

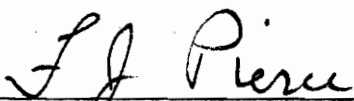
AN IMPLICIT NUMERICAL SOLUTION
OF THE TURBULENT THREE-DIMENSIONAL INCOMPRESSIBLE
BOUNDARY-LAYER EQUATIONS

by

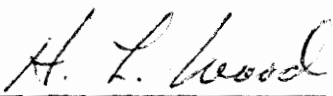
William Frederick Klinksiek

Thesis Submitted to the Graduate Faculty of the
Virginia Polytechnic Institute and State University
in Partial Fulfillment of the Requirements for the Degree of
DOCTOR OF PHILOSOPHY
in
Mechanical Engineering

APPROVED:


Chairman, Dr. F. J. Pierce


Dr. J. B. Jones


Dr. H. L. Wood


Dr. R. A. Comparin


Dr. C. K. Martin

June, 1971

Blacksburg, Virginia

LD
5655
V856
1971
K45
c. 2

ACKNOWLEDGEMENTS

The author gratefully acknowledges Dr. J. B. Jones for employing him as an Instructor in the Mechanical Engineering Department which allowed the author to further advance his graduate training. The author further extends his gratitude to the Army Research Office-Durham for partially funding this investigation which is part of a total research grant made to Dr. F. J. Pierce.

It has been a privilege to have Drs. F. J. Pierce (Chairman), J. B. Jones, R. A. Comparin, H. L. Wood and C. K. Martin as his advisory committee and the author extends his sincere appreciation for their advice, time, criticism and encouragement during the preparation of this thesis.

In addition, the author expresses his gratitude to Miss Willie Mae Hylton for typing the major portion of the manuscript.

Finally, to his wife, Sharon, the author expresses his appreciation for her understanding, patience, and encouragement during the past four years.

TABLE OF CONTENTS

	<u>Page</u>
TITLE PAGE	i
ACKNOWLEDGEMENTS	ii
TABLE OF CONTENTS	iii
LIST OF FIGURES	v
TABLE OF NOMENCLATUREviii
I. INTRODUCTION	1
II. REVIEW OF LITERATURE	3
III. INVESTIGATION	8
A. The Governing Equations	8
B. The Eddy-Viscosity Model	13
C. Finite Difference Formulation	15
1. Two-Dimensional and Plane of Symmetry Formulation	16
2. Three-Dimensional Formulation	23
D. Generation of Boundary Conditions and Initial Conditions	31
E. Solution Technique	39
F. The Continuity Equation	42
G. Stability and Convergence	44
IV. RESULTS	52
A. Laminar Two-Dimensional Solution	52
B. Turbulent Two-Dimensional Flow	60
C. Plane of Symmetry and Three-Dimensional Results	73
V. SUMMARY AND CONCLUSIONS	106

	<u>Page</u>
VI. BIBLIOGRAPHY	109
VII. APPENDIX A (Computer Program)	114
VIII. VITA	145

LIST OF FIGURES

		<u>Page</u>
3.1	Two-Dimensional Finite Difference Grid	17
3.2	Three-Dimensional Finite Difference Grid	24
3.3	Schematic Drawing of Johnston's Test Geometry. . .	32
3.4	Schematic Drawing of Hornung and Joubert's Test Geometry	33
3.5	Experimental Station Locations for Johnston's Test Geometry	35
3.6	Experimental Station Locations for Hornung and Joubert's Test Geometry	37
4.1	\bar{U} -Velocity Profile Compared with Blasius Solution for $\Delta X = \delta$	53
4.2	\bar{V} -Velocity Profile Compared with Blasius Solution for $\Delta X = \delta$	54
4.3	\bar{U} -Velocity Profile Compared with Blasius Solution for $\Delta X = \delta/2$ and $\Delta X = 4\delta$	55
4.4	\bar{V} -Velocity Profile Compared with Blasius Solution for $\Delta X = \delta/2$ and $\Delta X = 4\delta$	56
4.5	Skin-Friction Coefficient Compared with Blasius Solution	57
4.6	Development of Streamwise Turbulent Velocity Profiles Compared with the Law of the Wall	61
4.7	Development of θ_{11} and δ_1^* Compared with a Momentum Integral Analysis	63
4.8	Turbulent Skin-Friction Coefficient Compared with the Ludwig and Tillmann Correlation	64
4.9	Initial Law of the Wall Fit to Schubauer and Klebanoff's Experimental Data at $X = 19.0$ ft. . .	66

	<u>Page</u>
4.10	Initial \bar{U} -Velocity Profile for Schubauer and Klebanoff Geometry in Physical Coordinates at X = 19.0 ft 67
4.11	\bar{U} -Velocity Profile Compared with Schubauer and Klebanoff's Experimental Data at X = 20.5 ft . 69
4.12	\bar{U} -Velocity Profile Compared with Schubauer and Klebanoff's Experimental Data at X = 21.5 ft . 70
4.13	Initial \bar{U} -Velocity Profile fit to Johnston's Experimental Data at Station D-8 74
4.14	External Velocity Field on the Plane of Symmetry for the Johnston Geometry 75
4.15a	\bar{U} -Velocity Profile Compared with Johnston's Experimental Data at Station D-6 78
4.15b	\bar{U} -Velocity Profile Compared with Johnston's Experimental Data at Station D-X8 79
4.15c	\bar{U} -Velocity Profile Compared with Johnston's Experimental Data at Station D-4 80
4.15d	\bar{U} -Velocity Profile Compared with Johnston's Experimental Data at Station D-X6 81
4.16	Cross-Flow Velocity Gradients Compared with Johnston's Experimental Data at Station D-X6 . . . 82
4.17	Development of θ_{11} on the Plane of Symmetry Compared with Johnston's Experimental Data 84
4.18	Development of δ_1^* on the Plane of Symmetry Compared with Johnston's Experimental Data 85
4.19a	U_g and W_g Velocity Profiles Compared with Johnston's Experimental Data at Stations B-4 and F-4 86
4.19b	U_g and W_g Velocity Profiles Compared with Johnston's Experimental Data at Stations A-4 and G-4 87

	<u>Page</u>
4.20a	$U_{\bar{s}}$ and $W_{\bar{s}}$ Velocity Profiles Compared with Johnston's Experimental Data at Stations B-X6 and F-X6 88
4.20b	$U_{\bar{s}}$ and $W_{\bar{s}}$ Velocity Profiles Compared with Johnston's Experimental Data at Stations A-X6 and G-X6 89
4.21	Variation of Angle of Skewing Compared with Johnston's Experimental Data at Stations A-4 and G-4 91
4.22	Variation of Angle of Skewing Compared with Johnston's Experimental Data at Stations B-X6 and F-X6 92
4.23	Variation of Angle of Skewing in the Near Wall Region Compared with Johnston's Experimental Data at Stations B-X6 and F-X6 93
4.24	Development of θ_{11} off the Plane of Symmetry Compared with Johnston's Experimental Data . . . 94
4.25	Development of δ_1^* off the Plane of Symmetry Compared with Johnston's Experimental Data . . . 95
4.26	Development of θ_{13} off the Plane of Symmetry Compared with Johnston's Experimental Data . . . 96
4.27	\bar{U} -Velocity Profile Compared with Hornung and Joubert's Experimental Data at Station 10 . . 99
4.28	$U_{\bar{s}}$ and $W_{\bar{s}}$ Velocity Profiles Compared with Hornung and Joubert's Experimental Data at Station 12 . . 100
4.29	$U_{\bar{s}}$ and $W_{\bar{s}}$ Velocity Profiles Compared with Hornung and Joubert's Experimental Data at Station 14 . . 101
4.30	Variation of the X Component of the Laminar and Turbulent Shear Stress 104
4.31	Variation of the Z Component of the Laminar and Turbulent Shear Stress 105

TABLE OF NOMENCLATURE

A	van Driest's damping factor
A*	Distance of origin translation
A _{eff}	Modified value of A
A'(j)	Matrix coefficient
C'(j)	Matrix coefficient
D' _i (j)	Matrix coefficients
D' _i '(j)	Matrix coefficients
D _{ij}	Instantaneous rate-of-strain tensor: $\frac{\partial \bar{u}_i}{\partial X_j} + \frac{\partial \bar{u}_j}{\partial X_i}$
\bar{D}_{ij}	Time average rate-of-strain tensor: $\frac{\partial \bar{u}_i}{\partial X_j} + \frac{\partial \bar{u}_j}{\partial X_i}$
E _i (j)	Recurrence coefficients
F	Function
F _i	Body force vector
F _i (j)	Recurrence coefficients
G	Function
H	Dummy variable
L	Nondimensionalized mixing length
P	Instantaneous pressure
\bar{P}	Time average pressure
P'	Turbulent pressure fluctuation
Q ₀	Reference velocity
Q _i	Velocity vector with components (U, V, W)
\bar{Q}_i	Time average velocity vector with components (\bar{U} , \bar{V} , \bar{W})

Q'_i	Turbulent velocity fluctuation vector with components (U', V', W')
Q_{s_∞}	External streamline coordinate velocity
$\bar{Q}_{\infty i}$	External velocity vector with components ($\bar{U}_\infty, \bar{V}_\infty, \bar{W}_\infty$)
$S'_i(j)$	Matrix Coefficients
TE	Truncation error
X_i	Displacement vector with components (X, Y, Z)
b	Reference length
e, exp	Exponentiation with respect to the Napierian base
i, j, k	Indices
ℓ	Mixing length
r_1, r_2, r_3	Coefficients defined in Eq. 3.23
$s_1, s_2, s_3,$ $s_4, s_5, s_6,$ s_7, s_8, t	Coefficients defined in Eqs. 3.23 and 3.31
u, v, w	Nondimensionalized velocity components corresponding to $\bar{U}, \bar{V},$ and \bar{W} respectively
$\bar{u}, \bar{v}, \bar{w}$	Space averaged velocity components in finite difference grid
u_∞, w_∞	Nondimensionalized external velocity components corresponding to \bar{U}_∞ and \bar{W}_∞ , respectively
$\bar{u}_\infty, \bar{w}_\infty$	Spaced average external velocity components in finite difference grid
U_s, W_s	Streamline coordinate velocity components
u^*	Shear velocity = $\left(\frac{\tau_w}{\rho}\right)^{\frac{1}{2}}$
u^+	$\frac{\bar{U}}{u^*}$

wz	$\frac{\partial w}{\partial z}$ (nondimensionalized)
\overline{wz}	Space average value of wz in finite difference grid
wz_∞	External value of wz
$\overline{wz_\infty}$	Space average value of wz_∞ in finite difference grid
x, y, z	Nondimensional displacements corresponding to $X, Y,$ and $Z,$ respectively
y^+	$\frac{Y u^*}{\nu}$
$\left. \begin{array}{l} \Delta x, \Delta y_+, \\ \Delta y_-, \Delta z \end{array} \right\}$	Finite difference increments
α_s	Angle of skewing with respect to free stream streamline coordinate direction
α, β, γ	Amplification factors
δ	Boundary-layer thickness
δ_1^*, δ_3^*	Displacement thicknesses with respect to streamline coordinates
ϵ	Eddy viscosity
ϵ_m	Nondimensionalized eddy viscosity
θ	Parameter defined in Eq. 3.57
$\left. \begin{array}{l} \theta_{11}, \theta_{13}, \\ \theta_{31}, \theta_{33} \end{array} \right\}$	Momentum thicknesses with respect to streamline coordinates
μ	Dynamic viscosity
ν	Kinematic viscosity
π	3.1415926...
ρ	Density
σ	Step size parameter
τ_{x_l}, τ_{z_l}	Components of the laminar shear stress in the X and Z directions, respectively
τ_{x_t}, τ_{z_t}	Components of the turbulent shear stress in the X and Z directions, respectively

τ_{W_x}, τ_{W_z}

Wall shear stresses in the X and Z directions,
respectively

 τ_w

Total wall shear stress

 ϕ

Parameter defined in Eq. 3.57

I. INTRODUCTION

For many years momentum integral techniques have been used to predict the growth and general characteristics of two-dimensional turbulent boundary-layer flows. Not until large digital computers were introduced were numerical solutions of the two-dimensional boundary-layer equations feasible. With the development of such computers, and because of the large quantity of empirical input which momentum integral methods require, Spalding [1], in his recent review of the state of the art, recommended abandonment of any further effort in this area, favoring instead numerical solution techniques applied directly to the governing partial differential equations.

For three-dimensional turbulent boundary-layer flows, the momentum integral approach requires even more empirical input. The general case has two momentum integral equations, one each for the free-stream and transverse directions, and at least seven unknowns. For example, in addition to a velocity profile model in the free-stream direction, an additional empirical model must be introduced for the cross-flow velocity profile. A wall shear stress correlation is required, and except for the recent work of Pierce and Krommenhoek [2], there has been relatively little evidence substantiating the applicability of the two-dimensional wall shear stress correlations to three-dimensional flows. Generally, one "variation of form parameter" type ancillary equation is required for closure of the system of equations. The appropriate form of such an equation is open for two-dimensional turbulent boundary-layer

flows, with Thompson [3] suggesting that an entrainment equation yields the best results. Hence, any extension of the various forms of this ancillary equation to three-dimensional flow circumstances is open to some question. A similar difficulty with empirical input arises when attempting numerical solutions of the equations of motion for three-dimensional turbulent flows because a model for the shear stress variation through the boundary layer is required. However, this is the only necessary empirical input in such a solution.

The momentum integral analysis does, however, have one advantage over numerical solutions of the partial differential equations. The integral method requires the solution of only one set of finite difference equations at each free stream location. On the other hand, numerical solutions of the partial differential equations require the solution of a set of simultaneous equations at each free stream location for each boundary layer node location. Thus, the momentum integral technique generally has a substantially smaller computational time than does the alternative approach.

The emphasis of this present investigation is to develop a numerical technique by which the equations of motion for an incompressible three-dimensional turbulent boundary layer can be solved in a reasonable length of computational time and predict accurately the detailed characteristics of the flow field.

II. REVIEW OF LITERATURE

When attempting a solution of the equations of motion for turbulent boundary layer flows the major difficulty is in the modeling of the apparent or turbulent stress terms. There are generally two different approaches used to obtain the necessary equations to describe the turbulent shear stresses. The first approach was introduced by Boussinesq [4] in which an eddy viscosity was applied to describe the stress field. Prandtl [5] introduced the mixing length concept which can be used to generate one formulation for the eddy viscosity. The second approach was introduced by Townsend [6] in which the shear stress profile was obtained from a modified form of the turbulent energy equation. Many investigators (van Driest [7], Cebeci [8], Mellor [9], Mellor and Gibson [10], Pletcher [11] and Maise and McDonald [12]) have followed the mixing length concept or more generally the eddy viscosity concept, and have introduced various functional forms for the eddy viscosity or the mixing length in two-dimensional turbulent boundary-layer flows. One advantage of either the eddy viscosity or the mixing length approach is the introduction of only one empirical function to correlate the shear stress variation with known flow parameters. Bradshaw, Ferris and Atwell [13] modified the concepts presented by Townsend [6] slightly and developed an equation for the turbulent shear stresses using the turbulent energy equation. However, to accomplish this development, they had to introduce three empirical functions to correlate the shear stresses with the turbulent energy, the viscous dissipation, and the turbulence diffusion. They noted that with this shear

model, the governing equations were hyperbolic in form. This allowed the use of the method of characteristics to obtain the solution. Recently, Bradshaw [14] has extended this model to three-dimensional turbulent boundary-layer flows and again applied the method of characteristics to obtain a solution. Nash [15] used a simple explicit difference analysis for his three-dimensional turbulent boundary layer investigation and incorporated the Bradshaw model for the outer flow regions where viscous shear stresses are negligible. These latter two solutions fit to the law of the wall in the near-wall region where the viscous stresses are not negligible as assumed in the outer region model proposed by Bradshaw. Donaldson and Rosenbaum [16] have approached the problem in a manner similar to Bradshaw. However, instead of forming a contraction on the turbulence generation equations to produce the turbulent energy equation, they used the method of invariant modeling to form a system of equations for the individual turbulent stress terms. Their basic assumptions, however, are similar to those of Bradshaw and differ only in the mathematical detail. One advantage of Donaldson and Rosenbaum's method is the introduction of only one empirical function for which they are currently developing an expression.

Smith and Cebeci [17] applied a Levy-Lees transformation to the two-dimensional turbulent boundary-layer equations and used a simple implicit analog to obtain a set of finite difference equations. Because of their linearization technique, they had to incorporate an iterative procedure at each location in their solution to obtain successively better values of the eddy viscosity and other fluid properties. Their

results showed good agreement with experiment for incompressible turbulent boundary-layer flows subjected to favorable, zero, and adverse pressure gradients.

Hartree and Womersley [18] transformed the two-dimensional equations of motion for a laminar boundary layer in such a manner as to form an ordinary differential equation for the cross flow direction, which can be integrated using a Runge-Kutta method, and a finite difference equation in the streamwise direction. Smith and Clutter [19] used this technique for two-dimensional laminar boundary-layer flows and formed their finite differences using a simple implicit scheme. Smith, Jaffe and Lind [20] extended this method to two-dimensional turbulent boundary layer flows again using a simple implicit scheme. Mellor [21] also used this technique to predict turbulent boundary layer behavior on the plane of symmetry in convergent and divergent flow fields.

Der and Raetz [22] applied a rather complicated coordinate transformation on the laminar three-dimensional boundary layer equations and solved these equations using an explicit Dufort-Frankel difference analog. Dwyer [23] noted that their method converged too slowly for most practical problems. Thus, he applied the transformation used by Sowerby [24], which is almost identical to the Blasius transformation, to the three-dimensional laminar boundary layer equations. Dwyer then applied a simplified extension of the Crank-Nicholson finite difference method to the equations to obtain a solution. He noted that for one three-dimensional geometry for which there were 72,000 net nodal locations, the computational time on a General Electric 635 computer was

approximately five minutes.

Flügge-Lotz and Blottner [25] studied laminar two-dimensional boundary-layer flows in both transformed and physical coordinates using a Crank-Nicholson finite difference model to develop their final governing equations. Their results showed good agreement with the various similarity solutions available for such flows. They stated that great care must be taken when the initial input profile was not available from some analytical solution. Thus, most of these solutions actually started at some distance from the leading edge where a similarity profile could be obtained. Fussell [26] applied several different coordinate transformations for two-dimensional laminar flows and studied the agreement among various numerical methods. He concluded that the Crank-Nicholson finite difference analog yielded better accuracy than simple implicit formulations especially when an iterative procedure was included.

Pletcher [11] applied the Dufort-Frankel finite difference method to the two-dimensional turbulent boundary layer equations and obtained good agreement with experimental data in favorable, zero, and adverse pressure gradient flows. East [27] generalized this method to three-dimensional turbulent boundary-layer flow circumstances and also obtained good agreement with the data presented by Johnston [28] and that presented by Hornung and Joubert [29]. East's method required lengthy computational time on the IBM-360 model 65. He reported that a solution for the Johnston geometry required one hour and fifteen minutes, and a solution for the Hornung and Joubert geometry required nearly two hours.

Hunt, Bushnell and Beckwith [30] simplified the equations of motion and energy for compressible turbulent boundary layers over swept infinite cylinders and generated the corresponding algebraic equations by expressing the various derivatives implicitly. They expressed the turbulent stresses in terms of an eddy viscosity and subsequently used the mixing length hypothesis to generate the eddy viscosity variation through the boundary layer. The results of their investigation were generally in good agreement with experimental data both with and without blowing at the surface of the cylinder.

In summary, it appears that the only calculation scheme for the full three-dimensional turbulent boundary layer equations and using a mixing length hypothesis is that by East [27], in which he uses a Dufort-Frankel finite-difference analogue. The alternative solution technique is that of Bradshaw [14] and Nash [15]. This latter method requires slightly more empirical input, and the turbulent shear stress model does not accommodate near-wall calculations where viscous stresses dominate and gradients are largest. The present study extends implicit methods to three-dimensional turbulent boundary flows, using an eddy viscosity model following from the mixing length hypothesis to minimize empirical input, and attempts to decrease the required computational time taking advantage of increased step sizes following from the general stability of such implicit methods.

III. INVESTIGATION

An implicit finite-difference technique was incorporated to solve the governing differential equations for a three-dimensional incompressible turbulent boundary-layer flow. The difference equations were written in such a manner as to form a set of quasi-linear algebraic equations whose coefficients constituted a tridiagonal matrix. The Thomas [31] algorithm was written to obtain the solution set, instead of the time-consuming matrix inversion techniques. Finally an analysis was undertaken to determine the stability and convergence of the finite-difference equations.

A. The Governing Equations

The equations of motion and continuity which govern the unsteady flow of an incompressible fluid are given by Hinze [4] as

$$\rho \frac{DQ_i}{Dt} = - \frac{\partial P}{\partial X_i} + \frac{\partial}{\partial X_j} [\mu D_{ji}] + F_i \quad \begin{array}{l} i=1,2,3 \\ j=1,2,3 \end{array} \quad (3.1)$$

$$\frac{\partial Q_j}{\partial X_j} = 0 \quad j=1,2,3 \quad (3.2)$$

where

$$D_{ij} = \frac{\partial Q_i}{\partial X_j} + \frac{\partial Q_j}{\partial X_i} \quad \begin{array}{l} i=1,2,3 \\ j=1,2,3 \end{array}$$

and $\frac{D}{Dt}$ is the substantial derivative.

To obtain a solution of these equations for turbulent flow, the equations can be time smoothed and the resultant mean-flow equations solved. One serious drawback of this approach is the introduction of

six additional unknowns in the form of apparent or Reynolds stresses.

The time-smoothing procedure is outlined in Hinze [4] and the resultant governing equations, in the absence of body forces, are

$$\rho \frac{D\bar{Q}_i}{Dt} = - \frac{\partial \bar{P}}{\partial X_i} + \frac{\partial}{\partial X_j} (\mu \bar{D}_{ji} - \rho \overline{Q'_i Q'_j}) \quad \begin{array}{l} i=1,2,3 \\ j=1,2,3 \end{array} \quad (3.3)$$

$$\frac{\partial \bar{Q}_j}{\partial X_j} = 0 \quad j=1,2,3 \quad (3.4)$$

where the following substitutions were made

$$Q_i = \bar{Q}_i + Q'_i$$

$$P = \bar{P} + P'$$

with Q'_i and P' representing the turbulent fluctuations of the velocity and the pressure, respectively, and the overbar signifying the time-average value.

According to Boussinesq's [4] hypothesis, the apparent "kinematic" turbulent stresses can be expressed as functions of mean velocity gradients and a scalar eddy viscosity as shown in Eq. 3.5.

$$- \overline{Q'_i Q'_j} = \epsilon \bar{D}_{ij} \quad \begin{array}{l} i=1,2,3 \\ j=1,2,3 \end{array} \quad (3.5)$$

With this hypothesis the equations of motion become

$$\rho \frac{D\bar{Q}_i}{Dt} = - \frac{\partial \bar{P}}{\partial X_i} + \frac{\partial}{\partial X_j} [(\mu + \rho \epsilon) \bar{D}_{ji}] \quad \begin{array}{l} i=1,2,3 \\ j=1,2,3 \end{array} \quad (3.6)$$

Equations 3.6 and 3.4 were reduced from 4 equations and 4 unknowns to 3 equations and 3 unknowns by making the typical boundary-layer assumptions for flow over a surface defined by the plane, $Y = 0$. This procedure is outlined in Schlichting [32] for two-dimensional flows and

was extended by East [27] in some detail for three-dimensional turbulent flows. The further assumption, that outside the boundary layer the effects of the wall were negligible, allowed the use of Euler's equation to obtain a first approximation to the external pressure field. Thus, Eqs. 3.6 and 3.4 become

$$\rho \bar{Q}_j \frac{\partial \bar{Q}_i}{\partial X_j} = \rho \bar{Q}_{\infty k} \frac{\partial \bar{Q}_{\infty i}}{\partial X_k} + \frac{\partial}{\partial Y} [(\mu + \rho \epsilon) \frac{\partial \bar{Q}_i}{\partial Y}] \quad \begin{array}{l} i=1,3 \\ j=1,2,3 \\ k=1,3 \end{array} \quad (3.7)$$

$$\frac{\partial \bar{Q}_j}{\partial X_j} = 0 \quad j=1,2,3 \quad (3.8)$$

for steady flow.

Equations 3.7 and 3.8 were non-dimensionalized by the following substitutions

$$\bar{U} = u Q_0 \quad (3.9a)$$

$$\bar{V} = v \left(\frac{b}{Q_0 v} \right) - \frac{1}{2} \quad (3.9b)$$

$$\bar{W} = w Q_0 \quad (3.9c)$$

$$X = xb \quad (3.9d)$$

$$Y = y \left(\frac{vb}{Q_0} \right)^{\frac{1}{2}} \quad (3.9e)$$

$$Z = zb \quad (3.9f)$$

$$\epsilon = v \epsilon_m \quad (3.9g)$$

to form the final set of equations to be solved.

$$uu_x + vu_y + wu_z = u_\infty u_{\infty x} + w_\infty u_{\infty z} + [(1 + \epsilon_m) u_y]_y \quad (3.10a)$$

$$uw_x + vw_y + ww_z = u_\infty w_{\infty x} + w_\infty w_{\infty z} + [(1 + \epsilon_m) w_y]_y \quad (3.10b)$$

$$u_x + v_y + w_z = 0 \quad (3.10c)$$

The subscripts x , y and z denote the partial derivative of a quantity,

for example: $\frac{\partial u}{\partial x} = u_x$.

By the nature of the boundary-layer approximations the problem was reduced from a boundary-value problem in the three coordinate directions to an initial-value problem with respect to the variables x and z and a boundary-value problem with respect to y .

In some flow geometries a region of essentially two-dimensional flow exists upstream of the three-dimensional flow field under consideration. Thus to generate the initial values of u , v , and w for the $x = 0$ plane, the momentum and continuity equations are easily simplified for a two-dimensional turbulent boundary-layer flow and the resultant two-dimensional solution can be used to initiate the three-dimensional solution.

The initial conditions on the $z = 0$ plane depend on the physical flow circumstance to be studied. One class of three-dimensional boundary-layer flows which is governed by Eqs. 3.10 is typified by flow over a nearly-flat infinite swept wing. For this case, the derivatives with respect to z are all identically zero with the proper choice of coordinate system orientation, hence, eliminating the necessity for the z -direction initial conditions. External boundary-layer flows over a flat plate with an obstruction constitute another class of flows that may be

considered for solution. For the condition in which the obstruction is a symmetrically shaped object, a plane of symmetry exists along the stagnation streamline and becomes the initial condition for the z-direction. For the case when the object is asymmetric, care must be taken in generating the z-boundary condition because of the curvature of the stagnation free-stream streamline. For the asymmetric circumstance a streamline-coordinate set would probably be more suitable. Thus, the present investigation will be directed toward this second class of flows, and specifically, those cases when the obstruction is symmetric.

On the plane of symmetry, or for two-dimensional flows, the equations of motion and continuity are

$$u u_x + v u_y = u_\infty u_{\infty x} + [(1 + \epsilon_m) u_y]_y \quad (3.11a)$$

$$u_x + v_y + w_z = 0 \quad (3.11b)$$

and the z-momentum equation is identically equal to zero, which leaves only 2 equations but 3 unknowns. To remedy this situation the z-momentum equation was differentiated with respect to z and a third equation was generated for the unknown $\frac{\partial w}{\partial z}$ (which will be denoted as wz).

$$u(wz)_x + v(wz)_y + (wz)(wz) = u_\infty (wz)_{\infty x} + (wz_{\infty})^2 + [(1 + \epsilon_m) wz_y]_y \quad (3.12)$$

Equations 3.11 and 3.12 are the equations governing two-dimensional and plane of symmetry turbulent boundary-layer flows and also form the basis for generating the initial conditions for the three-dimensional solution.

B. The Eddy-Viscosity Model

There are many eddy-viscosity models available in the literature for two-dimensional boundary-layer flows. One such model that has gained wide-spread usage was introduced by Prandtl [4], who postulated that the eddy viscosity be formed as a function of a mixing length and a velocity gradient.

$$\epsilon = \ell^2 \frac{\partial \bar{U}}{\partial Y} \quad (3.13)$$

The quantity $\frac{\partial \bar{U}}{\partial Y}$ can also be represented as a function of the magnitude of the first rate-of-strain invariant [33]

$$\frac{\partial \bar{U}}{\partial Y} = \frac{1}{2} (\bar{D}_{ij} \bar{D}_{ij}) \quad \begin{array}{l} i=1,2 \\ j=1,2 \end{array} \quad (3.14a)$$

when only the highest order terms are retained, consistent with the two-dimensional boundary-layer approximations. Prandtl (see Goldstein [34]) extended the mixing length model to three-dimensional flows and developed an expression for the corresponding eddy viscosity.

$$\epsilon = \ell^2 (\bar{D}_{ij} \bar{D}_{ij}) / 2 \quad \begin{array}{l} i=1,2,3 \\ j=1,2,3 \end{array} \quad (3.15)$$

When the usual boundary-layer approximations are applied to the rate-of-strain invariant for three-dimensional boundary layers, the expression for the eddy viscosity model becomes

$$\epsilon = \ell^2 [(\bar{U}_Y)^2 + (\bar{W}_Y)^2]^{1/2} \quad (3.16a)$$

Non-dimensionally, this expression is written as

$$\epsilon_m = L^2 [(u_y)^2 + (w_y)^2]^{1/2} \quad (3.16b)$$

$$\text{where } L^2 = \frac{\ell^2 (Q_o b)^{3/2}}{b^2 \nu}$$

Several mixing-length models were considered for use in the present investigation. From the recent works of Pletcher [11] and East [27] the mixing length model, as proposed by Maise and McDonald [12], is taken as

$$\frac{\ell}{\delta} = 0.41 [1.0 - \exp(-y^+/A)] \left(\frac{y}{\delta}\right) \quad \text{for } \frac{y}{\delta} < 0.1 \quad (3.17a)$$

$$\begin{aligned} \frac{\ell}{\delta} = & 0.41 [1.0 - \exp(-y^+/A)] \left(\frac{y}{\delta}\right) \\ & - 1.53506 \left(\frac{y}{\delta} - 0.1\right)^2 + 2.75625 \left(\frac{y}{\delta} - 0.1\right)^3 \\ & - 1.88425 \left(\frac{y}{\delta} - 0.1\right)^4 \quad \text{for } 0.1 \leq \frac{y}{\delta} \leq 0.6 \end{aligned} \quad (3.17b)$$

$$\frac{\ell}{\delta} = 0.089 \left(\frac{y}{\delta}\right) \quad \text{for } \frac{y}{\delta} > 0.6 \quad (3.17c)$$

Although this correlation was for a zero pressure gradient flow, the numerical solutions of Pletcher [11] and East [27] indicate that the model yields very good agreement with experimental data when predicting the boundary layer growth of two-dimensional turbulent boundary-layer flows with a pressure gradient. Two other eddy viscosity models which deserve mention were presented by Smith and Cebeci [17]; and Mellor [9], and Mellor and Gibson [10]. As discussed by East [27], these models are easily adapted to plane of symmetry flows, but a generalization to three-dimensional flows is difficult to obtain, because the formulations both contain the term, δ_1^* . For two-dimensional and plane of symmetry flows, δ_3^* is zero and the extension to these circumstances is straightforward. However, for three-dimensional flows, δ_3^* is not equal to zero,

and a question arises whether to use δ_1^* only or replace the terms containing δ_1^* by some yet to be determined combination of δ_1^* and δ_3^* .

The value of A in Eqs. 3.17 was taken by the previous investigators as 26 after van Driest [7]. However, van Driest determined this value by obtaining a best fit to Laufer's data [35] which generally followed the law of the wall with the following constants

$$u^+ = \frac{1}{0.40} \ln y^+ + 5.24 \quad (3.18)$$

For equilibrium turbulent boundary-layer flows in two dimensions, Coles [36] studied some 500 profiles and suggested that the law of the wall constants should be as in Eq. 3.19.

$$u^+ = \frac{1}{0.41} \ln y^+ + 5.0 \quad (3.19)$$

To obtain a value of the parameter A, consistent with this set of constants, a procedure analogous to van Driest's was followed and the law of the wall formulation was closely approximated as

$$u^+ = \frac{1}{0.41} \ln y^+ + 5.07 \quad (3.20)$$

for a value of A of 25. This value was considered acceptable since van Driest noted that to fit Nikuradse's data, the parameter, A, was equal to 27 instead of 26.

C. Finite Difference Formulation

A Crank-Nicholson [37] implicit finite difference scheme was utilized for the following reasons:

- (i) For laminar two-dimensional boundary-layer flows the resultant equations have been shown to be stable and

convergent by Flügge-Lotz and Blottner [25].

(ii) The truncation errors are of order $(\Delta x)^2$, $(\Delta y)^2$ and $(\Delta z)^2$ which would minimize the computer time because of the larger step sizes that can be taken.

(iii) If the finite difference equations are written in such a manner as to form a tridiagonal matrix of coefficients, the solution of the difference equations does not require matrix inversion. Instead a simple algorithm can be written to obtain the solution.

1. Two-Dimensional and Plane of Symmetry Formulation

Figure 3.1 shows the grid construction used to generate the finite difference approximations for the two-dimensional and plane of symmetry flows. The difference approximations shown below are given for any variable H about the point $(i + \frac{1}{2}, j, k)$. The equations were written for a variable y -grid spacing allowing more dense node locations in regions of large gradients and fewer locations in regions of small gradients. Terms appearing in Eqs. 3.11a and 3.12 are given as

$$(H)_x = \frac{H(i+1, j, k) - H(i, j, k)}{\Delta x} - \frac{1}{24} (H)_{xxx} (\Delta x)^2 \quad (3.21a)$$

$$(H)_y = \frac{1}{2(\Delta y_+ + \Delta y_-)} \left\{ \frac{\Delta y_-}{\Delta y_+} [(H(i, j+1, k) - H(i, j, k)) + H(i+1, j+1, k) - H(i+1, j, k)) + \frac{\Delta y_+}{\Delta y_-} (H(i, j, k) - H(i, j-1, k) + H(i+1, j, k) - H(i+1, j-1, k))] \right\} - \frac{1}{6} (H)_{yyy} (\Delta y_+) (\Delta y_-) - \frac{1}{8} (H)_{xxy} (\Delta x)^2 \quad (3.21b)$$

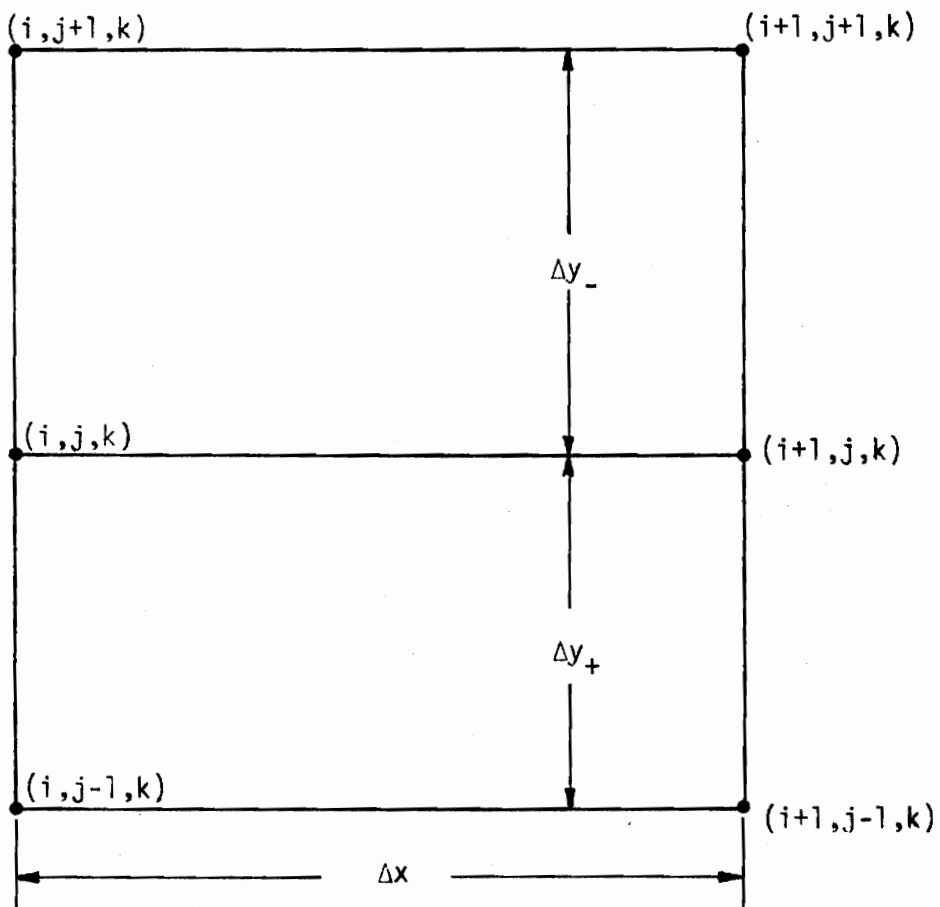


Fig. 3.1 Two-Dimensional Finite Difference Grid.

$$\begin{aligned}
& [(1+\epsilon_m)H_y]_y = \\
& \frac{1}{(\Delta y_+ + \Delta y_-)} \{ [1+\epsilon_m(i+1, j+\frac{1}{2}, k)] \frac{H(i+1, j+1, k) - H(i+1, j, k)}{\Delta y_+} \\
& - [1+\epsilon_m(i+1, j-\frac{1}{2}, k)] \frac{H(i+1, j, k) - H(i+1, j-1, k)}{\Delta y_-} \\
& + [1+\epsilon_m(i, j+\frac{1}{2}, k)] \frac{H(i, j+1, k) - H(i, j, k)}{\Delta y_+} \\
& - [1+\epsilon_m(i, j-\frac{1}{2}, k)] \frac{H(i, j, k) - H(i, j-1, k)}{\Delta y_-} \} \\
& - \frac{1}{8} [(1+\epsilon_m)H_y]_{xxy} (\Delta x)^2 - \{ \frac{1}{24} [(1+\epsilon_m)H_y]_{yyy} \\
& + \frac{1}{12} [(1+\epsilon_m)H_{yy}]_{yy} - \frac{1}{24} [(1+\epsilon_m)H_{yyy}]_y \} \cdot \\
& [(\Delta y_+)^2 - (\Delta y_+)(\Delta y_-) + (\Delta y_-)^2] - \frac{1}{4} [(1+\epsilon_m)_x H_{xy}]_y (\Delta x)^2 \\
& - \{ \frac{1}{4} [(1+\epsilon_m)_y H_y]_y + \frac{1}{3} [1+\epsilon_m] H_{yyy} + \frac{1}{4} (1+\epsilon_m)_y H_{yyy} \} (\Delta y_+ - \Delta y_-) \quad (3.21c)
\end{aligned}$$

For the case of equal grid spacing in the y direction, these finite-difference approximations are in agreement with Flügge-Lotz and Blottner [25].

Equation 3.21a is used to represent the terms u_x and wz_x in Eqs. 3.11a and 3.12. The derivatives with respect to y in these two equations are obtained using Eq. 3.21b and the terms containing the derivative of the laminar and turbulent stresses are formulated using Eq. 3.21c. The nonlinear coefficients in Eqs. 3.11a and 3.12 were assumed to be known from the previous node location and are given as space-average quantities as shown in Eq. 3.22 for any variable H.

$$\bar{H} = \frac{H(i+1,j,k) + H(i,j,k)}{2} \quad (3.22)$$

Thus, $H(i+1,j,k)$ is equal to $H(i,j,k)$ as a first approximation and an iterative procedure is used to determine successively better approximations to $H(i+1,j,k)$. The details of this iterative scheme are given in a later section.

To simplify the resultant difference equations the following definitions are introduced.

$$r_1 = \frac{\bar{v}(\Delta y_-)\Delta x}{2\bar{u}(\Delta y_+)(\Delta y_+ + \Delta y_-)} \quad (3.23a)$$

$$r_2 = \frac{\bar{v}(\Delta y_+)\Delta x}{2\bar{u}(\Delta y_-)(\Delta y_+ + \Delta y_-)} \quad (3.23b)$$

$$r_3 = \frac{(\bar{w}z)\Delta x}{2\bar{u}} \quad (3.23c)$$

$$s_1 = \frac{(1+\epsilon_m(i+1, j+\frac{1}{2}, k))}{\bar{u}} \left\{ \frac{\Delta x}{(\Delta y_+)(\Delta y_+ + \Delta y_-)} \right\} \quad (3.23d)$$

$$s_2 = \frac{(1+\epsilon_m(i+1, j-\frac{1}{2}, k))}{\bar{u}} \left\{ \frac{\Delta x}{(\Delta y_-)(\Delta y_+ + \Delta y_-)} \right\} \quad (3.23e)$$

$$s_3 = \frac{(1+\epsilon_m(i, j+\frac{1}{2}, k))}{\bar{u}} \left\{ \frac{\Delta x}{(\Delta y_+)(\Delta y_+ + \Delta y_-)} \right\} \quad (3.23f)$$

$$s_4 = \frac{(1+\epsilon_m(i, j-\frac{1}{2}, k))}{\bar{u}} \left\{ \frac{\Delta x}{(\Delta y_-)(\Delta y_+ + \Delta y_-)} \right\} \quad (3.23g)$$

With this notation the difference approximations for the momentum equations become

x-momentum

$$\begin{aligned}
& (-r_2 - s_2)u(i-1, j-1, k) + (r_1 - s_1)u(i+1, j+1, k) \\
& + (1 + r_2 - r_1 + s_2 + s_1)u(i+1, j, k) + (-r_2 - s_4)u(i, j-1, k) \\
& + (r_1 - s_3)u(i, j+1, k) + (-1 + r_2 - r_1 + s_4 + s_3)u(i, j, k) \\
& = \frac{\bar{u}_\infty}{\bar{u}} \frac{u_\infty(i+1, k) - u_\infty(i, k)}{\bar{u}} \quad (3.24a)
\end{aligned}$$

(z-momentum)_z

$$\begin{aligned}
& (-r_2 - s_2)wz(i+1, j-1, k) + (r_1 - s_1)wz(i+1, j+1, k) \\
& + (1 + r_2 - r_1 + s_2 + s_1 + r_3)wz(i+1, j, k) + (-r_2 - s_4)wz(i, j-1, k) \\
& + (r_1 - s_3)wz(i, j+1, k) + (-1 + r_2 - r_1 + s_4 + s_3 + r_3)wz(i, j, k) \\
& = \frac{\bar{u}_\infty}{\bar{u}} \frac{wz_\infty(i+1, k) - wz_\infty(i, k)}{\bar{u}} + (\overline{wz_\infty})^2 \quad (3.24b)
\end{aligned}$$

For compactness these additional quantities are introduced

$$A'(j) = -r_2 - s_2 \quad (3.25a)$$

$$S'_1(j) = 1 + r_2 - r_1 + s_2 + s_1 \quad (3.25b)$$

$$S'_2(j) = 1 + r_2 - r_1 + s_2 + s_1 + r_3 \quad (3.25c)$$

$$C'(j) = r_1 - s_1 \quad (3.25d)$$

$$\begin{aligned}
D'_1(j) &= \frac{\bar{u}_\infty}{\bar{u}} [u_\infty(i+1, k) - u_\infty(i, k)] \\
&- (-r_2 - s_4)u(i, j-1, k) - (r_1 - s_3)u(i, j+1, k) \\
&- (-1 + r_2 - r_1 + s_3 + s_4)u(i, j, k) \quad (3.25e)
\end{aligned}$$

$$\begin{aligned}
D'_2(j) &= \frac{\bar{u}}{\bar{u}} [wz(i+1, k) - wz(i, k)] \\
&- (r_2 - s_4)wz(i, j-1, k) - (r_1 - s_3)wz(i, j+1, k) \\
&- (-1 + r_2 - r_1 + s_3 + s_4 + r_3)wz(i, j, k) \quad (3.25f)
\end{aligned}$$

The resultant algebraic equations to be solved are shown below.

x-momentum

$$A'(j) u(i+1, j-1, k) + S'_1(j) u(i+1, j, k) + C'(j) u(i+1, j+1, k) = D'_1(j) \quad j = 2, 3 \dots n \quad (3.26a)$$

(z-momentum)_z

$$A'(j) w_z(i+1, j-1, k) + S'_2(j) w_z(i+1, j, k) + C'(j) w_z(i+1, j+1, k) = D'_2(j) \quad j = 2, 3 \dots n \quad (3.26b)$$

Note that both Eqs. 3.26a and 3.26b have a matrix of coefficients that is tridiagonal (i.e., the matrix contains non-zero elements only on the principal diagonal and the two diagonals to either side). The details of the method of solution will be discussed in a later section of this chapter.

Two finite-difference formulations of the continuity equation (Eq. 3.11b) are posed for use in the solution. Method I evaluates the derivatives at the point $(i+1, j-\frac{1}{2}, k)$ on Fig. 3.1 and utilizes a backward difference scheme for the x derivative.

$$v_y = \frac{1}{\Delta y_-} [v(i+1, j, k) - v(i+1, j-1, k)] - \frac{1}{24} (v)_{yyy} (\Delta y_-)^2 \quad (3.27a)$$

$$u_x = \frac{1}{2\Delta x} [u(i+1, j, k) + u(i+1, j-1, k) - u(i, j, k) - u(i, j-1, k)] + \frac{1}{2} (u)_{xx} \Delta x \quad (3.27b)$$

$$w_z = \frac{1}{2} [w_z(i+1, j, k) + w_z(i+1, j-1, k)] - \frac{1}{8} u_{yy} (\Delta y_-)^2 \quad (3.27c)$$

Method II evaluates the derivatives at the point $(i+\frac{1}{2}, j-\frac{1}{2}, k)$ on Fig. 3.1 so that the resultant finite difference approximations are

$$\begin{aligned} (v)_y &= \frac{1}{2\Delta y_-} [v(i+1, j, k) + v(i, j, k) - v(i+1, j-1, k) \\ &- v(i, j-1, k)] \\ &- \frac{1}{8} (v)_{xxy} (\Delta x)^2 - \frac{1}{24} (v)_{yyy} (\Delta y_-)^2 \end{aligned} \quad (3.28a)$$

$$\begin{aligned} (u)_x &= \frac{1}{2\Delta x} [u(i+1, j, k) + u(i+1, j-1, k) - u(i, j, k) \\ &- u(i, j-1, k)] - \frac{1}{24} (u)_{xxx} (\Delta x)^2 - \frac{1}{8} (u)_{xyy} (\Delta y_-)^2 \end{aligned} \quad (3.28b)$$

$$\begin{aligned} w_z &= \frac{1}{4} [wz(i+1, j, k) + wz(i, j, k) + wz(i+1, j-1, k) + wz(i, j-1, k)] \\ &- \frac{1}{8} u_{xx} (\Delta x)^2 - \frac{1}{8} u_{yy} (\Delta y)^2 \end{aligned} \quad (3.28c)$$

Thus, the continuity equation is written in the following two forms:

Method I

$$\begin{aligned} v(i+1, j, k) &= v(i+1, j-1, k) - \frac{\Delta y_-}{2\Delta x} [u(i+1, j, k) \\ &+ u(i+1, j-1, k) - u(i, j, k) - u(i, j-1, k)] - \frac{\Delta y_-}{2} [wz(i+1, j, k) \\ &+ wz(i+1, j-1, k)] \end{aligned} \quad (3.29a)$$

Method II

$$\begin{aligned} v(i+1, j, k) &= v(i+1, j-1, k) + v(i, j-1, k) - v(i, j, k) \\ &- \frac{\Delta y_-}{x} [u(i+1, j, k) + u(i+1, j-1, k) - u(i, j, k) - u(i, j-1, k)] \\ &- \frac{\Delta y_-}{2} [wz(i, j, k) + wz(i, j-1, k) + wz(i+1, j, k) + wz(i+1, j-1, k)] \end{aligned} \quad (3.29b)$$

The choice of which continuity expression to use was the subject of a brief analysis and the findings will be presented in a later section.

2. Three-Dimensional Formulation

Figure 3.2 shows the grid used to model the finite differences for the three-dimensional problem. The difference formulations are shown below using a Crank-Nicholson finite difference scheme extended to three dimensions about the point $(i+\frac{1}{2}, j, k-\frac{1}{2})$ for any variable, H. Again a variable grid spacing in the y direction was used. Typical derivative terms appearing in Eqs. 3.10a and 3.10b are given as

$$H_x = \frac{1}{2\Delta x} [H(i+1, j, k) + H(i+1, j, k-1) - H(i, j, k) - H(i, j, k-1)] - \frac{1}{8} (H)_{xzz} (\Delta z)^2 - \frac{1}{24} (H)_{xxx} (\Delta x)^2 \quad (3.30a)$$

$$H_z = \frac{1}{2\Delta z} [H(i+1, j, k) + H(i, j, k) - H(i+1, j, k-1) - H(i, j, k-1)] - \frac{1}{8} (H)_{xxz} (\Delta x)^2 - \frac{1}{24} (H)_{zzz} (\Delta z)^2 \quad (3.30b)$$

$$H_y = \frac{1}{4(\Delta y_+ + \Delta y_-)} \left\{ \left(\frac{\Delta y_-}{\Delta y_+} \right) [H(i, j+1, k) - H(i, j, k) + H(i, j+1, k-1) - H(i, j, k-1) + H(i+1, j+1, k) - H(i+1, j, k) + H(i+1, j+1, k-1) - H(i+1, j, k-1)] \right. \\ \left. + \left(\frac{\Delta y_+}{\Delta y_-} \right) [H(i, j, k) - H(i, j-1, k) + H(i, j, k-1) - H(i, j-1, k-1) + H(i+1, j, k) - H(i+1, j-1, k) + H(i+1, j, k-1) - H(i+1, j-1, k-1)] \right\} \\ - \frac{1}{6} (H)_{yyy} (\Delta y_+) (\Delta y_-) - \frac{1}{8} (H)_{yxx} (\Delta x)^2 - \frac{1}{8} (H)_{yzz} (\Delta z)^2 \quad (3.30c)$$

$$[(1+\epsilon_m) H_y]_y =$$

$$\frac{1}{2(\Delta y_+ + \Delta y_-)} \left\{ [1+\epsilon_m (i+1, j+\frac{1}{2}, k)] \frac{H(i+1, j+1, k) - H(i+1, j, k)}{\Delta y_+} \right.$$

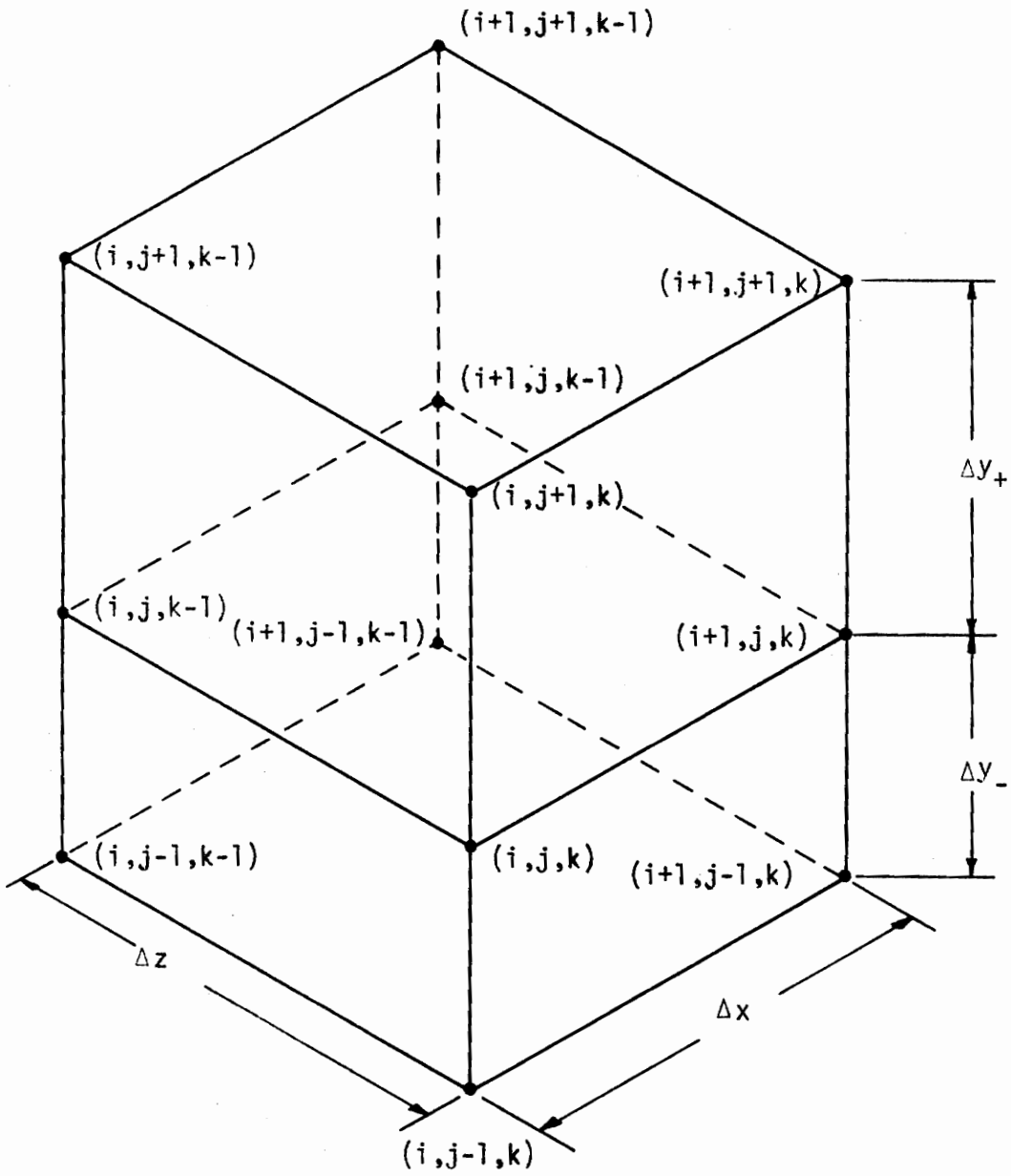


Fig. 3.2 Three-Dimensional Finite Difference Grid.

$$\begin{aligned}
& - [1+\epsilon_m(i+1, j-\frac{1}{2}, k)] \frac{H(i+1, j, k) - H(i+1, j-1, k)}{\Delta y_-} \\
& + [1+\epsilon_m(i+1, j+\frac{1}{2}, k-1)] \frac{H(i+1, j+1, k-1) - H(i+1, j, k-1)}{\Delta y_+} \\
& - [1+\epsilon_m(i+1, j-\frac{1}{2}, k-1)] \frac{H(i+1, j, k-1) - H(i+1, j-1, k-1)}{\Delta y_-} \\
& + [1+\epsilon_m(i, j+\frac{1}{2}, k)] \frac{H(i, j+1, k) - H(i, j, k)}{\Delta y_+} \\
& - [1+\epsilon_m(i, j-\frac{1}{2}, k)] \frac{H(i, j, k) - H(i, j-1, k)}{\Delta y_-} \\
& + [1+\epsilon_m(i, j+\frac{1}{2}, k-1)] \frac{H(i, j+1, k-1) - H(i, j, k-1)}{\Delta y_+} \\
& - [1+\epsilon_m(i, j-\frac{1}{2}, k-1)] \frac{H(i, j, k-1) - H(i, j-1, k-1)}{\Delta y_-} \\
& - \frac{1}{8} [1+\epsilon_m] H_y]_{\text{xxxy}} (\Delta x)^2 - \frac{1}{8} [(1+\epsilon_m) H_y]_{\text{zzzy}} (\Delta z)^2 - \frac{1}{4} [(1+\epsilon_m) H_{xy}]_y (\Delta x)^2 \\
& - \frac{1}{4} [(1+\epsilon_m) H_{zy}]_y (\Delta z)^2 - \left\{ \frac{1}{24} [(1+\epsilon_m) H_y]_{\text{yyy}} + \frac{1}{12} [(1+\epsilon_m) H_{yy}]_{\text{yy}} \right. \\
& - \frac{1}{24} [(1+\epsilon_m) H_{\text{yyy}}]_y \} [(\Delta y_+)^2 - (\Delta y_+)(\Delta y_-) + (\Delta y_-)^2] \\
& - \frac{1}{4} [(1+\epsilon_m) H_y]_y (\Delta y_+ - \Delta y_-) - \frac{1}{3} (1+\epsilon_m) H_{\text{yyy}} (\Delta y_+ - \Delta y_-) \\
& - \frac{1}{4} (1+\epsilon_m) H_{\text{yy}} (\Delta y_+ - \Delta y_-) \tag{3.30d}
\end{aligned}$$

Five additional new parameters are introduced to simplify the three-dimensional finite-difference equations.

$$s_5 = \frac{\Delta x}{\bar{u}(\Delta y_+)(\Delta y_+ + \Delta y_-)} [1+\epsilon_m(i+1, j+\frac{1}{2}, k-1)] \tag{3.31a}$$

$$s_6 = \frac{\Delta x}{\bar{u}(\Delta y_-)(\Delta y_+ + \Delta y_-)} [1+\epsilon_m(i+1, j-\frac{1}{2}, k-1)] \tag{3.31b}$$

$$s_7 = \frac{\Delta x}{\bar{u}(\Delta y_+)(\Delta y_+ + \Delta y_-)} [1+\epsilon_m(i, j+\frac{1}{2}, k-1)] \tag{3.31c}$$

$$s_8 = \frac{\Delta x}{\bar{u}(\Delta y_+) (\Delta y_+ + \Delta y_-)} [1 + \epsilon_m (i, j - \frac{1}{2}, k - 1)] \quad (3.31d)$$

$$t = \frac{\bar{w} \Delta x}{\bar{u} \Delta z} \quad (3.31e)$$

where the notation of the overbar is changed from the definition given in Eq. 3.22 to

$$\bar{H} = \frac{1}{4} [H(i+1, j, k) + H(i+1, j, k-1) + H(i, j, k) + H(i, j, k-1)] \quad (3.32)$$

With the use of Eqs. 3.30, 3.31, and 3.22 (with the noted change in the definition of \bar{H}) and linearizing the resultant equations, with the same procedure as outlined for the two-dimensional equations the finite difference approximations for the three-dimensional turbulent boundary-layer equations become

x-momentum

$$\begin{aligned} & (-r_2 - s_2)u(i+1, j-1, k) + (r_1 - s_1)u(i+1, j+1, k) \\ & + (1 + r_2 - r_1 + s_2 + s_1 + t)u(i+1, j, k) + (-r_2 - s_4)u(i, j-1, k) \\ & + (r_1 - s_3)u(i, j+1, k) + (-1 + r_2 - r_1 + s_4 + s_3 + t)u(i, j, k) \\ & + (-r_2 - s_6)u(i+1, j-1, k-1) + (r_1 - s_5)u(i+1, j+1, k-1) \\ & + (1 + r_2 - r_1 + s_6 + s_5 - t)u(i+1, j, k-1) + (-r_2 - s_8)u(i, j-1, k-1) \\ & + (r_1 - s_7)u(i, j+1, k-1) + (-1 + r_2 - r_1 + s_8 + s_7 - t)u(i, j, k-1) \\ & = \frac{\bar{u}_\infty}{\bar{u}} [u_\infty(i+1, k) - u_\infty(i, k) + u_\infty(i+1, k-1) - u_\infty(i, k-1)] \\ & + \frac{\bar{w}_\infty \Delta x}{\bar{u} \Delta z} [u_\infty(i+1, k) + u_\infty(i, k) - u_\infty(i+1, k-1) - u_\infty(i, k-1)] \end{aligned} \quad (3.33a)$$

z-momentum

$$\begin{aligned}
& (-r_2 - s_2)w(i+1, j-1, k) + (r_1 - s_1) w(i+1, j+1, k) \\
& + (1 + r_2 - r_1 + s_2 + s_1 + t)w(i+1, j, k) + (-r_2 - s_4)w(i, j-1, k) \\
& + (r_1 - s_3)w(i, j+1, k) + (-1 + r_2 - r_1 + s_4 + s_3 + t)w(i, j, k) \\
& + (-r_2 - s_6)w(i+1, j-1, k-1) + (r_1 - s_5)w(i+1, j+1, k-1) \\
& + (1 + r_2 - r_1 + s_6 + s_5 - t)w(i+1, j, k-1) + (-r_2 - s_8)w(i, j-1, k-1) \\
& + (r_1 - s_7)w(i, j+1, k-1) + (-1 + r_2 - r_1 + s_8 + s_7 - t)w(i, j, k-1) \\
& = \frac{\bar{u}_\infty}{u} [w_\infty(i+1, k) - w_\infty(i, k) + w_\infty(i+1, k-1) - w_\infty(i, k-1)] \\
& + \frac{\bar{w}_\infty \Delta X}{u \Delta z} [w_\infty(i+1, k) - w_\infty(i+1, k-1) + w_\infty(i, k) - w_\infty(i, k-1)] \quad (3.33b)
\end{aligned}$$

The definition of $A'(j)$ and $C'(j)$ are retained (see Eqs. 3.25a and 3.25d) and the additional variables $S'_3(j)$, $S'_4(j)$, $D'_3(j)$ and $D'_4(j)$ were defined to cast the equations of motion into the general tridiagonal form.

$$S'_3(j) = S'_4(j) = r_2 - r_1 + s_2 + s_1 + t + 1 \quad (3.34a)$$

$$D'_3(j) = \frac{\bar{u}_\infty}{u} [u_\infty(i+1, k) - u_\infty(i, k) + u_\infty(i+1, k-1) - u_\infty(i, k-1)]$$

$$+ \frac{\bar{w}_\infty \Delta X}{u \Delta z} [u_\infty(i+1, k) - u_\infty(i+1, k-1) + u_\infty(i, k) - u_\infty(i, k-1)]$$

$$- \{ (-r_2 - s_4) u(i, j-1, k) + (r_1 - s_3) u(i, j+1, k) \}$$

$$+ (-1 + r_2 - r_1 + s_4 + s_3 + t)u(i, j, k) + (-r_2 - s_6)u(i+1, j-1, k-1)$$

$$+ (r_1 - s_5)u(i+1, j+1, k-1) + (1 + r_2 - r_1 + s_6 + s_5 - t) u(i+1, j, k-1)$$

$$+ (-r_2 - s_8)u(i, j-1, k-1) + (r_1 - s_7)u(i, j+1, k-1)$$

$$+ (-1 + r_2 - r_1 + s_8 + s_7 - t)u(i, j, k-1) \quad (3.34b)$$

$$\begin{aligned}
D'_4(j) &= \frac{\bar{u}_\infty}{u} [w_\infty(i+1,k) - w_\infty(i,k) + w_\infty(i+1,k-1) - w_\infty(i,k-1)] \\
&+ \frac{\bar{w}_\infty \Delta x}{u \Delta z} [w_\infty(i+1,k) - w_\infty(i+1,k-1) + w_\infty(i,k) - w_\infty(i,k-1)] \\
&- \{(-r_2 - s_4)w(i,j-1,k) + (r_1 - s_3)w(i,j+1,k) \\
&+ (-1 + r_2 - r_1 + s_4 + s_3 + t)w(i,j,k) + (-r_2 - s_6)w(i+1,j-1,k-1) \\
&+ (r_1 - s_5)w(i+1,j+1,k-1) + (1 + r_2 - r_1 + s_6 + s_5 - t)w(i+1,j,k-1) \\
&+ (-r_2 - s_8)w(i,j-1,k-1) + (r_1 - s_7)w(i,j+1,k-1) \\
&+ (-1 + r_2 - r_1 + s_8 + s_7 - t)w(i,j,k-1)\} \tag{3.34c}
\end{aligned}$$

Thus the momentum equations are written as

x-momentum

$$\begin{aligned}
A'(j)u(i+1,j-1,k) + S'_3(j)u(i+1,j,k) \\
+ C'(j)u(i+1,j+1,k) = D'_3(j) \quad j = 2,3, \dots n \tag{3.35a}
\end{aligned}$$

z-momentum

$$\begin{aligned}
A'(j)w(i+1,j-1,k) + S'_4(j)w(i+1,j,k) \\
+ C'(j)w(i+1,j+1,k) = D'_4(j) \quad j = 2,3, \dots n \tag{3.35b}
\end{aligned}$$

Equations 3.35 are the final form of the momentum equations that are solved in the three-dimensional turbulent boundary layer problem posed in this investigation.

Again an adequate finite difference representation of the continuity equation had to be formulated to complete the set of governing equations. Analogous to the two-dimensional problem formulation, two methods of approximating the continuity equation are proposed.

The first method consists of writing the derivatives about the point $(i+1, j-\frac{1}{2}, k)$ in Fig. 3.2, similar to method I presented for the two-dimensional problem.

$$v_y = \frac{v(i+1, j, k) - v(i+1, j-1, k)}{\Delta y_-} - \frac{1}{24} (v)_{yyy} (\Delta y_-)^2 \quad (3.36a)$$

$$u_x = \frac{1}{2\Delta x} \{u(i+1, j, k) - u(i, j, k) + u(i+1, j-1, k) - u(i, j-1, k)\} \\ + \frac{1}{2} (u)_{xx} (\Delta x) \quad (3.36b)$$

$$w_z = \frac{1}{2\Delta z} \{w(i+1, j, k) - w(i+1, j, k-1) + w(i+1, j-1, k) - w(i+1, j-1, k-1)\} \\ + \frac{1}{2} (w)_{zz} (\Delta z) \quad (3.36c)$$

With Eqs. 3.36, the finite difference approximation for Eq. 3.10c becomes

Method I

$$v(i+1, j+1, k) = v(i+1, j-1, k) - \frac{\Delta y_-}{2\Delta x} \{u(i+1, j, k) \\ - u(i, j, k) + u(i+1, j-1, k) - u(i, j-1, k)\} \\ - \frac{\Delta y_-}{2\Delta z} \{w(i+1, j, k) - w(i+1, j, k-1) \\ + w(i+1, j-1, k) - w(i+1, j-1, k-1)\} \quad (3.37)$$

The second method expresses the derivative approximations about the point $(i+\frac{1}{2}, j-\frac{1}{2}, k-\frac{1}{2})$ in Fig. 3.2. The resultant finite differences are

$$\begin{aligned}
u_x &= \frac{1}{4\Delta x} [u(i+1,j,k) - u(i,j,k) + u(i+1,j,k-1) - u(i,j,k-1) \\
&+ u(i+1,j-1,k) - u(i,j-1,k) + u(i+1,j-1,k-1) - u(i,j-1,k-1)] \\
&- \frac{1}{24} (u)_{xxx} (\Delta x)^2 - \frac{1}{8} (u)_{xyy} (\Delta y_-)^2 - \frac{1}{8} (u)_{xzz} (\Delta z)^2
\end{aligned} \tag{3.38a}$$

$$\begin{aligned}
v_y &= \frac{1}{4\Delta y_-} [v(i+1,j,k) - v(i+1,j-1,k) + v(i,j,k) - v(i,j-1,k) \\
&+ v(i+1,j,k-1) - v(i+1,j-1,k-1) + v(i,j,k-1) - v(i,j-1,k-1)] \\
&- \frac{1}{8} (v)_{xxy} (\Delta x)^2 - \frac{1}{8} (v)_{yzz} (\Delta z)^2 - \frac{1}{24} (v)_{yyy} (\Delta y_-)^2
\end{aligned} \tag{3.38b}$$

$$\begin{aligned}
w_z &= \frac{1}{4\Delta z} [w(i+1,j,k) - w(i+1,j,k-1) + w(i+1,j-1,k) - w(i+1,j-1,k-1) \\
&+ w(i,j,k) - w(i,j,k-1) + w(i,j-1,k) - w(i,j-1,k-1)] \\
&- \frac{1}{8} (w)_{zyy} (\Delta y_-)^2 - \frac{1}{8} (w)_{xxz} (\Delta x)^2 - \frac{1}{24} (w)_{zzz} (\Delta z)^2
\end{aligned} \tag{3.38c}$$

The resultant continuity expression is shown below for this set of finite difference approximations.

Method II

$$\begin{aligned}
v(i+1,j,k) &= v(i+1,j-1,k) + v(i+1,j-1,k-1) + v(i,j-1,k) \\
&+ v(i,j-1,k-1) - v(i+1,j,k-1) - v(i,j,k) - v(i,j,k-1) \\
&- \frac{\Delta y_-}{\Delta x} [u(i+1,j,k) - u(i,j,k) + u(i+1,j-1,k) - u(i,j-1,k) \\
&+ u(i+1,j,k-1) - u(i,j,k-1) + u(i+1,j-1,k-1) - u(i,j-1,k-1)] \\
&- \frac{\Delta y_-}{\Delta z} [w(i+1,j,k) - w(i+1,j,k-1) + w(i+1,j-1,k) - w(i+1,j-1,k-1) \\
&+ w(i,j,k) - w(i,j,k-1) + w(i,j-1,k) - w(i,j-1,k-1)]
\end{aligned} \tag{3.39}$$

Equations 3.37 and 3.39 constitute the proposed forms of the continuity equation to be used in the three-dimensional turbulent boundary-layer flow solution. A discussion as to the final choice

of form will be found in a later section of this chapter.

Finally, the consequences of the linearization technique used to develop the tridiagonal finite difference forms of the equations of motion will also be discussed in a later section of this chapter.

D. Generation of Boundary Conditions and Initial Conditions

Two three-dimensional flow geometries were investigated numerically and the results were compared to the corresponding experimental data presented by Johnston [28] and Hornung and Joubert [29]. Johnston's experimental apparatus consisted of a rectangular inlet duct from which the issuing jet impinged on an end wall 48 in. from the outlet of the channel. The jet was confined on the top and bottom by flat surfaces, and the boundary layer which developed on the floor of the test section was probed. A schematic of this geometry is shown in Fig. 3.3. Hornung and Joubert experimentally investigated the boundary layer growth on the floor of the large test section in which a vertical airfoil with a cylindrical front was placed perpendicular to the flow direction as shown in Fig. 3.4. The lead-in section was about 17 ft from the center of the cylinder and the channel was slightly divergent.

The initial condition and boundary conditions were generated in the same manner for both three-dimensional geometries as described below.

- (1) A two-dimensional zero pressure gradient turbulent boundary layer was developed from the leading edge of a flat plate with the following initial conditions as prescribed by Wu [38]

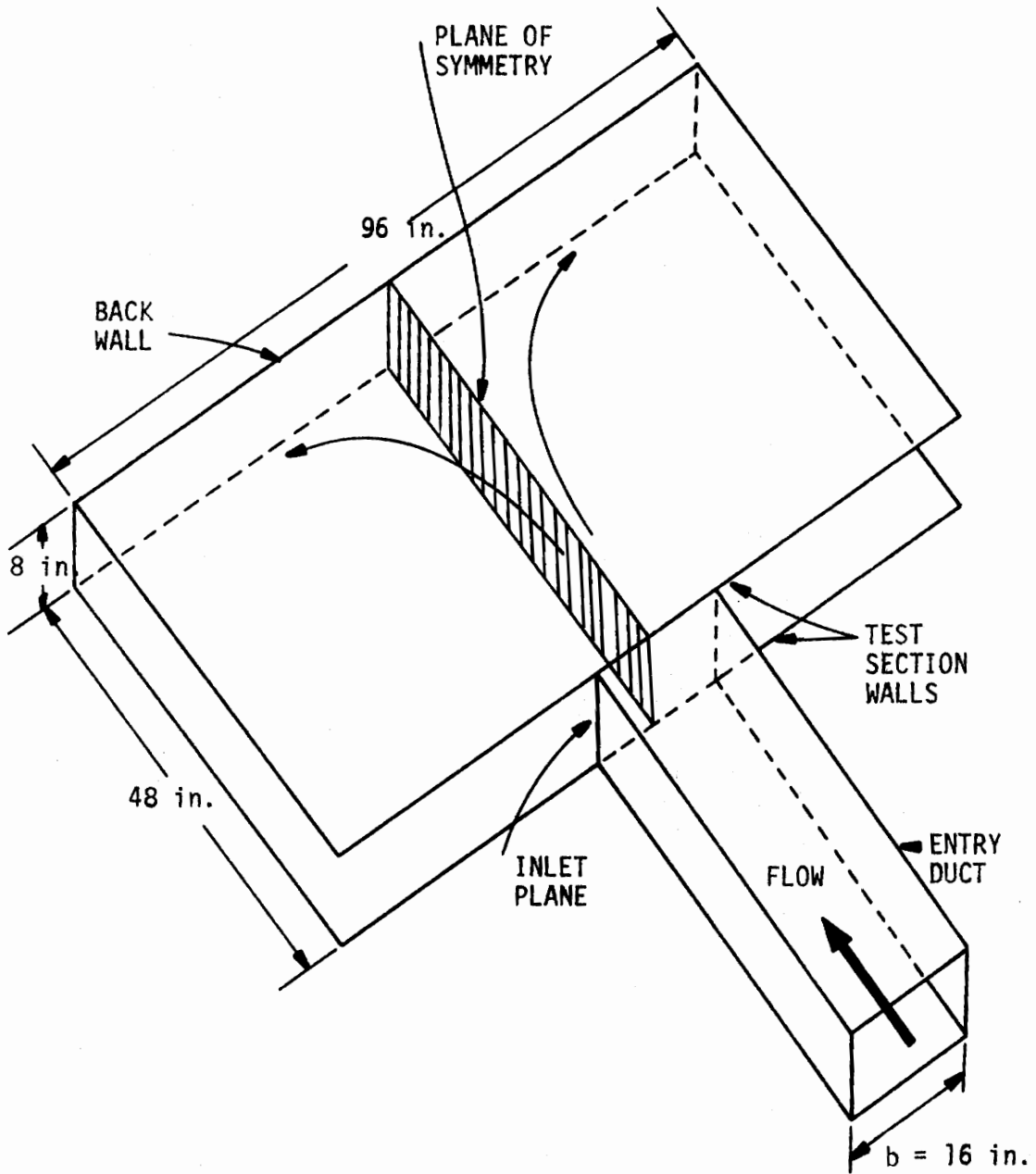


Fig. 3.3 Schematic Drawing of Johnston's Test Geometry.

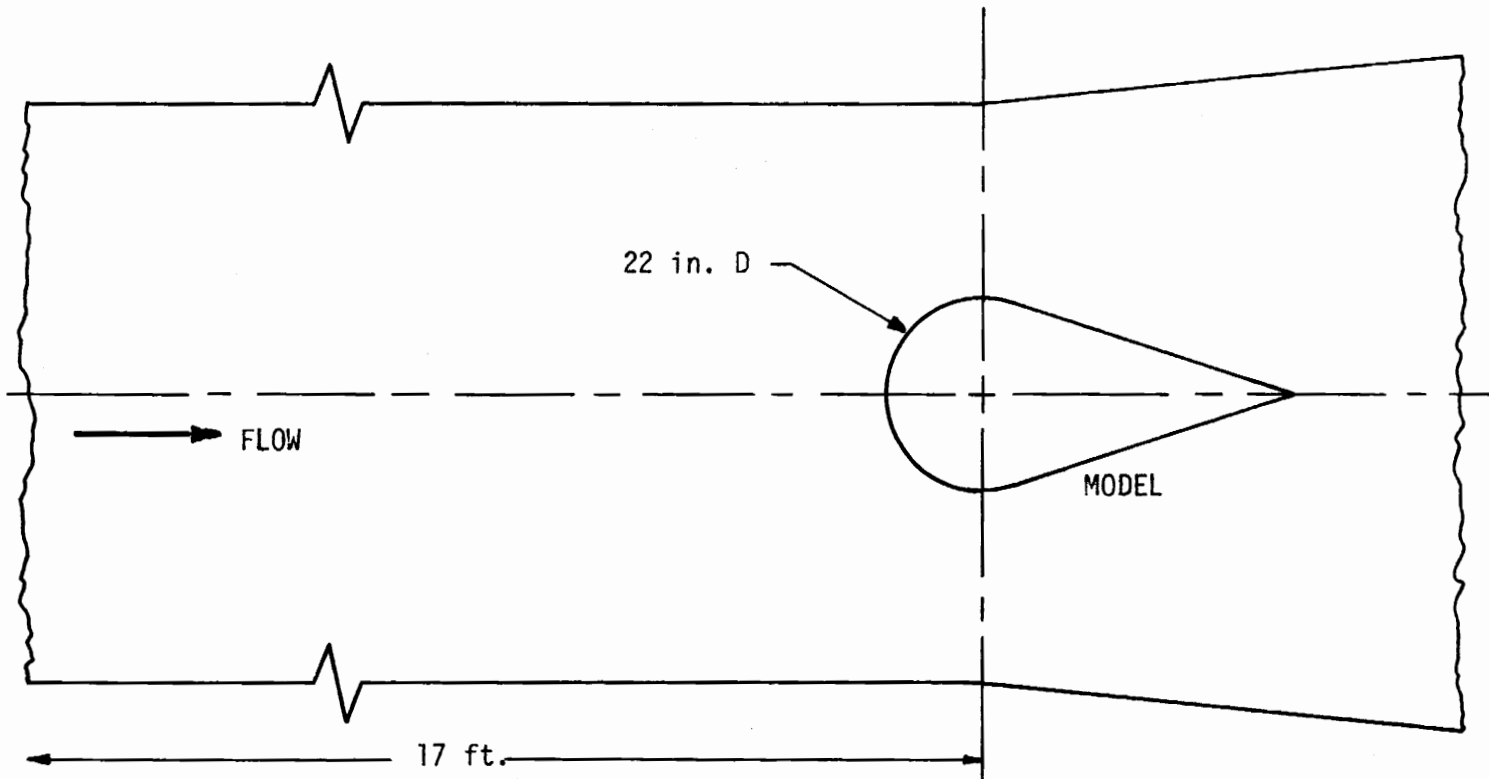


Fig. 3.4 Schematic Drawing of Hornung and Joubert's Test Geometry.

$$u(o,y,z) = u_{\infty}(o,z) \quad (3.40a)$$

$$v(o,y,z) = w(o,y,z) = wz(o,y,z) = 0 \quad (3.40b)$$

$$u(x,o,z) = v(x,o,z) = w(x,o,z) = wz(x,o,z) = 0 \quad (3.40c)$$

$$u(x,\delta,z) = u_{\infty}(x,\delta,z) \quad (3.40d)$$

$$w(x,\delta,o) = wz(x,\delta,o) = 0 \quad (3.40e)$$

This procedure could be modified for pressure gradient flows if the pressure gradient of the inlet channel were known.

However, for the cases studied either the pressure gradient was nearly zero (Johnston's experiment) or it was not specified (Hornung and Joubert's experiment).

(2) At some distance down the flat plate the plane of symmetry solution was initiated using the previously determined two-dimensional profile. To proceed from this point the pressure gradient was prescribed by the potential flow solution for the given geometry.

(3) The plane of symmetry solution was continued until a match point was reached where the resultant solution was compared to the available experimental data.

(4) The lengths of the two-dimensional solution and the plane-of-symmetry solution were adjusted appropriately and steps (1), (2), and (3) were repeated until the desired fit was obtained. For the Johnston geometry the match point was at station D-8 as shown in Fig. 3.5. This point also corresponded to the location at which the plane of symmetry solution was started, since this match point was in a

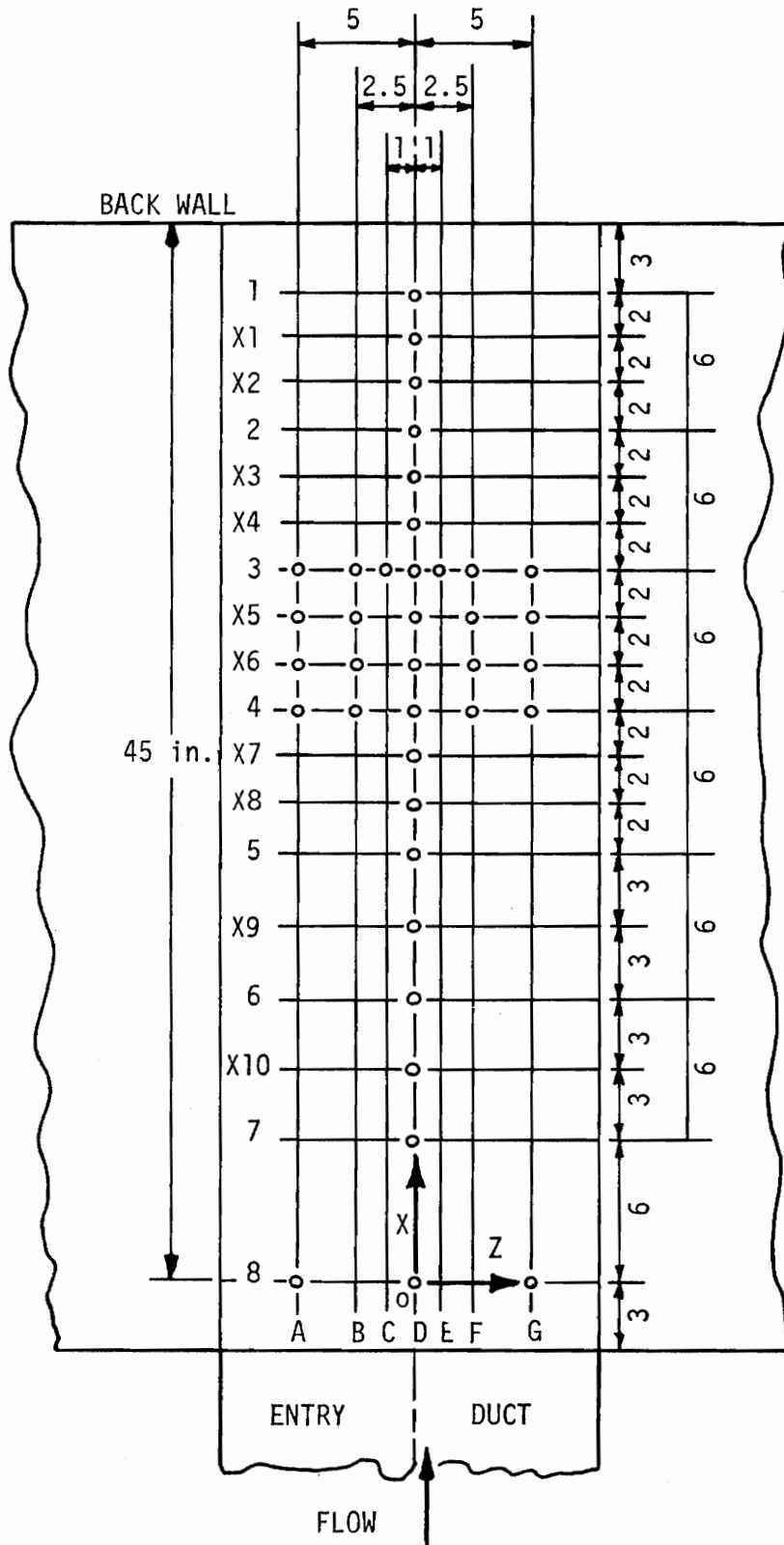


Fig. 3.5 Experimental Station Locations for Johnston's Test Geometry.

region far enough from the end wall so that a fully two-dimensional profile could be assumed. For the Hornung and Joubert geometry (see Fig. 3.6) the match point corresponded to station 10 at which there were strong three-dimensional effects. Thus, the plane of symmetry solution had to be initiated at some point upstream where the three-dimensional effects were negligible.

(5) After an adequate fit was obtained by steps (1) - (4) at the match point, the complete three-dimensional solution was obtained where the appropriate two-dimensional profile was used as the x-direction initial condition, and the plane of symmetry solution was generated simultaneously to provide the initial conditions in the z-direction for the full three-dimensional solution.

Two modifications were introduced when beginning the full three-dimensional solution. Instead of assuming w and wz equal to zero as provided by the two-dimensional solution, these quantities were assumed to have the corresponding free-stream values which were considered to more accurately represent these profiles. Also, the u -profile was proportionally weighted along the $X=0$ plane to insure that the resultant profiles matched at the boundary layer edge with the potential flow solution off the plane of symmetry. This procedure did, however, retain the general shape of the profile off the plane of symmetry when compared to the profile on the plane of symmetry at the match point.

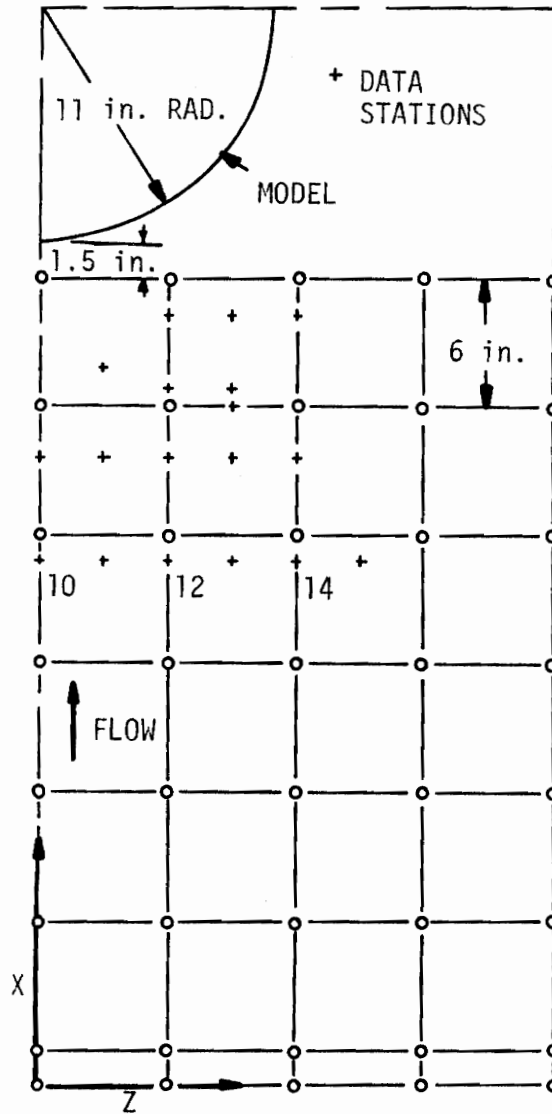


Fig. 3.6 Experimental Station Locations for Hornung and Joubert's Test Geometry.

Certain circumstances can occur for which the assumption of a zero pressure gradient inlet section may have questionable validity. Thus, the program was sufficiently generalized to allow a profile to be read in to initiate either a two- or three-dimensional solution. These input profiles can be obtained from a variety of sources such as a known analytical solution, experimental correlations typified by the wall-wake formulation [39], curve fits to experimental data, or a two-dimensional pressure gradient solution previously obtained from the program itself.

As mentioned previously the pressure gradients were generated for the three-dimensional flow solution from potential flow theory. Milne-Thompson [40] and Pai [41] have detailed derivations for the impinging jets problem which are applicable to the Johnston geometry. Their results were non-dimensionalized as set forth in Eq. 3.9, where Q_0 was equal to the velocity of the jet and b was equal to the width of the jet at an infinite distance from the end wall. The resultant equations are

$$F = 0 = -\pi \left(x - \frac{A^*}{b}\right) - \frac{1}{2} \ln \left[\frac{(1+u_\infty)^2 + w_\infty^2}{(1-u_\infty)^2 + w_\infty^2} \right] - \frac{1}{2} \tan^{-1} \frac{2u_\infty}{1-u_\infty^2 - w_\infty^2} \quad (3.41a)$$

$$G = 0 = -\pi z - \frac{1}{2} \ln \left[\frac{(1-w_\infty)^2 + u_\infty^2}{(1+w_\infty)^2 + u_\infty^2} \right] + \frac{1}{2} \tan^{-1} \frac{2w_\infty}{1-u_\infty^2 - w_\infty^2} \quad (3.41b)$$

where A^* is a convenient distance that the origin was shifted along the x axis. Equation 3.41b was differentiated with respect to z and the following expression was obtained for wz on the plane of symmetry

$$wz = \frac{\pi}{4} [1 - u_\infty^4] \quad (3.41c)$$

Unfortunately, u_∞ and w_∞ could not be expressed explicitly in terms of x and z . Thus, an extension of the Newton-Raphson method (see Traub [42])

was used to solve the simultaneous equations for u_∞ and w_∞ at each x and z location. The potential flow solution for Hornung and Joubert's geometry was taken as that of a uniform flow approaching a right circular cylinder. The expressions for the velocities were non-dimensionalized such that Q_0 was the velocity of the uniform stream at an infinite distance from the cylinder and b was equal to the radius of the cylinder. Again A^* shifted the origin along the x axis.

$$u_\infty = 1 - \frac{\left(\frac{A^*}{b} - x\right)^2 - z^2}{\left[\left(\frac{A^*}{b} - x\right)^2 + z^2\right]^2} \quad (3.42a)$$

$$w_\infty = 2\left(\frac{A^*}{b} - x\right) z \frac{1}{\left[\left(\frac{A^*}{b} - x\right)^2 + z^2\right]^2} \quad (3.42b)$$

and on the plane of symmetry

$$wz = \frac{2}{\left(\frac{A^*}{b} - x\right)^3} \quad (3.42c)$$

E. Solution Technique

Equations 3.26 and 3.35 can be represented in a general tridiagonal system of $n - 1$ equations in the form

$$S'_i(2)H(2) + C'(2)H(3) = D''_i(2) \quad (3.43a)$$

$$A'(j)H(j-1) + S'_i(j)H(j) + C'(j)H(j+1) = D''_i(j) \quad j = 3, 4, \dots, n-1 \quad (3.43b)$$

$$A'(n)H(n-1) + S'_i(n) = D''_i(n) \quad (3.43c)$$

for $i = 1, 2, 3, 4$ depending on the desired equation of motion to be solved, and $H(j)$ is a dummy variable which correspondingly becomes

$u(i+1,j,k)$, $wz(i+1,j,k)$ $u(i+1,j,k)$ or $w(i+1,j,k)$.

The variable $D_i''(j)$ is introduced to more clearly show the nature of the tridiagonal scheme $D_i''(j)$ can be related to $D_i'(j)$ as follows

$$D_i''(2) = D_i'(2) - A(2)H(1) \quad (3.44a)$$

$$D_i''(j) = D_i'(j) \quad j = 3, 4, \dots, n-1 \quad (3.44b)$$

$$D_i''(n) = D_i'(n) - A(n)H(n+1) \quad (3.44c)$$

where the following equivalences are applied

$$u_{\infty}(i,k) = u(i,n+1,k)$$

$$w_{\infty}(i,k) = w(i,n+1,k)$$

$$wz_{\infty}(i,k) = wz(i,n+1,k)$$

Ames [31] outlines the use of the Thomas algorithm and a similar procedure is used in this investigation. To begin the solution, a Gaussian elimination was applied to Eqs. 3.43 to transform the matrix into an upper bidiagonal form.

$$H(2) + E_i(2)H(3) = F_i(2) \quad (3.45a)$$

$$H(j) + E_i(j)H(j+1) = F_i(j) \quad j = 3, 4, \dots, n-1 \quad (3.45b)$$

$$H(n) = F_i(n) \quad (3.45c)$$

for $i = 1, 2, 3, 4$ and the coefficients $E_i(j)$ and $F_i(j)$ were calculated using the following recurrence formulae

$$E_i(2) = \frac{C_i'(2)}{S_i'(2)} \quad (3.46a)$$

$$F_i(2) = \frac{D_i''(2)}{S_i'(2)} \quad (3.46b)$$

$$E_i(j) = \frac{C'(j)}{S'_i(j) - A'(j) E_i(j-1)} \quad j = 3,4 \dots n \quad (3.46c)$$

$$F_i(j) = \frac{D''_i(j) - A'(j)F_i(j-1)}{S'_i(j) - A'(j)E_i(j-1)} \quad j = 3,4 \dots n \quad (3.46d)$$

where $C'(n) = 0$ by Eq. 3.43c. From Eq. 3.45c, $H(n)$ was determined and by successive substitutions into Eq. 3.47 below the remaining values of $H(j)$ were obtained.

$$H(j) = F_i(j) - E_i(j) H(j+1) \quad j = n-1, n-2 \dots 2 \quad (3.47)$$

This method of solution was far superior to matrix inversion techniques because of the great reduction in the number of calculations necessary to solve the large system of equations.

When the finite difference equations were developed, the quantities \bar{u} , \bar{v} , \bar{w} , \bar{wz} , $\epsilon_m(i+1, j+\frac{1}{2}, k)$ and $\epsilon_m(i+1, j-\frac{1}{2}, k)$ were assumed to be known in order to linearize the equations. Since all of the quantities are functions of the variables to be determined at the new location an iterative procedure had to be followed when solving the finite difference equations at each new x and z location.

- i) The velocity profiles at station (i, j, k) were projected forward to station $(i+1, j, k)$ for all j and k .
- ii) The finite difference equations were solved and a first approximation to the desired velocity profiles was obtained at station $(i+1, j, k)$ for each j .
- iii) The results of step (ii) were used to generate new coefficients for the finite difference equations.
- iv) Steps (ii) and (iii) were repeated to provide a second

approximation as suggested by Flügge-Lotz and Blottner [25].

- v) Steps (ii) through (iv) were then repeated for all values of k .
- vi) Steps (i) through (v) were finally repeated for each x step.

To minimize the number of equations to be solved, the number of grid locations in the y -direction was increased as the boundary layer grew.

Convergence to the solution was determined to be a function of both the step size and the number of iterations at each location. The number of iterations was set at two as suggested by Flügge-Lotz and Blottner [25], and therefore only the step size affected the results. The effects of the variable grid spacing will be demonstrated in the next chapter.

F. The Continuity Equation

Except for the case when a known analytical solution can be used as initial conditions, the input v -velocity profile is generally unknown. Because of the boundary layer approximations, the leading edge of a surface over which the boundary layer grows is singular in that a simple analysis shows that the v component of velocity should be infinite. However, from the physical viewpoint this value is unrealistic. In reality the v -velocity should be some small value and for lack of any other value it was assumed to be equal to zero as described earlier.

Consider a two-dimensional boundary-layer flow which is subjected to a mildly favorable pressure gradient, a zero pressure gradient, or an adverse pressure gradient. An initial preference of the method II continuity equation is obvious because of the smaller truncation error when compared to method I. However, a simple analysis shows that this continuity equation may give rise to large oscillations of the v-velocity profile. Consider the first two x steps away from the initial location and the nearest y location to the wall. From Eq. 3.29b the resultant v-velocities are

$$v(2,2,k) = - \frac{\Delta y}{\Delta x} [u(2,2,k) - u(1,2,k)] \quad (3.48)$$

and

$$v(3,2,k) = - \frac{\Delta y}{\Delta x} [u(3,2,k) - u(2,2,k)] \quad (3.49)$$

These two equations are combined to yield

$$v(3,2,k) = - \frac{\Delta y}{\Delta x} [(u(1,2,k) - u(2,2,k)) - (u(2,2,k) - u(3,2,k))] \quad (3.50)$$

Since the derivative of u with respect to x is a decreasing function for these circumstances, the quantity, $u(1,2,k) - u(2,2,k)$, is larger than the quantity, $u(2,2,k) - u(3,2,k)$. Thus, the v component of velocity becomes negative at the second step while it is positive at the first step. This oscillation can also be shown to continue further downstream. Several short computer runs were made to determine whether the solution would eventually converge with this initial oscillation. Unfortunately, the results diverged and eventually gave unacceptable answers. Thus, method I (with the corresponding truncation errors being larger than

method II) had to be used for the continuity equation in two-dimensional flow circumstances when the v-velocity was unknown at the inlet.

A similar result can also be shown to exist for three-dimensional flows when method II was used.

Thus, for both two-dimensional and three-dimensional flows, the corresponding method I was used for all calculations presented in this investigation. With this procedure the truncation errors in the continuity equation could be large in regions of large pressure gradients which may necessitate the use of smaller step sizes than would in principle be possible with the method II continuity equations.

G. Stability and Convergence

No general method exists for the determination of stability and convergence of simultaneous non-linear finite difference equations. However, with several reasonable assumptions an extension of the existing methods for single and simultaneous linear finite difference equations can be made to analyze the finite difference equations presented in this investigation.

To show convergence of the solution of the finite difference equations to that of the partial differential equations one must show both consistency and stability of the difference equations according to Lax's equivalence theorem [43]:

"Given a properly posed initial value problem and a finite-difference approximation to it that satisfies the consistency condition, stability is the necessary and sufficient condition for convergence."

Since the two-dimensional and three-dimensional equations were derived and expressed in a similar manner it is sufficient to investigate in detail only the three-dimensional equations for convergence, with the two-dimensional equations a simplification of the three-dimensional case. However, these equations are non-linear and stability criteria are generally formulated for linear equations. Thus, the assumption was made that the stability requirements for the quasi-linear finite difference equations presented in this investigation are identical to the requirements for the actual non-linear finite-difference equations. This assumption is generally referred to as a "local" stability requirement.

The consistency of the finite difference equations can be easily obtained by the following procedure. Substitute Eqs. 3.30 into Eqs. 3.10 neglecting the higher order terms, again assuming that the various coefficients are linear in Eqs. 3.10. Expand each nodal velocity in a Taylor series about the point $(i+\frac{1}{2}, j, k-\frac{1}{2})$ and substitute this result into the expression obtained in the previous step. From this equation subtract the original differential equation. The difference between these two will give the truncation error, which should approach zero as Δx , Δy , and Δz approach zero uniformly in the limit. Using this procedure the truncation error was determined:

1) for the x-momentum equation as

$$\begin{aligned} TE_x = & O(\Delta x)^2 + O(\Delta z)^2 + O(\Delta y_+ - \Delta y_-) \\ & + O(\Delta y_+)^2 + O(\Delta y_-)^2 + O(\Delta y_+ \Delta y_-) \end{aligned}$$

2) for the z-momentum equation as

$$\begin{aligned} TE_z &= O(\Delta x)^2 + O(\Delta z)^2 + O(\Delta y_+ - \Delta y_-) \\ &+ O(\Delta y_+)^2 + O(\Delta y_-)^2 \\ &+ O(\Delta y_+ \Delta y_-) \end{aligned}$$

3) and for the continuity equation as

$$TE_c = O(\Delta x) + O(\Delta y_+)^2 + O(\Delta z)$$

where the notation $O(\Delta x)$ means "of order Δx " and the actual forms of the error terms are equivalent to those introduced in Eqs. 3.21, 3.27, 3.28, 3.30, 3.36 and 3.38. This formulation further imposed the condition that the velocities and eddy viscosity were many-fold differentiable with respect to x , y and z . Since this latter restriction is fulfilled, the truncation error goes to zero as Δx , Δy and Δz go to zero, and thus, the consistency requirement is satisfied.

The second requirement was that of stability. East [27] applied the von Neumann stability criteria [43] to his three-dimensional explicit finite-difference equations. A procedure similar to his was incorporated for the present investigation. However, one major departure of East's technique was necessary in the formulation of the growth terms for the error velocity introduced in the derivation. East allowed a periodic variation of the error in the z direction of the form $\exp [(-1)^{\frac{1}{2}} k_y \Delta z]$. However, this form is properly applicable for the case where a boundary-value problem exists in the z -coordinate direction. For the present investigation, with an initial-value problem existing in both the x and z directions, the growth of any computer error should be of an exponential

nature in both directions as discussed in [43] for initial value problems.

To obtain the stability criteria only the x-momentum equation was considered since the z-momentum equation was of exactly the same form and yields identical results.

Because of the complexity of the finite difference equations the assumption is made that the eddy viscosity is a function of only the y coordinate. This assumption implies a priori that the change of the eddy viscosity with x and z does not affect the stability of the equations. However, the assumption seems to be reasonable for small grid spacing since the stability analysis is concerned only with the case when step sizes in the initial value problem approach zero [43]. With this assumption, the following relations follow to simplify the coefficients in Eq. 3.33a.

$$s_1 = s_3 = s_5 = s_7 \quad (3.52a)$$

and

$$s_2 = s_4 = s_6 = s_8 \quad (3.52b)$$

Using Eqs. 3.52, Eq. 3.33a becomes

$$\begin{aligned} & (-r_2 - s_2)u(i+1, j-1, k) + (r_1 - s_1)u(i+1, j+1, k) \\ & + (1 + r_2 - r_1 + s_2 + s_1 + t)u(i+1, j, k) + (-r_2 - s_2)u(i, j-1, k) \\ & + (r_1 - s_1)u(i, j+1, k) + (-1 + r_2 - r_1 + s_2 + s_1 + t)u(i, j, k) \\ & + (-r_2 - s_2)u(i+1, j-1, k-1) + (r_1 - s_1)u(i+1, j+1, k-1) \\ & + (1 + r_2 - r_1 + s_2 + s_1 - t)u(i+1, j, k-1) + (-r_2 - s_2)u(i, j-1, k-1) \\ & + (r_1 - s_1)u(i, j+1, k-1) + (-1 + r_2 - r_1 + s_2 + s_1 - t)u(i, j, k-1) \end{aligned}$$

$$\begin{aligned}
&= \frac{\bar{u}_\infty}{\bar{u}} [u_\infty(i+1,k) - u_\infty(i,k) + u_\infty(i+1,k-1) - u_\infty(i,k-1)] \\
&+ \frac{\bar{w}_\infty \Delta x}{\bar{u} \Delta z} [u_\infty(i+1,k) + u_\infty(i,k) - u_\infty(i+1,k-1) - u_\infty(i,k-1)] \quad (3.53)
\end{aligned}$$

The exact numerical solution is perturbed to allow for the error introduced by the finite word length of the computer. Thus, $u(i,j,k) + \dot{u}(i,j,k)$ is the assumed actual value obtained from the calculation, and this quantity is also a solution of the finite difference equation to the accuracy of the computer. Thus, Eq. 3.53 is perturbed by the quantity $\dot{u}(i,j,k)$ and Eq. 3.53 is subtracted from the perturbed equation which yields

$$\begin{aligned}
&(-r_2 - s_2) \dot{u}(i+1,j-1,k) + (r_1 - s_1) \dot{u}(i+1,j+1,k) \\
&+ (1 + r_2 - r_1 + s_2 + s_1 + t) \dot{u}(i+1,j,k) + (-r_2 - s_2) \dot{u}(i,j-1,k) \\
&+ (r_1 - s_1) \dot{u}(i,j+1,k) + (-1 + r_2 - r_1 + s_2 + s_1 + t) \dot{u}(i,j,k) \\
&+ (-r_2 - s_2) \dot{u}(i+1,j-1,k-1) + (r_1 - s_1) \dot{u}(i+1,j+1,k-1) \\
&+ (1 + r_2 - r_1 + s_2 + s_1 - t) \dot{u}(i+1,j,k-1) + (-r_2 - s_2) \dot{u}(i,j-1,k-1) \\
&+ (r_1 - s_1) \dot{u}(i,j+1,k-1) + (-1 + r_2 - r_1 + s_2 + s_1 - t) \dot{u}(i,j,k-1) \\
&= 0 \quad (3.54)
\end{aligned}$$

This manipulation used to obtain Eq. 3.54 eliminated the boundary conditions at the free-stream which are assumed to be known exactly, and hence would not generate an unbounded error.

According to the von Neumann stability criterion, the error must be bounded to insure stability. To determine the condition for which Eq. 3.33a is stable the following substitution was made for $\dot{u}(i,j,k)$.

$$\dot{u}(i,j,k) = u_0 \exp [i\alpha\Delta x + (-1)^{\frac{1}{2}} j\beta\Delta y_{\pm} + k\gamma\Delta z] \quad (3.55)$$

where an exponential growth was assumed in both the x and z directions, with a harmonic error in the y direction. Equation 3.55 is substituted into Eq. 3.54 and some simplification gives

$$\begin{aligned} & (\phi + 1 + t + (-1)^{\frac{1}{2}}\theta) \exp(\alpha\Delta x + \gamma\Delta z) (\phi + 1 - t + (-1)^{\frac{1}{2}}\theta) + \exp(\alpha\Delta x) \\ & + (\phi - 1 + t + (-1)^{\frac{1}{2}}\theta) \exp(\gamma\Delta z) + (\phi - 1 - t + (-1)^{\frac{1}{2}}\theta) = 0 \end{aligned} \quad (3.56)$$

where

$$\phi = (r_2 + s_2)(1 - \cos\beta\Delta y_+) - (r_1 - s_1)(1 - \cos\beta\Delta y_-) \quad (3.57a)$$

$$\theta = (r_2 + s_2)\sin\beta\Delta y_+ + (r_1 - s_1)\sin\beta\Delta y_- \quad (3.57b)$$

For the error to be bounded the following conditions must be valid

$$|\exp(\alpha\Delta x)| \leq 1 \quad (3.58)$$

$$|\exp(\gamma\Delta z)| \leq 1 \quad (3.59)$$

Solving for $\exp(\alpha\Delta x)$ in Eq. 3.56 and applying the constraint from

Eq. 3.58 the following relation was derived for $\exp(\gamma\Delta z)$

$$(\phi + t)\exp(2\gamma\Delta z) + 2\phi \exp(\gamma\Delta z) + \phi - t \geq 0 \quad (3.60)$$

for all θ . The exponential term in Eq. 3.60 was determined using the quadratic equation as

$$\exp(\gamma\Delta z) \geq -\frac{\phi \pm t}{\phi + t} \quad (3.61)$$

The second constraint equation was applied to obtain the following condition for stability

$$\phi t \geq 0 \quad (3.62)$$

Since for positive w , t is always greater than or equal to 0, it follows that ϕ must also be greater than or equal to zero. Thus, the following relationship was obtained

$$(r_2 + s_2)(1 - \cos\beta\Delta y_+) - (r_1 - s_1)(1 - \cos\beta\Delta y_-) \geq 0 \quad (3.63)$$

For the case when $\Delta y_+ = \Delta y_-$ the equation reduced to

$$s_2 + s_1 \geq 0. \quad (3.64)$$

Since s_1 and s_2 are always positive, the equations are always stable and therefore convergent.

If $(1 - \cos\beta\Delta y_-)$ is less than $(1 - \cos\beta\Delta y_+)$ then a sufficient condition for stability is for $r_2 + s_2 - r_1 + s_1$ to be greater than zero. On the other hand, if $(1 - \cos\beta\Delta y_+)$ is less than $(1 - \cos\beta\Delta y_-)$ it is necessary for $r_2 + s_2 - r_1 + s_1$ to be greater than zero. To obtain some concept of the dependency of stability on the y grid spacing the result from these two cases was examined.

$$r_2 + s_2 - r_1 + s_1 \geq 0 \quad (3.65)$$

The author realized that a much more stringent stability criterion than Eq. 3.65 may have existed, but some useful results were obtained from Eq. 3.65. Using the definitions of r_1 , r_2 , s_1 , and s_2 shown in Eqs. 3.23, the following relationship was obtained from Eq. 3.65 for the v component of velocity.

$$\bar{v} \geq -2 \left[\frac{[1 + \epsilon_m(i+1, j-\frac{1}{2}, k)]\Delta y_- + [1 + \epsilon_m(i+1, j+\frac{1}{2}, k)]\Delta y_+}{(\Delta y_+)^2 - (\Delta y_-)^2} \right] \quad (3.66)$$

The expression in brackets is always positive, which implies that \bar{v} , at least under some circumstances, must be greater than some finite negative value.

This result partially explains the divergence of the solution when the method II continuity equations are used in conjunction with the zero v initial profile. Apparently the existence of the large oscillation in the v profile produces a large negative value of \bar{v} which subsequently causes the equations to become unstable and divergent.

IV. RESULTS

The primary purpose of this investigation was to develop an efficient finite-difference solution technique for the three-dimensional steady turbulent boundary layer equations for incompressible fluids. Before these results were obtained several short investigations were completed to insure that the program was yielding results consistent with two-dimensional flow theory and experiment.

These test cases included the following flow circumstances:

- i) A laminar two-dimensional boundary-layer with zero pressure gradient,
- ii) A turbulent two-dimensional boundary-layer with zero pressure gradient, and
- iii) A turbulent two-dimensional boundary layer with an adverse pressure gradient.

A complete copy of the computer program used for all the calculations presented in this investigation is given in Appendix A.

A. Laminar Two-Dimensional Solution

The classic Blasius solution for two-dimensional laminar boundary-layer flow over a flat plate was used to initially test the validity of the present numerical method. The results are shown in Figs. 4.1 - 4.5 and show an excellent agreement with the exact solution.

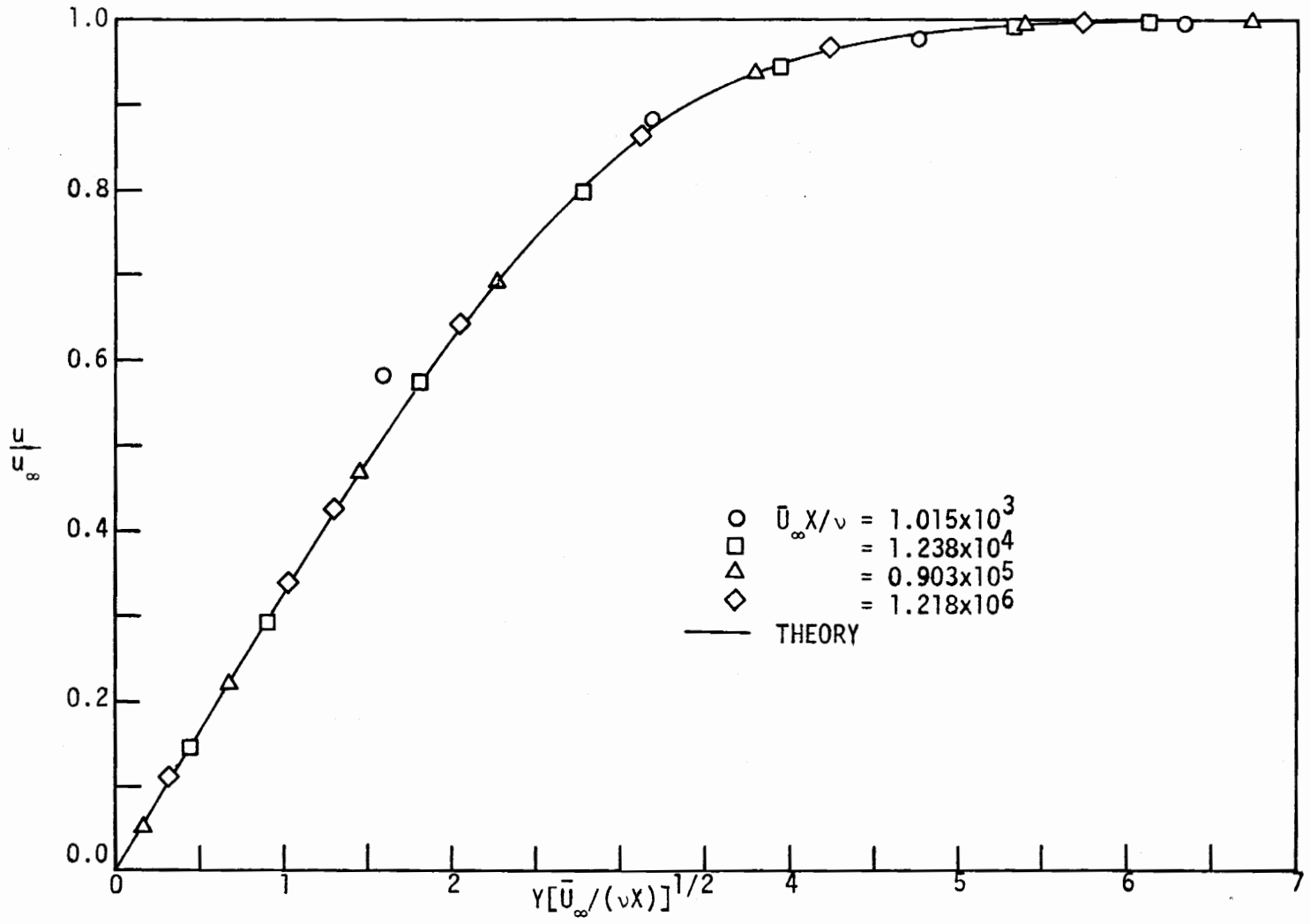


Fig. 4.1 \bar{U} -Velocity Profile Compared with Blasius Solution for $\Delta X = \delta$.

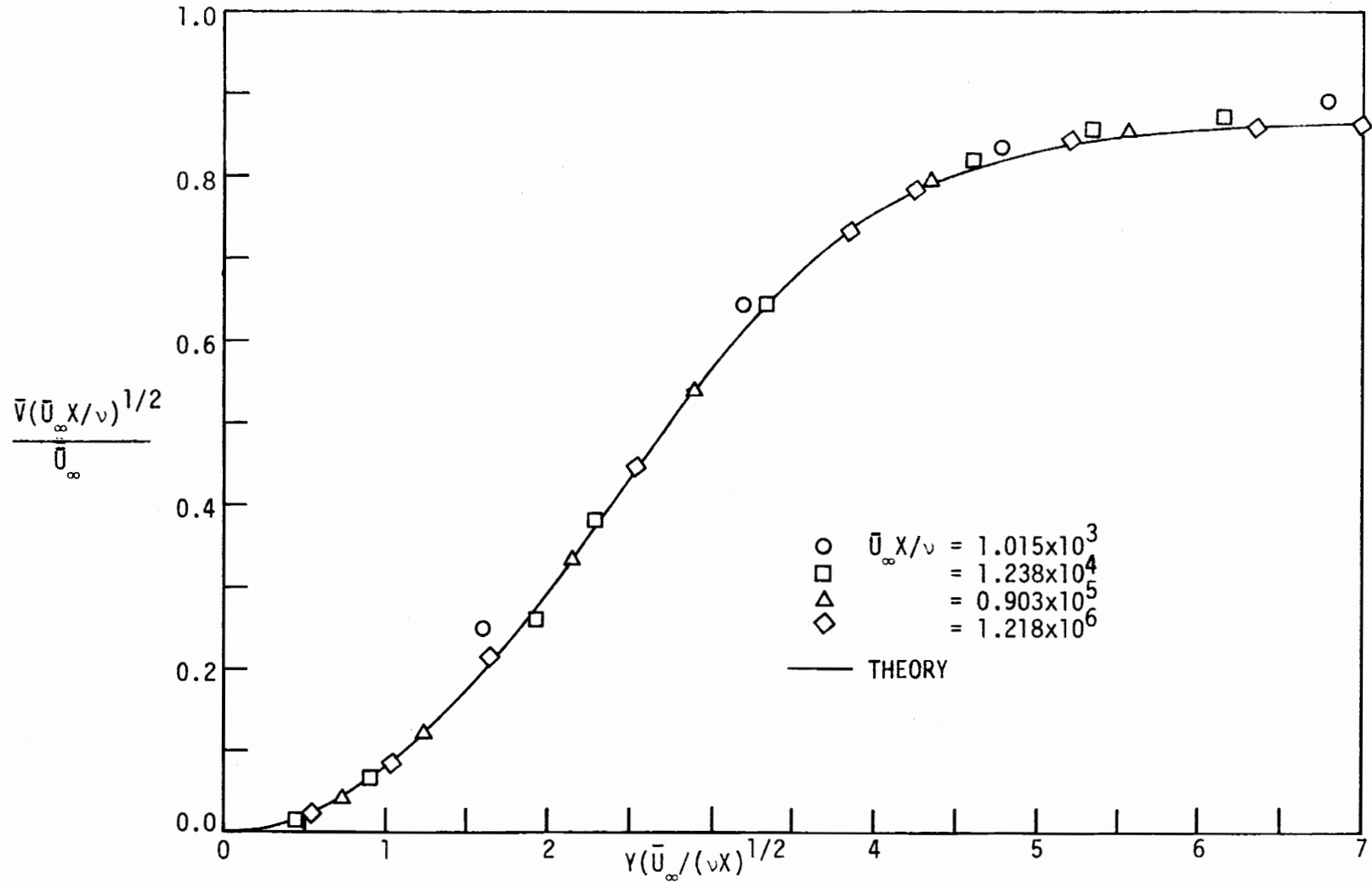


Fig. 4.2 \bar{v} -Velocity Profile Compared with Blasius Solution for $\Delta X = \delta$.

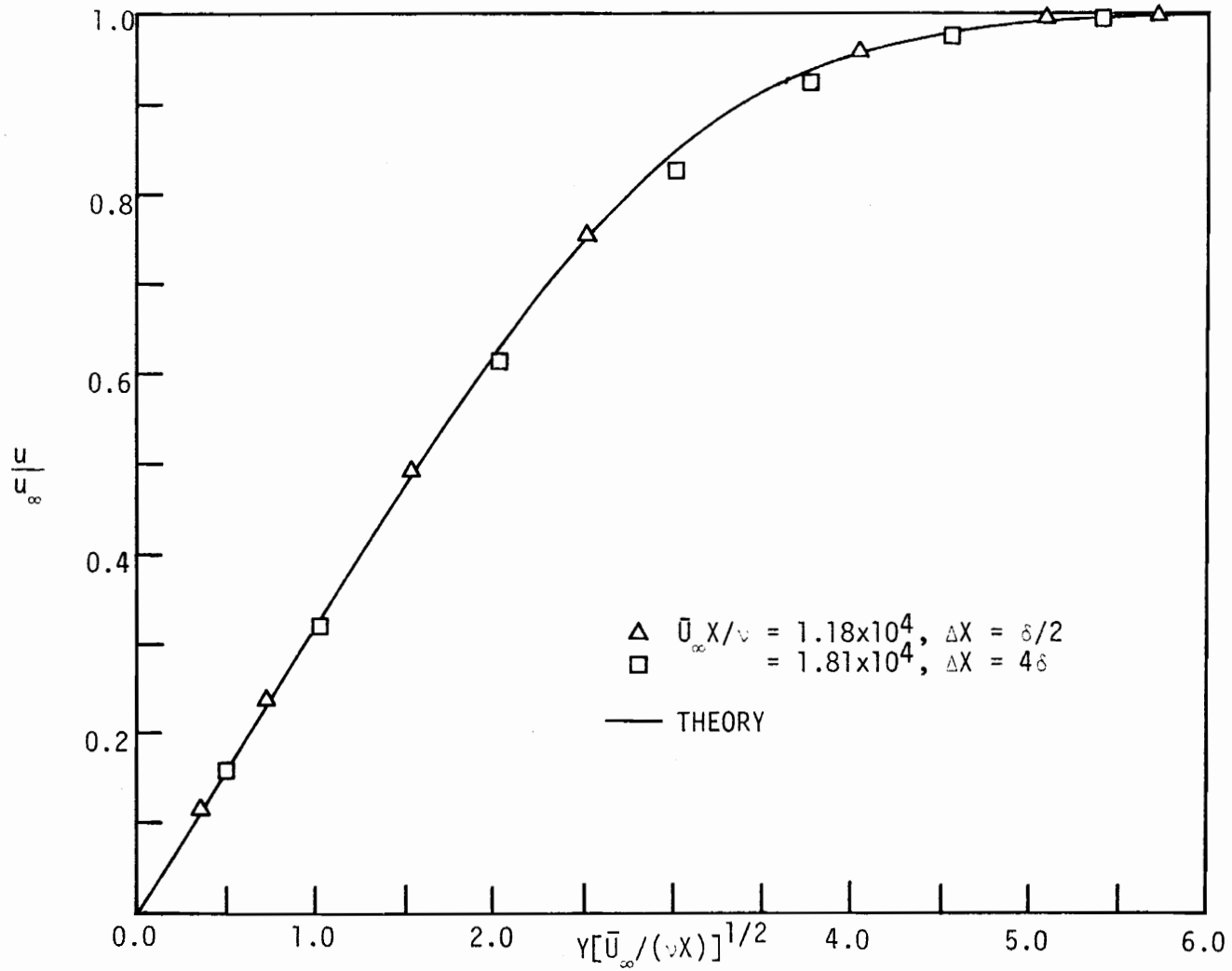


Fig. 4.3 \bar{U} -Velocity Profile Compared with Blasius Solution for $\Delta X = \delta/2$ and $\Delta X = 4\delta$.

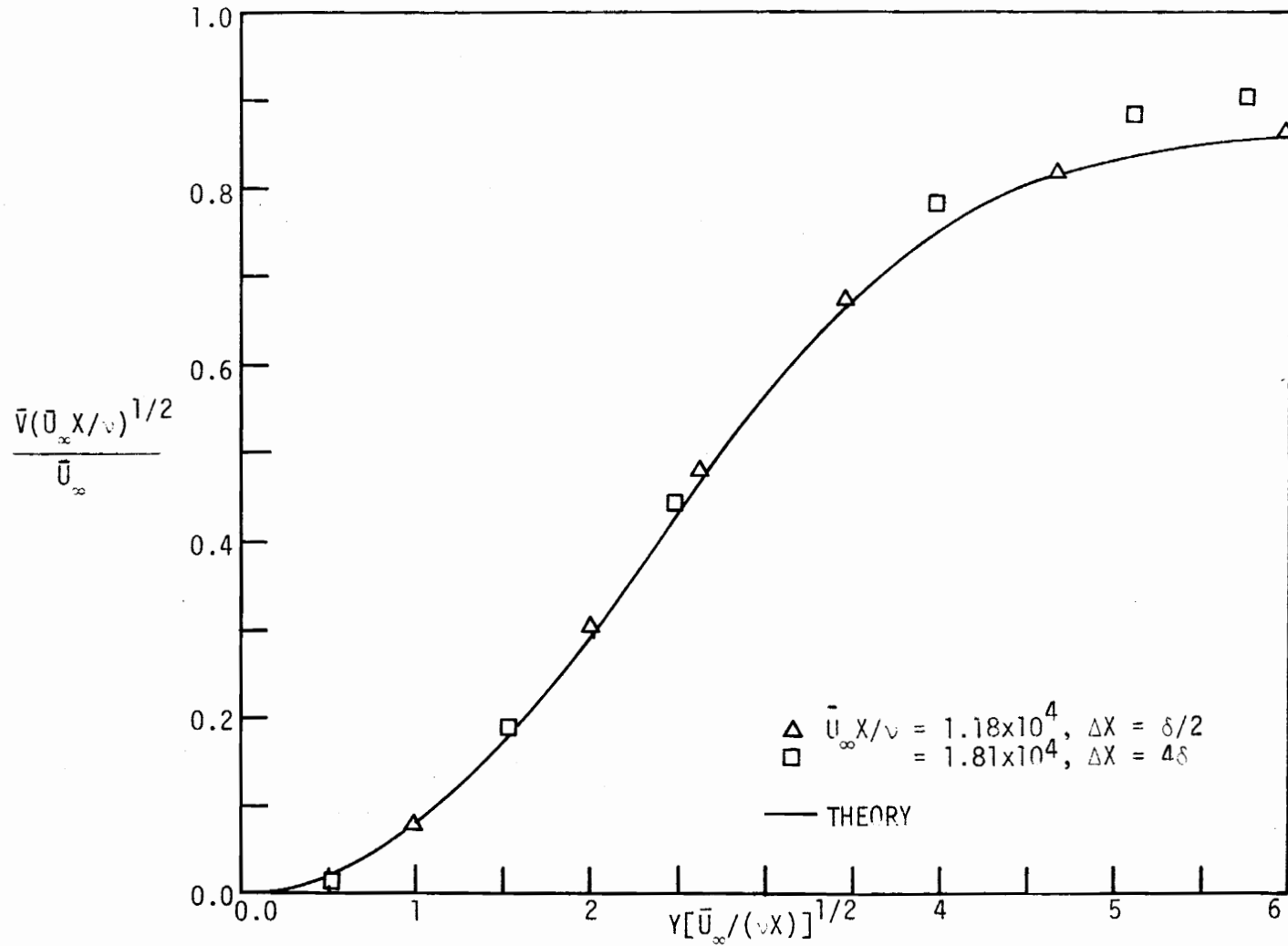


Fig. 4.4 \bar{V} -Velocity Profile Compared with Blasius Solution for $\Delta X = \delta/2$ and $\Delta X = 4\delta$.

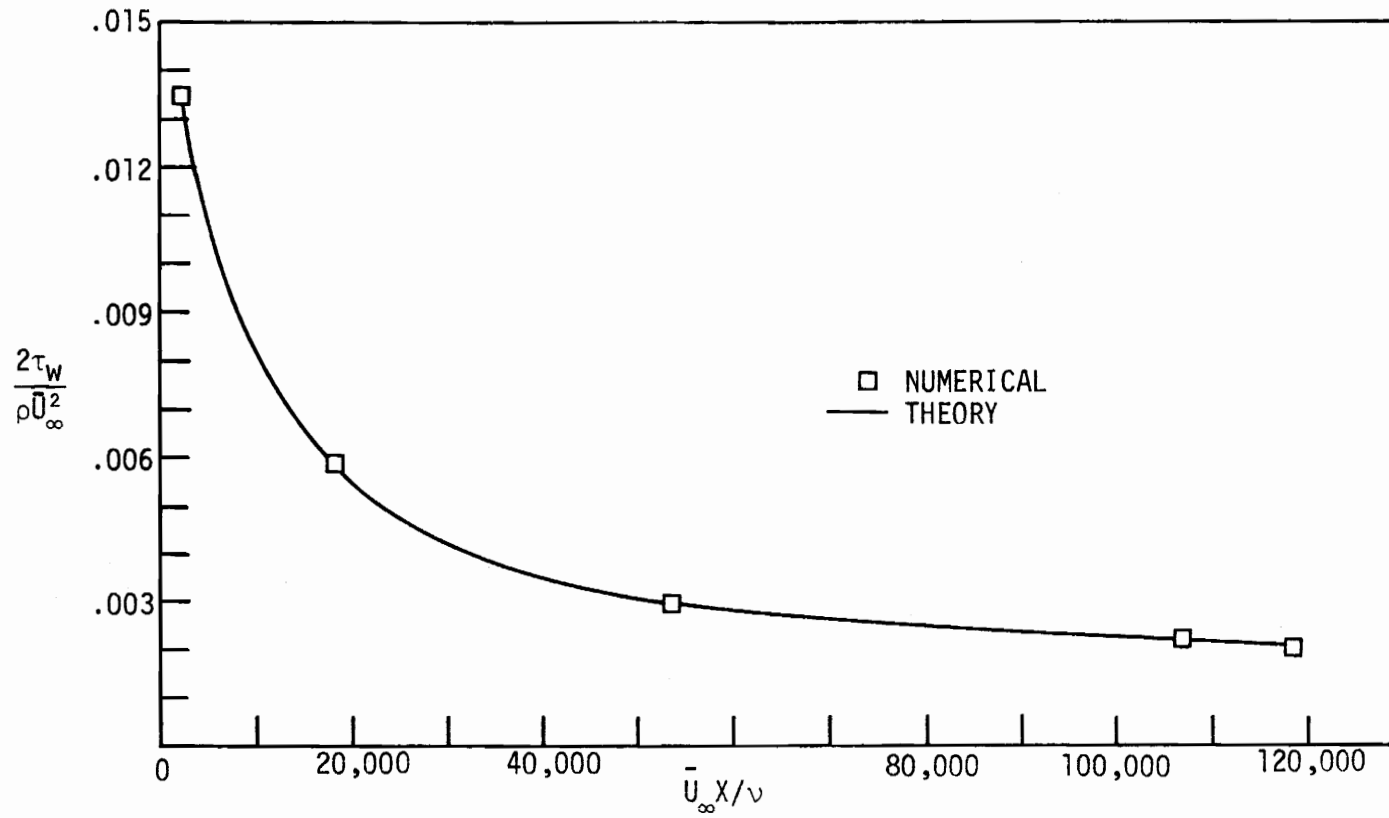


Fig. 4.5 Skin-Friction Coefficient Compared with Blasius Solution .

One of the major questions when solving a problem numerically is: How large a step size can be taken without affecting the results appreciably? Fig. 4.1 and 4.2 show the \bar{U} and \bar{V} profiles for a ΔX step equal to the boundary layer thickness. Obviously at the leading edge this criterion breaks down because at the leading edge the boundary-layer thickness is zero. Therefore, at the leading edge 20 steps, equal to 0.001 in., were taken in the X-direction. The step size was then increased by 10% per step until the step size was equal to the boundary layer thickness. The boundary layer thickness, δ , was set at the y-location where $\frac{u}{u_\infty} = 0.99$. The total solution, however was carried out in the y-direction until $\frac{u}{u_\infty} \geq 0.99999$ and at the next y-location the boundary conditions were imposed. The choice of the criterion for the solution thickness was somewhat arbitrary but the following reasoning justified to some extent this value. Several parametric studies for this flow circumstance showed that the results were virtually unaffected when the solution was only taken to $\frac{u}{u_\infty} \geq 0.9999$. However, it was desirable to insure that the outer region flow in the boundary layer was definitely not affected by the finite solution thickness. Thus, the higher limit was placed on the size of the solution thickness with the knowledge that the total number of grid points in the y-direction increased proportionally.

For the two- and three-dimensional turbulent flows to be investigated, the near wall region of the boundary layer is of some importance. To obtain a wall shear stress value from the velocity gradient

and the dynamic viscosity, the velocity gradient at the wall should be determined from the velocity field within the viscous sublayer. Also of importance, when investigating three-dimensional boundary layer flows, is the limiting wall streamline direction which again requires detailed knowledge of the velocity field in the immediate vicinity of the boundary surfaces. Thus, near the wall five y-grid locations spaced at .001 in. were used and at each subsequent y-location Δy was increased by 10%. Since the results for the laminar flow test case were in such good agreement with theory no further study was made for the y-grid spacing for this case.

Figures 4.3 and 4.4 show the typical dependence that the solution had on the ΔX increment. Since the results for $\Delta X = \frac{\delta}{2}$ were virtually indistinguishable from those of a step size of $\Delta X = \delta$, the latter step size was taken. Note also that for ΔX equal to 4δ , the computer solution began to show a definite deviation from the exact solution.

In all of these runs the \bar{v} -profile was not predicted as closely as was the \bar{u} profile. This small error was directly attributed to the finite difference approximation used for the continuity equation, Eq. 3.29a, for which the truncation error was of order Δx .

Figure 4.5 shows the variation of the skin friction coefficient with Reynolds number. For laminar flows and turbulent flows the wall shear stress is proportional to the velocity gradient at the wall. Thus this figure is a representation of the accuracy of predicted velocity gradients in the y direction at the wall, and also a check

on the method of determining the wall shear stress given below

$$\tau_w = \mu \frac{u(i, 2, k)}{\Delta y_-} \quad (4.1)$$

Again the good agreement substantiated the validity of the numerical solution.

B. Turbulent Two-Dimensional Flow

Because of the nature of turbulent flows, exact analytical solutions of the turbulent boundary-layer equations do not exist for even the simplest of flow geometries. To verify the validity of the computer program, experimental data, empirical correlations, and a simple momentum integral solution were used.

The results of the program were compared to the generally accepted wall-wake model proposed by Coles [36,39] and are shown in Fig. 4.6. This figure clearly shows the development of the wake profile as the velocity profile developed. In the outer regions the wake function reaches a maximum and for zero pressure gradient flows the equilibrium value for the "strength of the wake component" $\frac{\Delta u}{U_\infty \theta}$ should be approximately 2.7 according to Coles [36] for $\frac{U_\infty \theta}{\nu} \geq 6000$. The computer results shown in Fig. 4.6 for $\frac{U_\infty X}{\nu} = 5.48 \times 10^6$ had a value of $\frac{U_\infty \theta}{\nu}$ of approximately 9,000 and the "strength of the wake component" was slightly over 2.5. This latter value was within the scatter of the experimental data from which the average value of 2.7 was obtained.

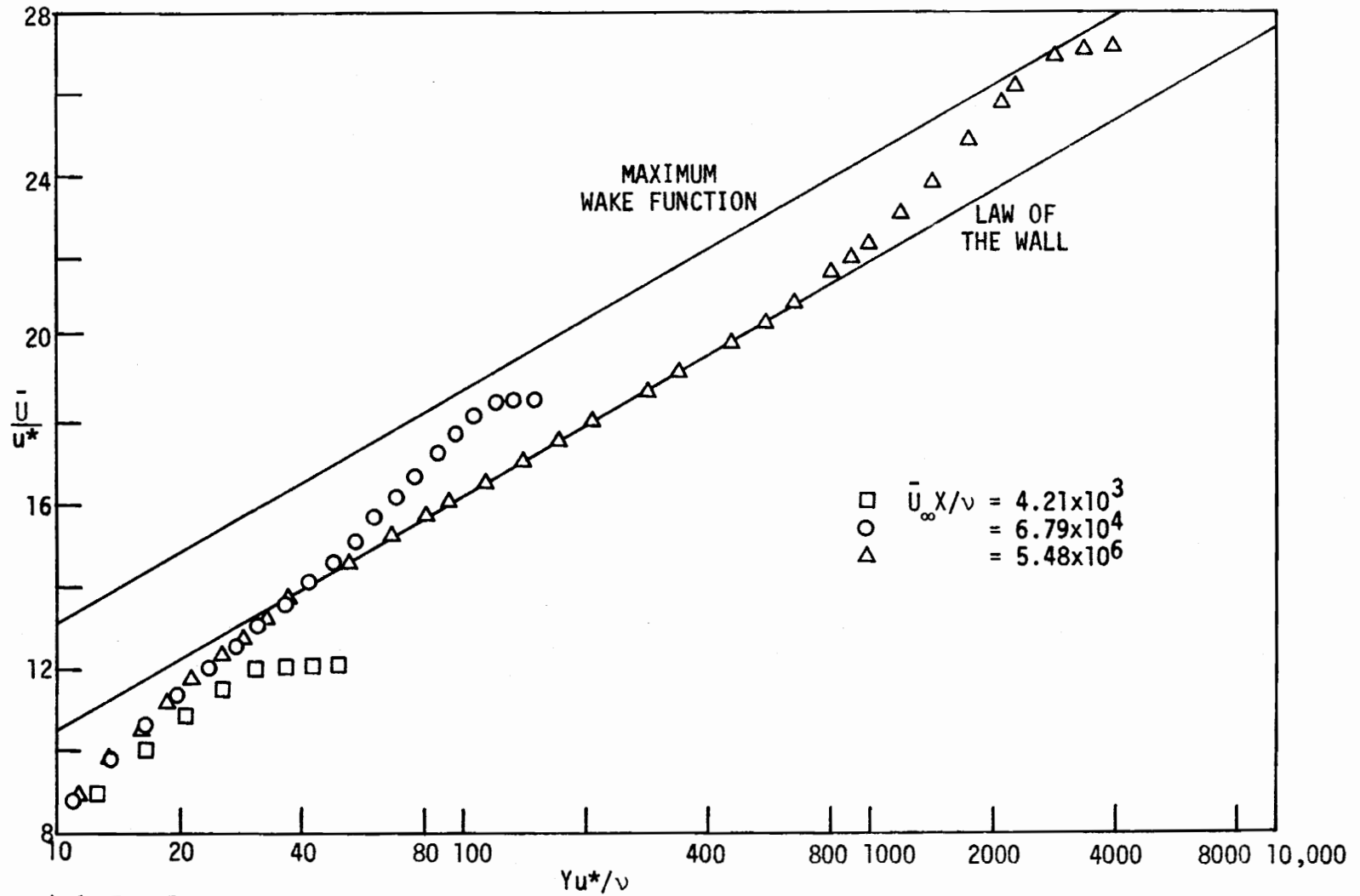


Fig. 4.6 Development of Streamwise Turbulent Velocity Profiles Compared with the Law of the Wall.

To check the solution further, the computer output was compared to the simple momentum integral analysis presented by Schlichting [32] for two-dimensional turbulent boundary layers over a flat plate where the one-seventh power law velocity profile was used in conjunction with the Blasius law of friction. Figure 4.7 shows that the results compare very favorably with the approximate momentum integral analysis for the variation of the integrated parameters θ_{11} and δ_1^* .

For the results presented above the procedure, for marching in the x-direction was exactly the same as for the laminar flow case discussed earlier and the rate of increase of the y increment, as the boundary layer edge was approached, was again 10%. Decreasing the X step to $\frac{1}{2} \delta$ had an insignificant effect on the results, and decreasing the rate of increase of the y increment to a value of 6% similarly yielded results which were indistinguishable from the results presented above.

The wall shear stress was calculated by Eq. 4.1 and is valid only if the first nodal point in the y-direction is within the laminar sublayer. The resultant skin friction coefficient is plotted in Fig. 4.8 where the Ludwig and Tillmann [44] empirical shear stress correlation was used for comparison. Note that the local θ_{11} and H integral parameters from the output were used in the formulation. Again the good correlation between the computer results and this empirical skin friction formulation gave further strength to the present analysis.

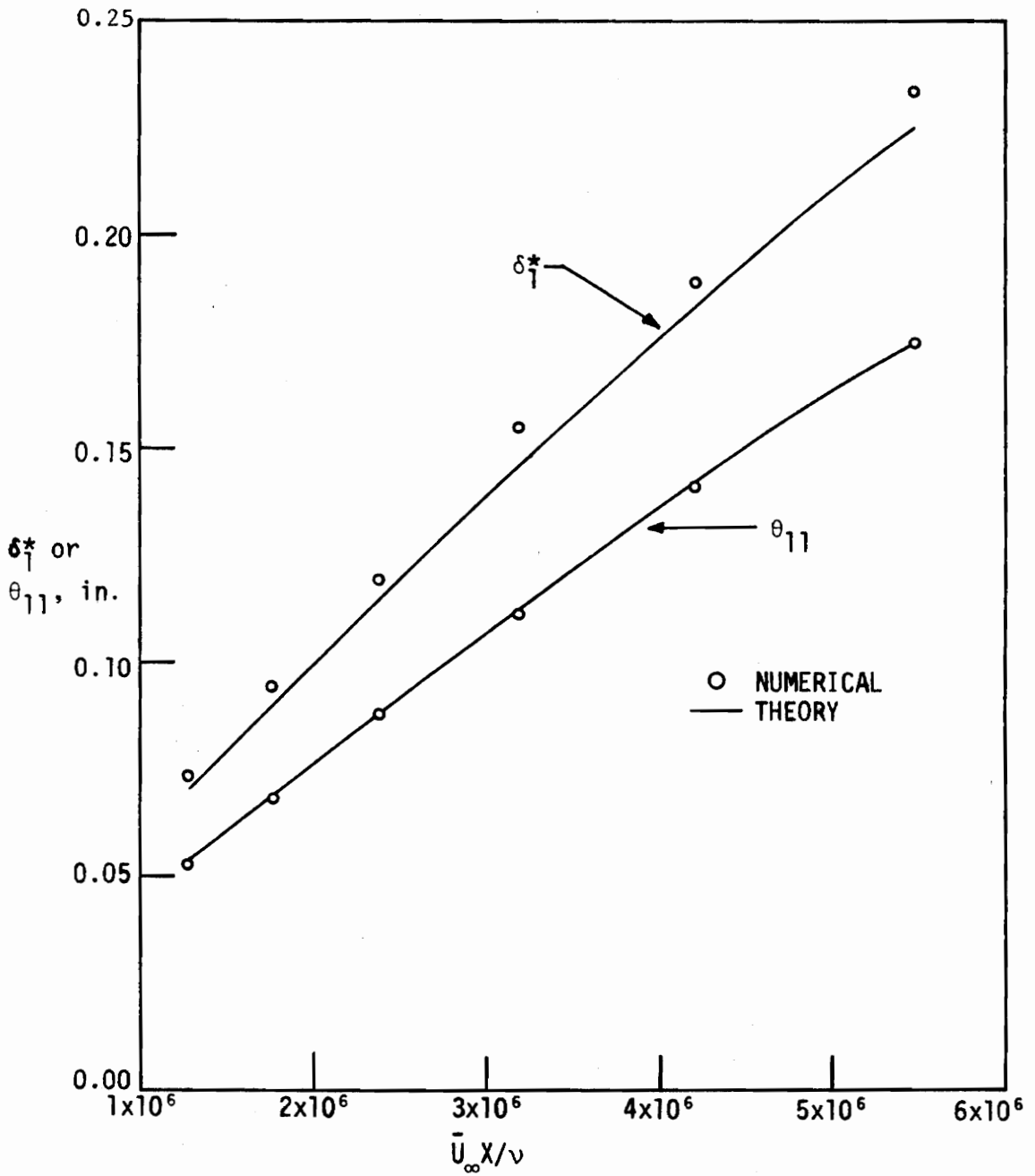


Fig. 4.7 Development of θ_{11} and δ_1^* Compared with a Momentum Integral Analysis.

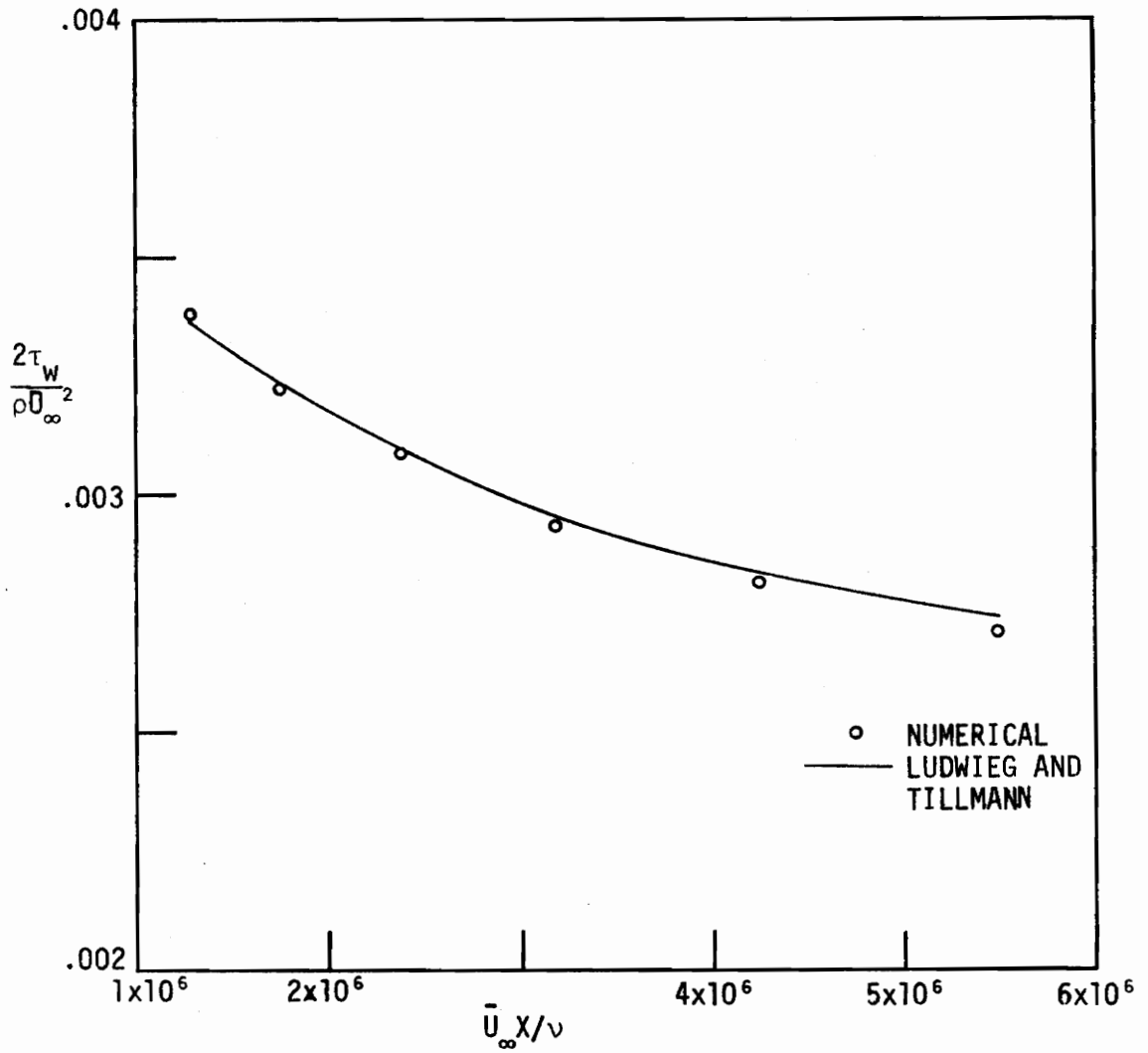


Fig. 4.8 Turbulent Skin-Friction Coefficient Compared with the Ludwig and Tillmann Correlation.

To investigate the solution for adverse pressure gradient flows, which are probably the most critical test cases, the data obtained by Schubauer and Klebanoff [45] in a mildly adverse pressure gradient were used for comparison. The initial profile was obtained from a best fit law of the wall profile (see Figs. 4.9 and 4.10) using the data, at the test location at 19 ft from the leading edge, given in the proceedings of the Stanford Conference [46].

$$\text{i) } \bar{U}_\infty = 154.1 \text{ ft/sec}$$

$$\text{ii) } \delta = 2.5798 \text{ in.}$$

$$\text{iii) } \frac{\bar{U}_\infty}{u^*} = 30.4$$

$$\text{iv) } \frac{2\tau_w}{\rho \bar{U}_\infty^2} = 0.002164$$

The external velocity field was approximated by Eq. 4.2 between $X = 19.0 \text{ ft}$ and $X = 21.5 \text{ ft}$.

$$\bar{U}_\infty = \frac{5.8425}{0.42231} (X - 17.3)^{0.44231} - 10X + 326.79 \quad (4.2)$$

where X is in ft and \bar{U}_∞ is in ft/sec.

The predicted velocity profiles are shown in Fig. 4.11 and 4.12 for $X = 20.5 \text{ ft}$ and $X = 21.5 \text{ ft}$, respectively.

Initial runs for adverse pressure gradient flows were made in which the Δx step size was equal to the boundary layer thickness. These results were compared to those for $\Delta X = \frac{1}{2} \delta$ and $\Delta X = \frac{1}{4} \delta$. The difference between the latter two runs and the run for $\Delta X = \delta$ cannot be shown graphically because of the small deviations between the runs. One measure of the difference between runs was to note the percentage change of the velocity at the first nodal location above the boundary surface

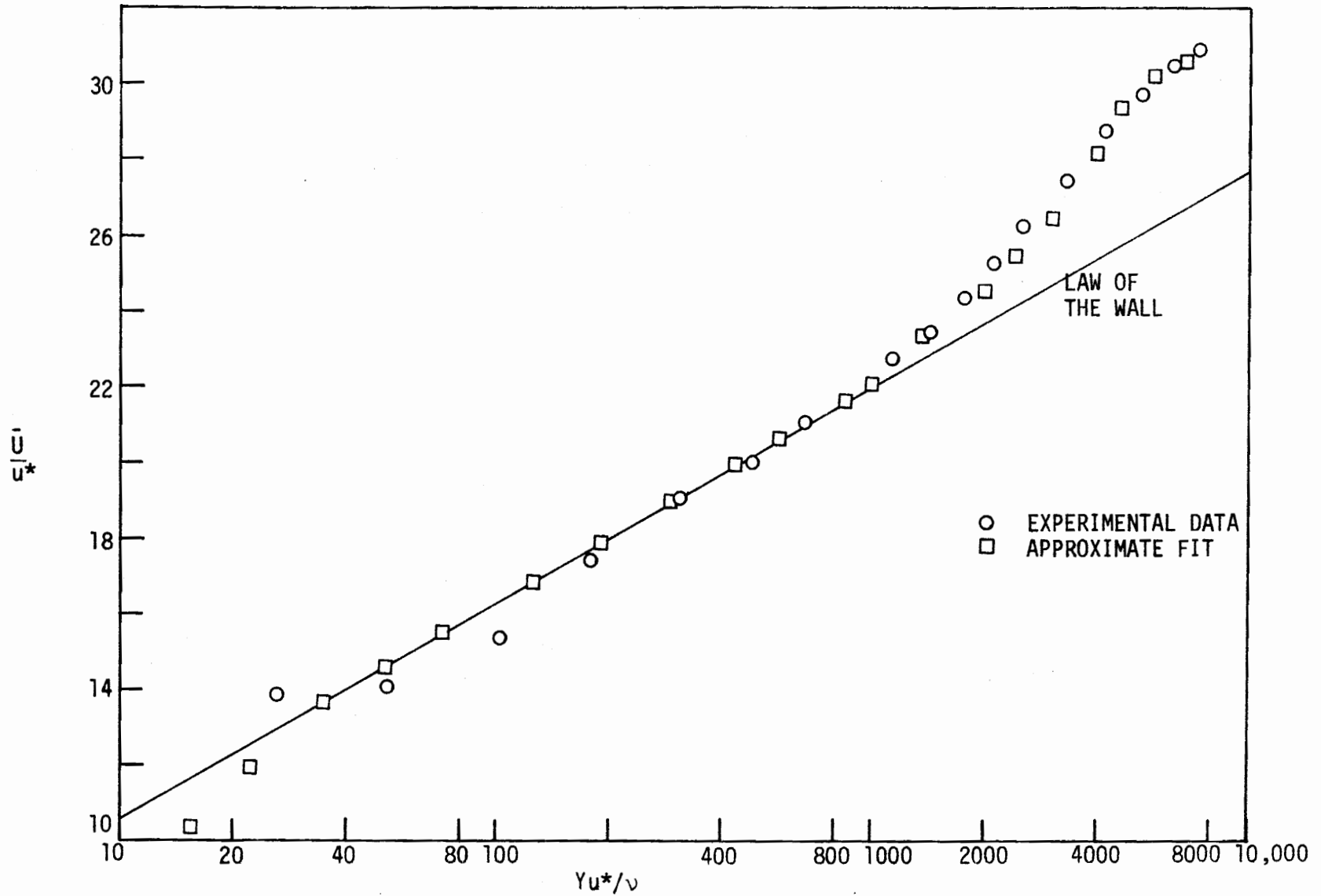


Fig. 4.9 Initial Law of the Wall Fit to Schubauer and Klebanoff's Experimental Data at X = 19.0 ft.

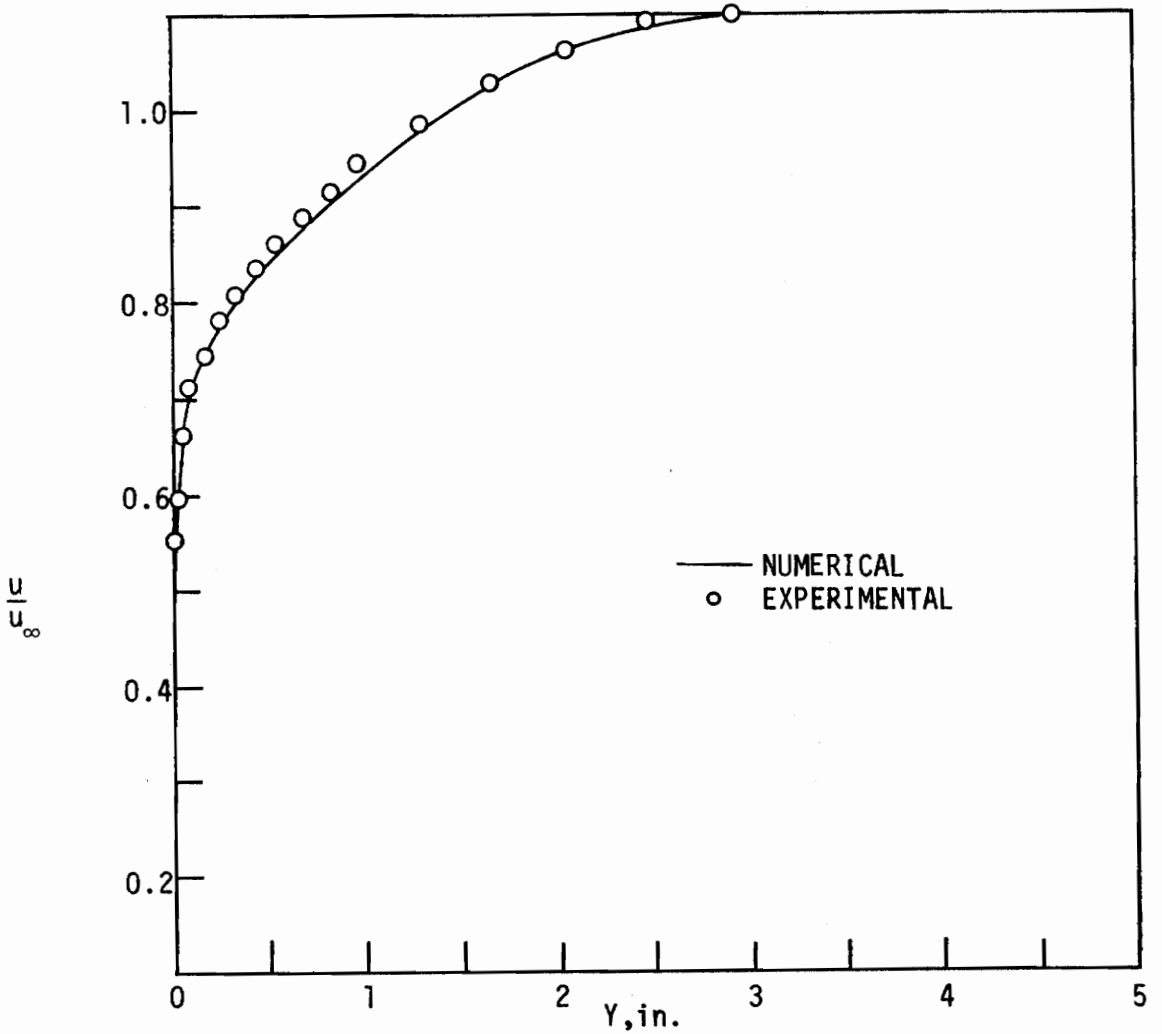


Fig. 4.10 Initial \bar{U} -Velocity Profile for Schubauer and Klebanoff Geometry in Physical Coordinates at $X = 19.0$ ft.

at an arbitrary distance downstream. The results, at the location $X = 21.5$ ft as the test point, were compared as described above, and yielded the following information:

<u>ΔX increment</u>	<u>Approximate Deviation (Compared to $\Delta X = \delta/4$)</u>
$\Delta X = \delta$	0.9%
$\Delta X = 1/2$	0.08%
$\Delta X = 1/4$	0%

It was desirable to have an increment in the X direction which would vary as the pressure gradient varied since for zero pressure gradient flows the ΔX step was equal to δ . Thus, the following parameter was introduced in an effort to modify the nondimensionalized X increment, x ,

$$\Delta x \leq \frac{u_{\infty}}{\frac{du_{\infty}}{dx}} \sigma \quad (4.3)$$

where σ is an arbitrary constant and ΔX was not to exceed the value of δ . For σ equal to 0.005, ΔX at 19 ft was approximately equal to δ but at $X = 21.5$, ΔX was just under $\frac{1}{2} \delta$. The deviation of this run for $\Delta X = \frac{1}{2} \delta$ was noted in the 4th significant digit. Reducing σ to a value of 0.003 yielded essentially the same results obtained for $\Delta X = \frac{1}{4} \delta$ and a further reduction in the value of σ yielded an insignificant change in the results. Thus the results shown in Figs. 4.11 and 4.12 are for a value of $\sigma = 0.003$. The Y increment was 0.002 in. for the first five grid locations, then successively increased by 10% through the boundary layer.

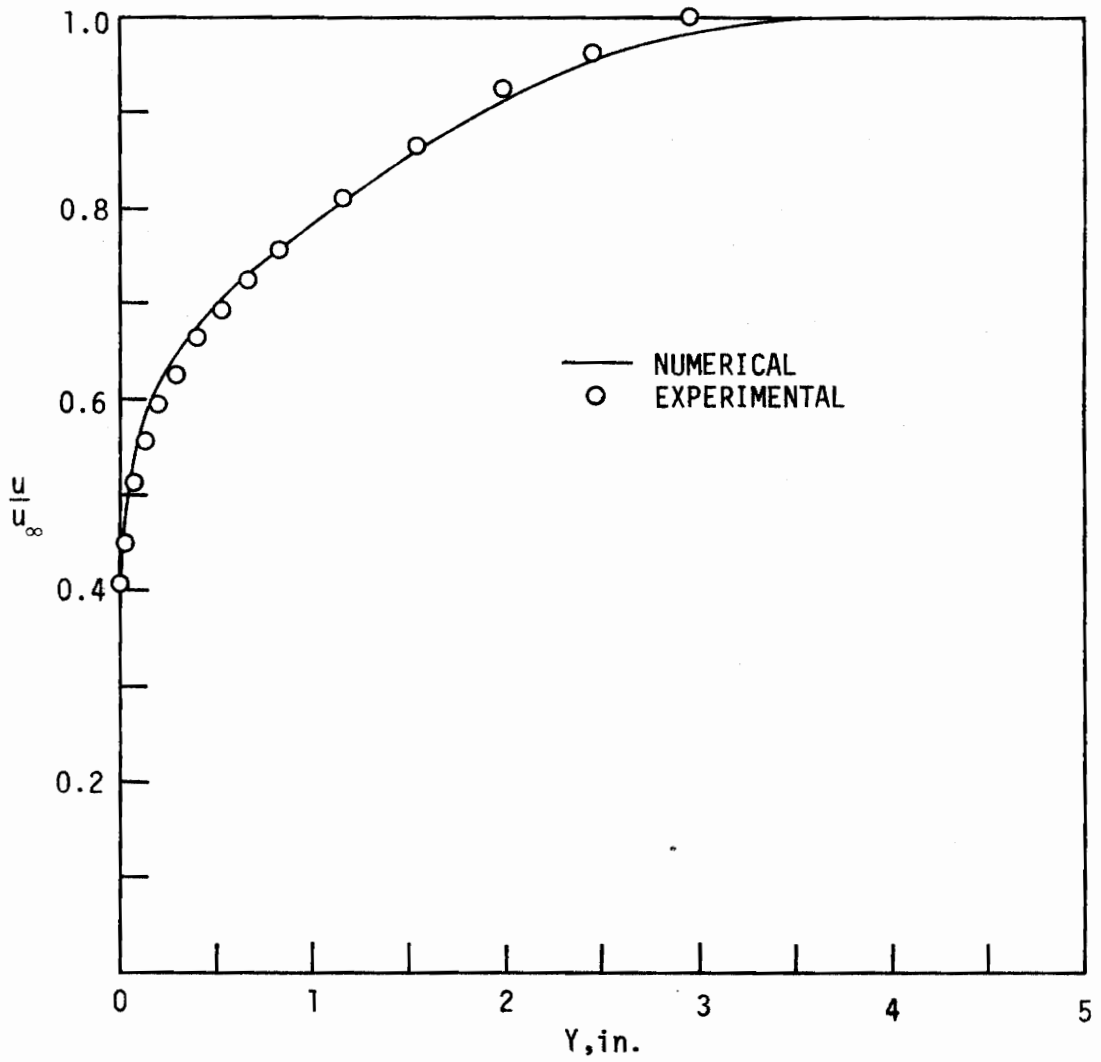


Fig. 4.11 \bar{U} -Velocity Profile Compared with Schubauer and Klebanoff's Experimental Data at $X = 20.5$ ft.

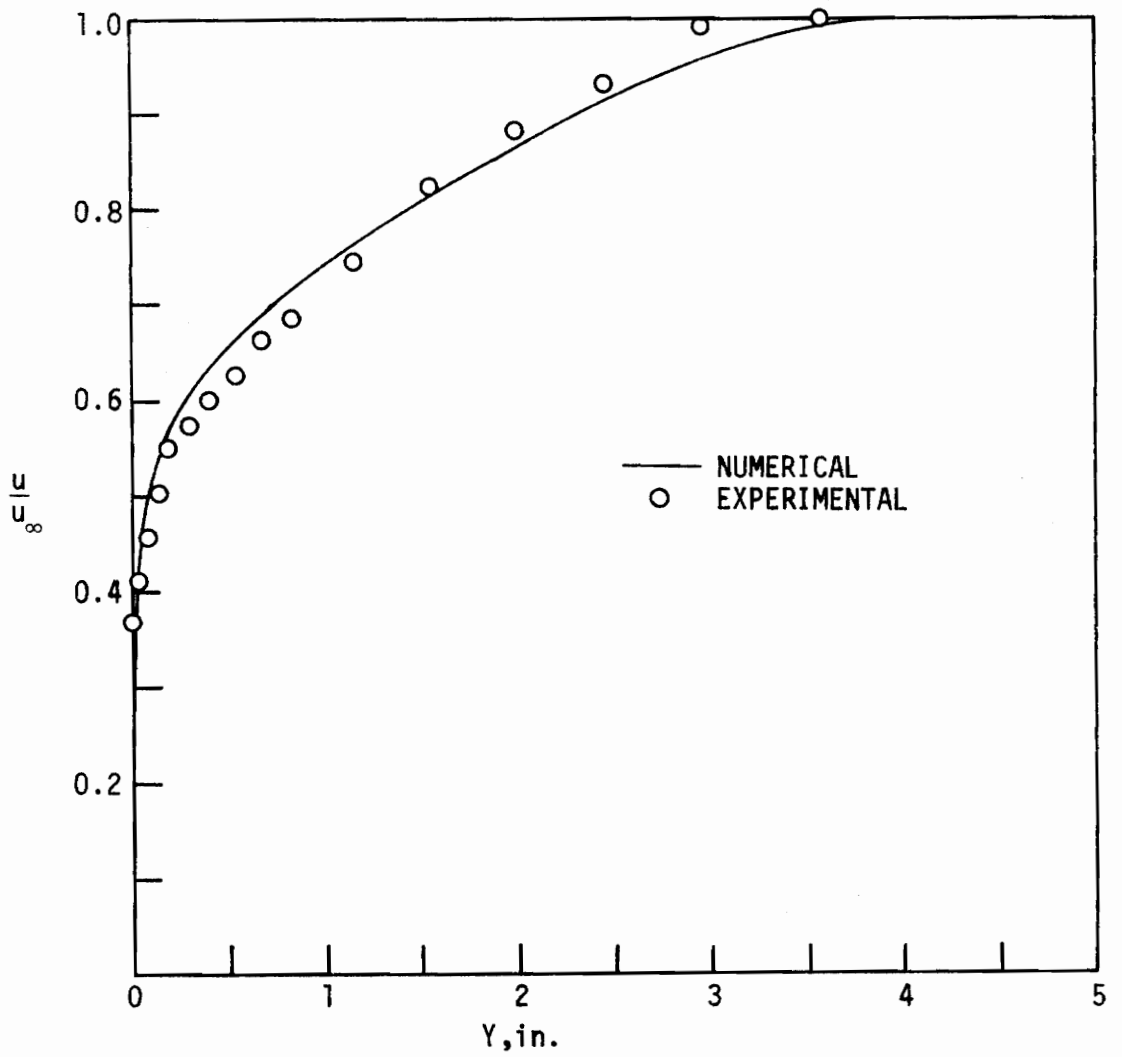


Fig. 4.12 \bar{U} -Velocity Profile Compared with Schubauer and Klebanoff's Experimental Data at $X = 21.5$ ft.

This increase of the Y increment near the wall from 0.001 in. to 0.002 in. was necessary to accommodate the thickness of the boundary layer under investigation, which was more than twice as thick as those previously mentioned. The first y location was, however, maintained within the laminar sublayer.

About 40 steps of 0.001 in. in the X direction were taken before the larger step sizes were imposed. This region allowed the computer solution to smooth out the input u-velocity profile to conform to the finite difference equations and allowed for the development of the v profile.

Finally Cebeci [8] has introduced a correction factor, to compensate for compressibility effect, boundary layer suction and blowing, and pressure gradients, on the parameter, A, introduced in the van Driest mixing length hypothesis, Eqs. 3.17a and 3.17b.

$$A_{\text{eff}} = A \left[1 - 11.8 \left(\frac{\bar{v} \bar{U}_{\infty} \frac{d\bar{U}_{\infty}}{dX}}{2 \left(\frac{\tau_w}{\rho} \right)^{3/2}} \right) \right] \quad (4.4)$$

Since this correction assumes previous knowledge of the wall shear stress, an iteration procedure was followed at each new location to determine the proper value of A_{eff} that was consistent with the shear stress. Using this correction factor the skin friction coefficient was decreased approximately 0.1% at $X = 21.5$ ft when compared to the results previously described. To generalize this model into three-dimensions would require the introduction of a non-scalar mixing length because

of the dependence of A_{eff} on the pressure gradient in the flow direction. This method to generalize the correction factor would have the following effects on the computer program.

- i) The introduction of another eddy viscosity would require approximately twice as many calculations to determine the eddy-viscosity parameters necessary in the finite difference equations.
- ii) A double iteration would be necessary to obtain values of A_{eff} in the x and z directions consistent with the wall shear stress vector, further increasing the computational time at each location.
- iii) The computer storage area requirements for the program would have to be increased by approximately 20% to allow for the additional eddy viscosity parameter and the associated additional object code storage.

With these considerations the decision was made not to incorporate this correction into the program for what appeared to be only a slight change in the results. However, it should be noted that the experimental work of Johnston [47] seems to indicate a nonisotropic nature of the mixing length for three-dimensional turbulent boundary-layer flows because the turbulent shear stress vector, with components τ_{x_t} and τ_{z_t} , does not align with the velocity gradient vector, with components \bar{U}_y and \bar{W}_y . He further mentioned that the difference between the direction of these two vectors cannot be attributed completely to experimental errors.

C. Plane of Symmetry and Three-Dimensional Results

Two three-dimensional solutions were obtained for which experimental data were available. The first solution was for the Johnston [28] data and the second was for the experimental data presented by Hornung and Joubert [29].

Figure 4.13 shows the match to the profile at station D-8 in the Johnston experiment. To obtain this match a two-dimensional boundary layer was developed from a leading edge of a flat plate some 62 in. before the match point with the external velocity equal to the velocity at the match point. The fit was a compromise between the following criteria:

- i) Matching the integrated parameters θ_{11} and δ_1^* as closely as possible,
- ii) Matching the actual velocity profile, and
- iii) Developing a profile over the approximate actual lead-in section length.

To generate an accurate solution, the free-stream flow field should approximate as closely as possible the actual flow condition encountered in the experiment. Figure 4.14 shows the experimentally measured field and the external velocity field as predicted from the potential flow solution for this geometry. Due to the slight acceleration of the fluid caused by boundary layer growth on the floor and the ceiling of the test section, the predicted external velocity noticeably deviated

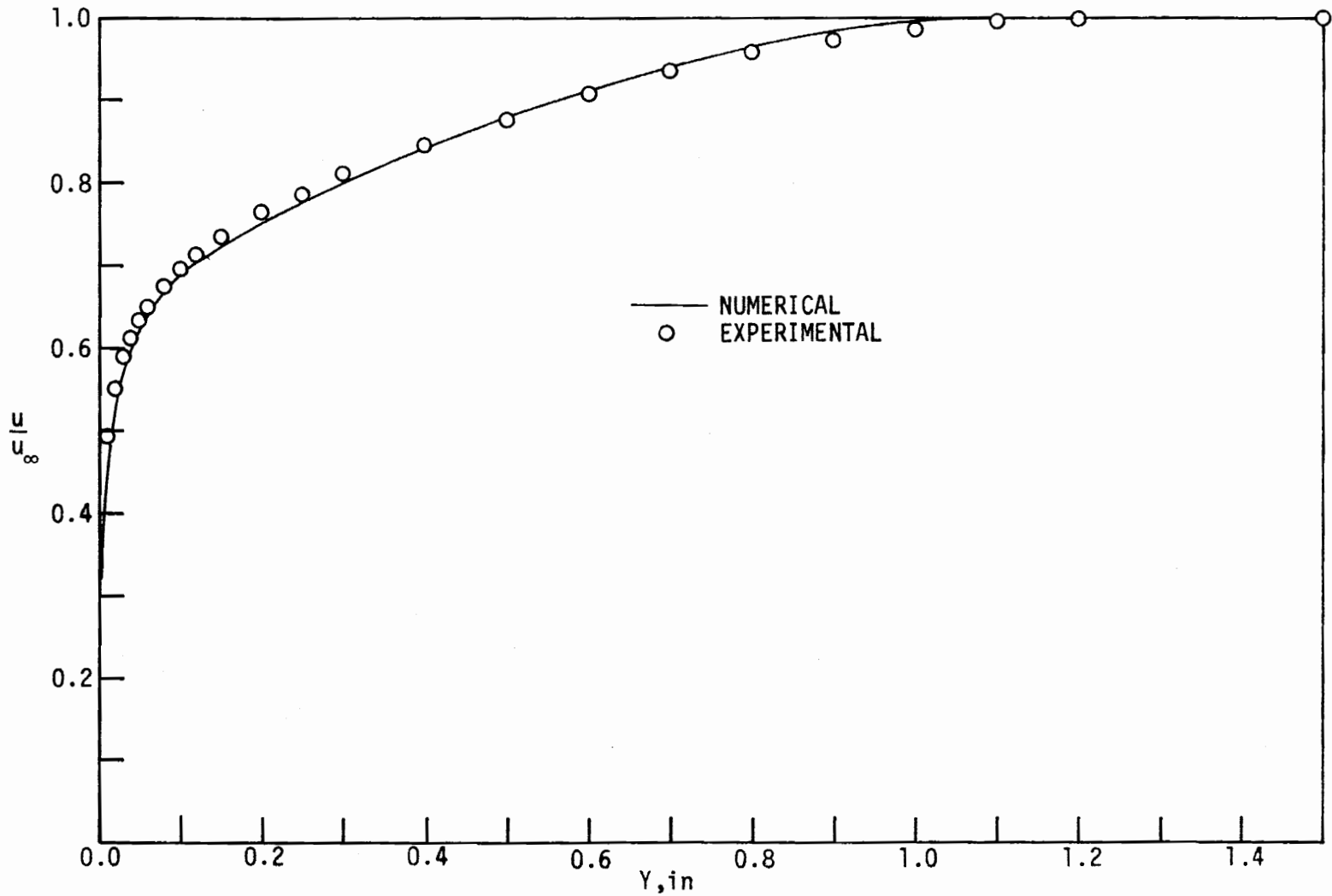


Fig. 4.13. Initial \bar{U} -Velocity Profile fit to Johnston's Experimental Data at Station D-8.

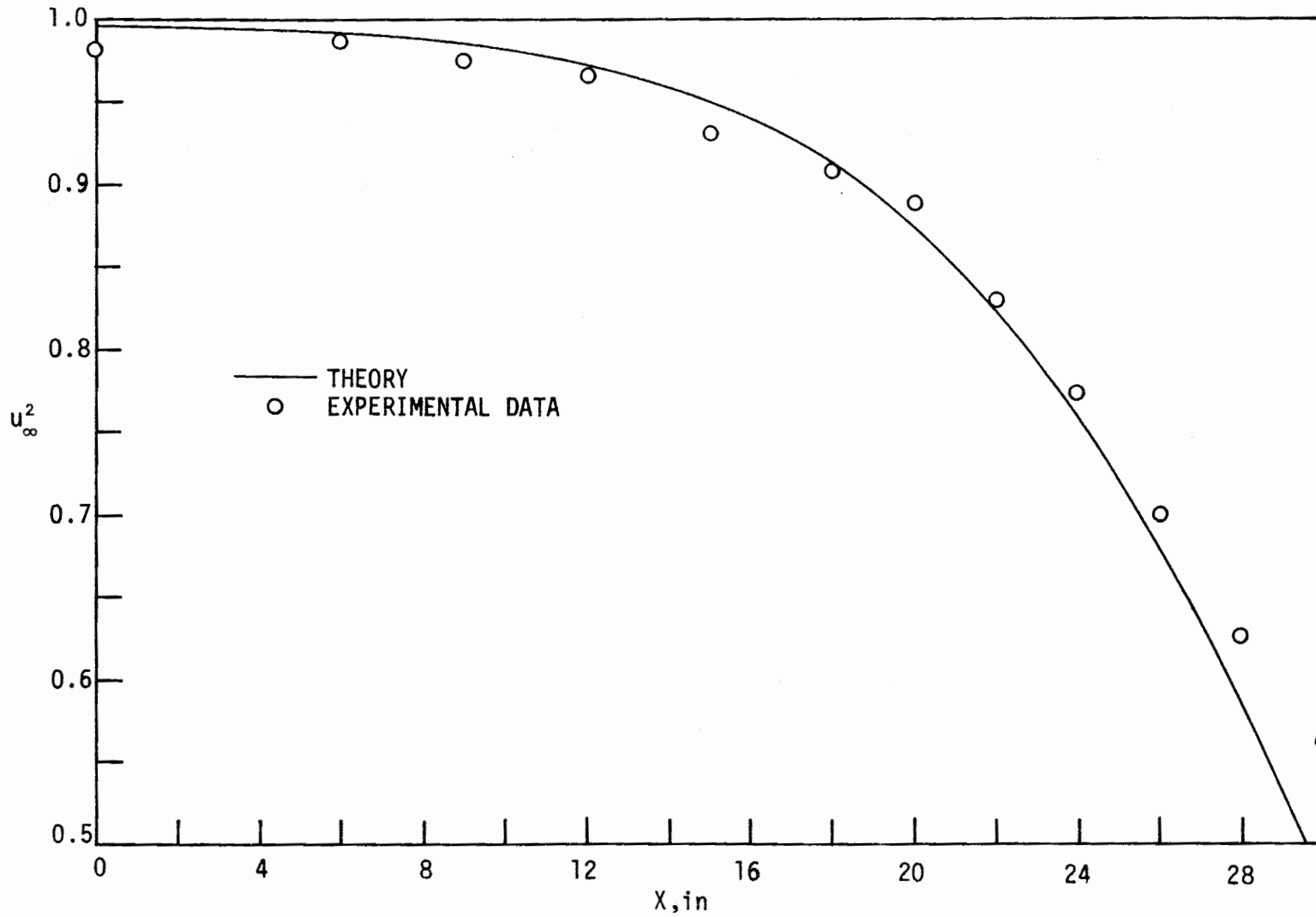


Fig. 4.14 External Velocity Field on the Plane of Symmetry for the Johnston Geometry.

from the actual velocity as the end wall was approached (especially after a distance of about 24 in. from station D-8). This deviation resulted in a larger adverse pressure gradient than actually experienced experimentally by Johnston. Thus, the information obtained from the computer solution should exhibit characteristics which are attributable to this larger adverse and therefore a larger transverse pressure gradient when compared to the experimental data.

This problem directly affected the location of the separation point along the plane of symmetry. The experimental results from observing the flow while smoke was injected into the stream and also using a wall streak test qualitatively showed the separation point on the plane of symmetry to be about 31 in. from station D-8. The computer results showed separation to occur at about 27.7 in. downstream of the match point or about 3.3 in. before the experimentally determined point. East [27] numerically showed separation to occur at approximately 28 in. The reason for the difference between these two numerical solutions was not precisely determined, but it is noted that the nature of the finite difference approximations are dissimilar to the extent that one of the truncation error terms in the Dufort-Frankel finite difference approximations is $(\frac{\Delta x}{\Delta y})^2 u_{xx}$. For flows near separation u_{xx} becomes large and the solution is directly affected by this truncation error which possibly accounts for the discrepancy noted above. For the present numerical technique the corresponding truncation error term for the momentum equation was $u_{xxx} (\Delta x)^2$, a much smaller term.

Figures 4.15a through 4.15d show typical predicted u-velocity profiles along the plane of symmetry. For all of these cases the velocity near the wall was underpredicted. This was partially caused by the initial fit at station D-8 which also exhibits this same characteristic due to the necessary compromise to obtain the match point profile.

For the plane of symmetry solution, the quantity wz was calculated from Eq. 3.24b. However, only an approximate comparison with experimental evidence was possible because of the large z spacing between data locations. Figure 4.16 shows the results at the location 26 in. from the match point. The wz derivative was approximated by taking a simple difference using the data nearest the plane of symmetry. Also shown on this figure are the results presented by Mellor [21] and East [27]. The numerical wz profile seemed to overpredict the experimental data. This is expected since wz reaches a maximum on the plane of symmetry and the derivative formed from the experimental data was obtained by using the w velocities at $Z = \pm 2.5$ in., therefore predicting lower values than actually expected. Further downstream, comparison was impossible since the present program predicted separation before the next experimental location. East was able to compare with Mellor's results at both 28 in. and 30 in. because they both fit a polynomial expression to the experimental velocity field on the plane of symmetry. However, when the present solution at 27.7 in. is compared to their results at 28 in. and the experimental results

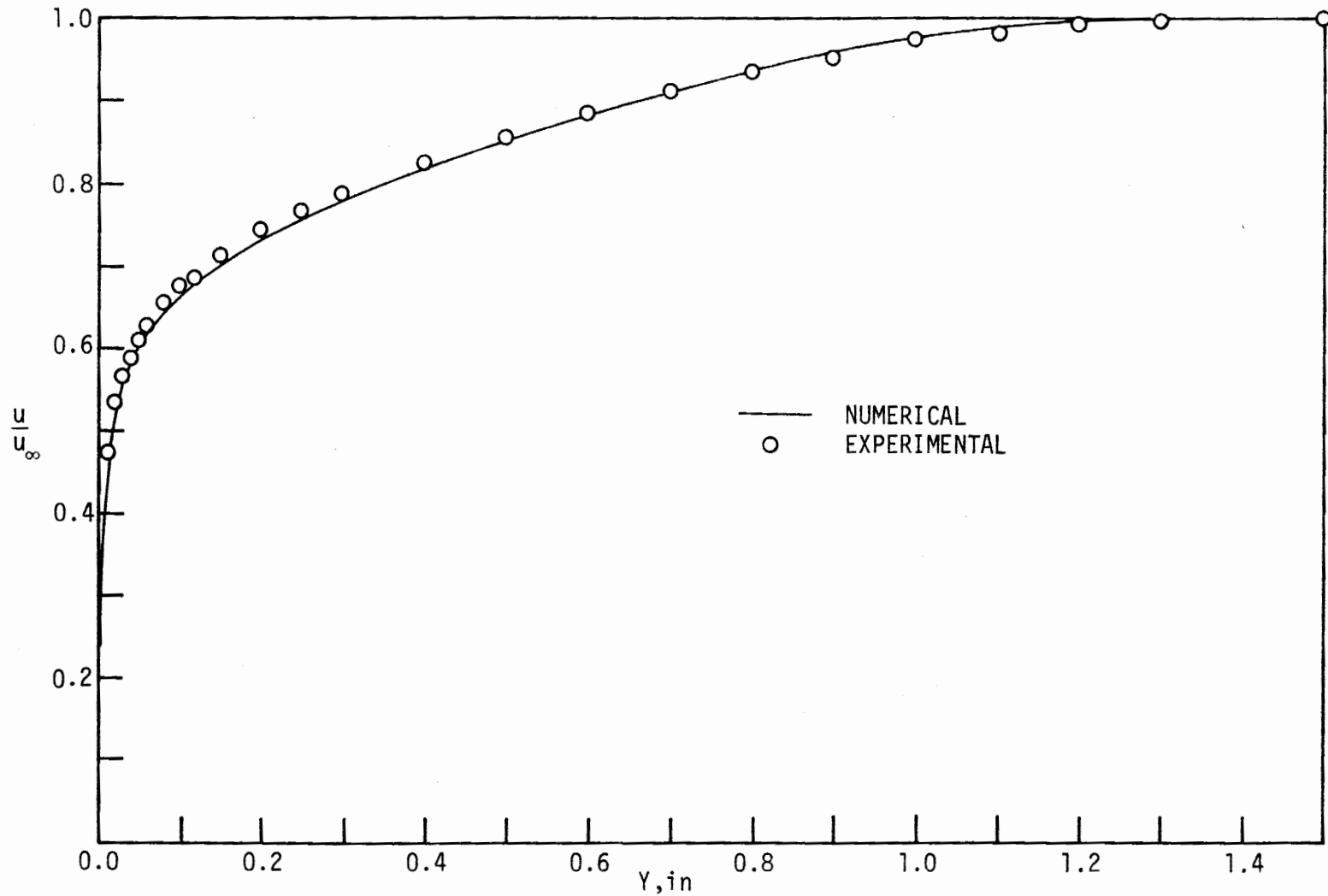


Fig. 4.15a \bar{U} -Velocity Profile Compared with Johnston's Experimental Data at Station D-6.

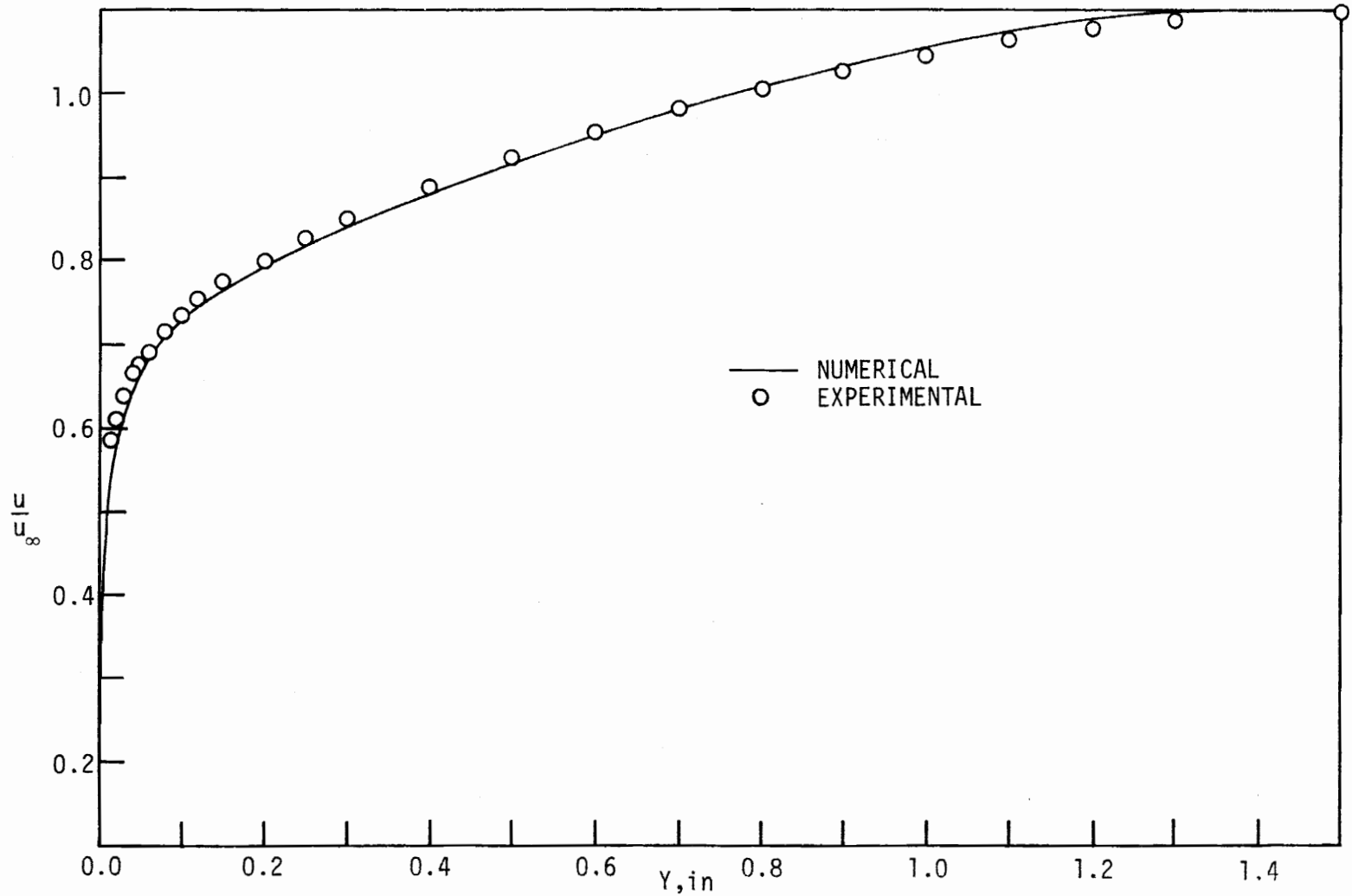


Fig. 4.15b \bar{U} -Velocity Profile Compared with Johnston's Experimental Data at Station D-X8.

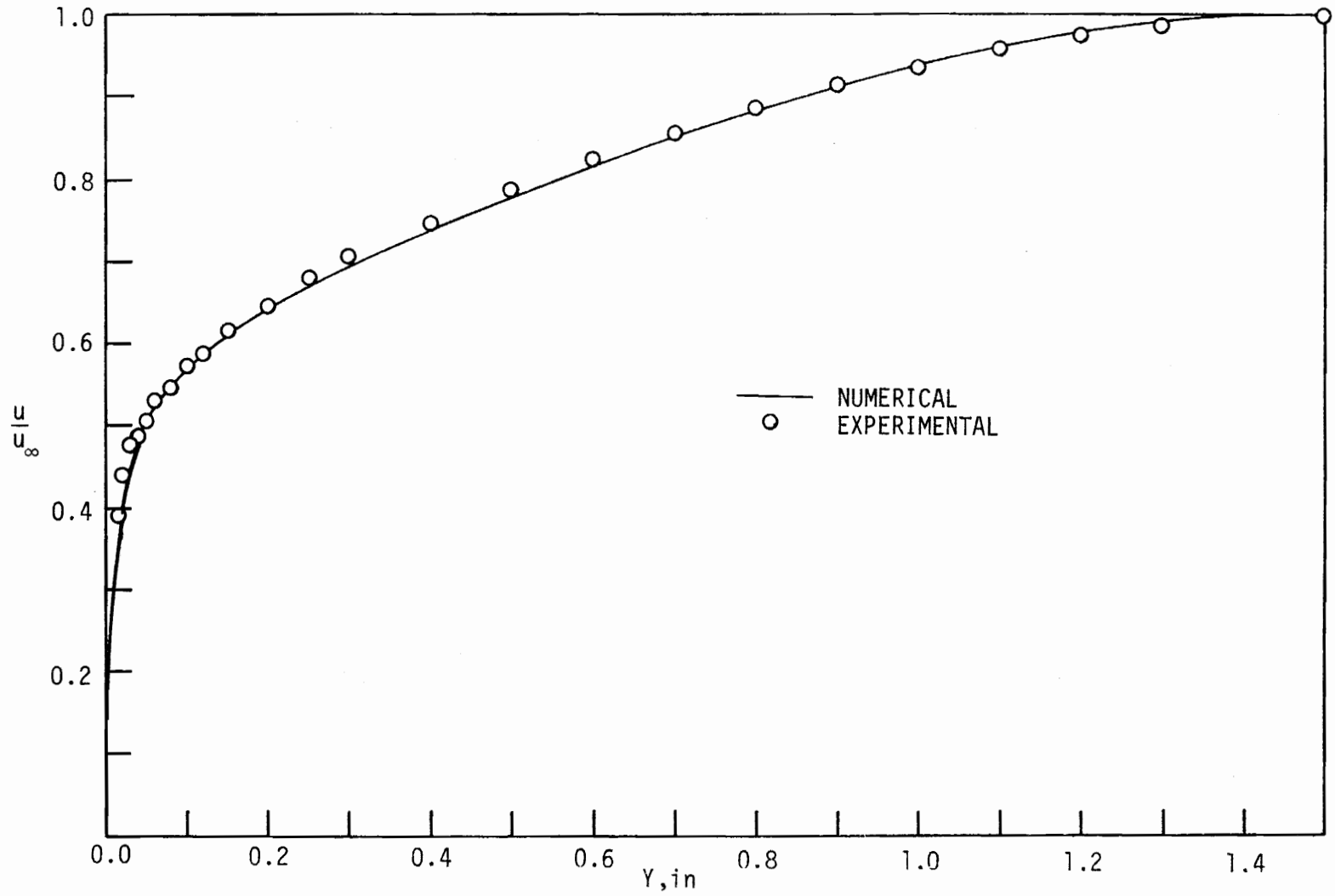


Fig. 4.15c \bar{U} -Velocity Profile Compared with Johnston's Experimental Data at Station D-4.

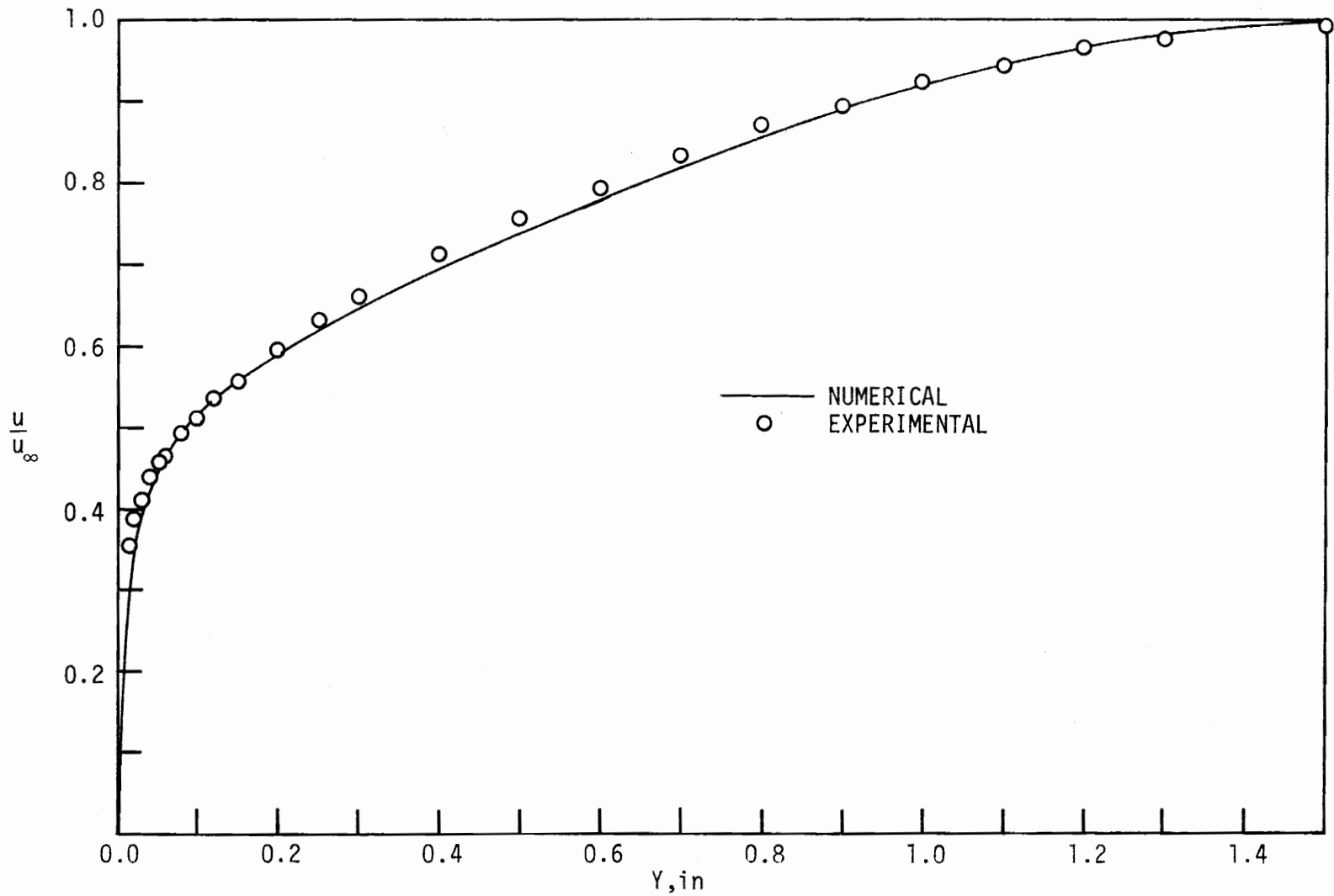


Fig. 4.15d \bar{u} -Velocity Profile Compared with Johnston's Experimental Data at Station D-X6.

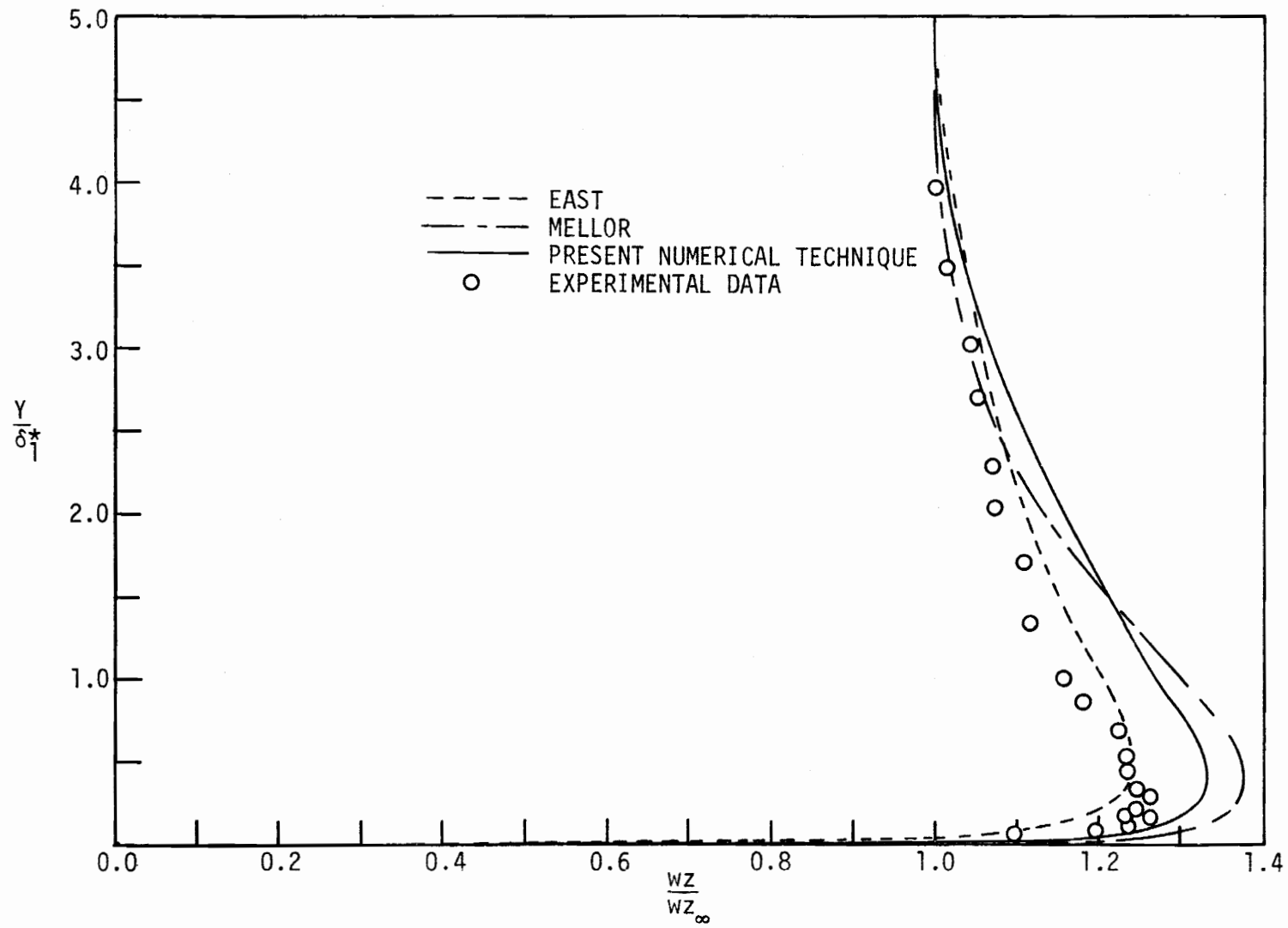


Fig. 4.16 Cross-Flow Velocity Gradients Compared with Johnston's Experimental Data at Station D-X6.

at 28 in., the present analysis yielded a result similar to the results shown in Fig. 4.16.

Figure 4.17 shows the variation of the momentum thickness along the plane of symmetry. The numerical solution predicted this growth very well up to about 26 in., where the momentum thickness began to increase more rapidly than the experimental results. This is due to the discrepancy between the actual and theoretical free-stream velocity fields, especially in velocity gradients. A similar result is shown in Fig. 4.18 for the development of δ_1^* along the plane of symmetry.

Figures 4.19 and 4.20 show the velocity profiles obtained off the plane of symmetry. The results are shown in streamline coordinates because this is generally the format in which experimental profiles are presented in the literature. The U_s -velocity profiles were generally in good agreement with the experimental profiles. The W_s component of velocity was consistently slightly larger than that of the experimental profiles. This same effect was experienced by East and the probable cause was the larger cross-flow pressure gradient obtained from the potential flow solution, as discussed earlier.

Many experimentalists (Francis and Pierce [48], Klinksiek and Pierce [49], Gardow [50], Johnston [28], Hornung and Joubert [29], Smith [51], Smith [52], Lewkowicz [53]) have recorded data which seem to imply the existence of a collateral layer in the near wall region of three-dimensional turbulent boundary-layer flows. However,

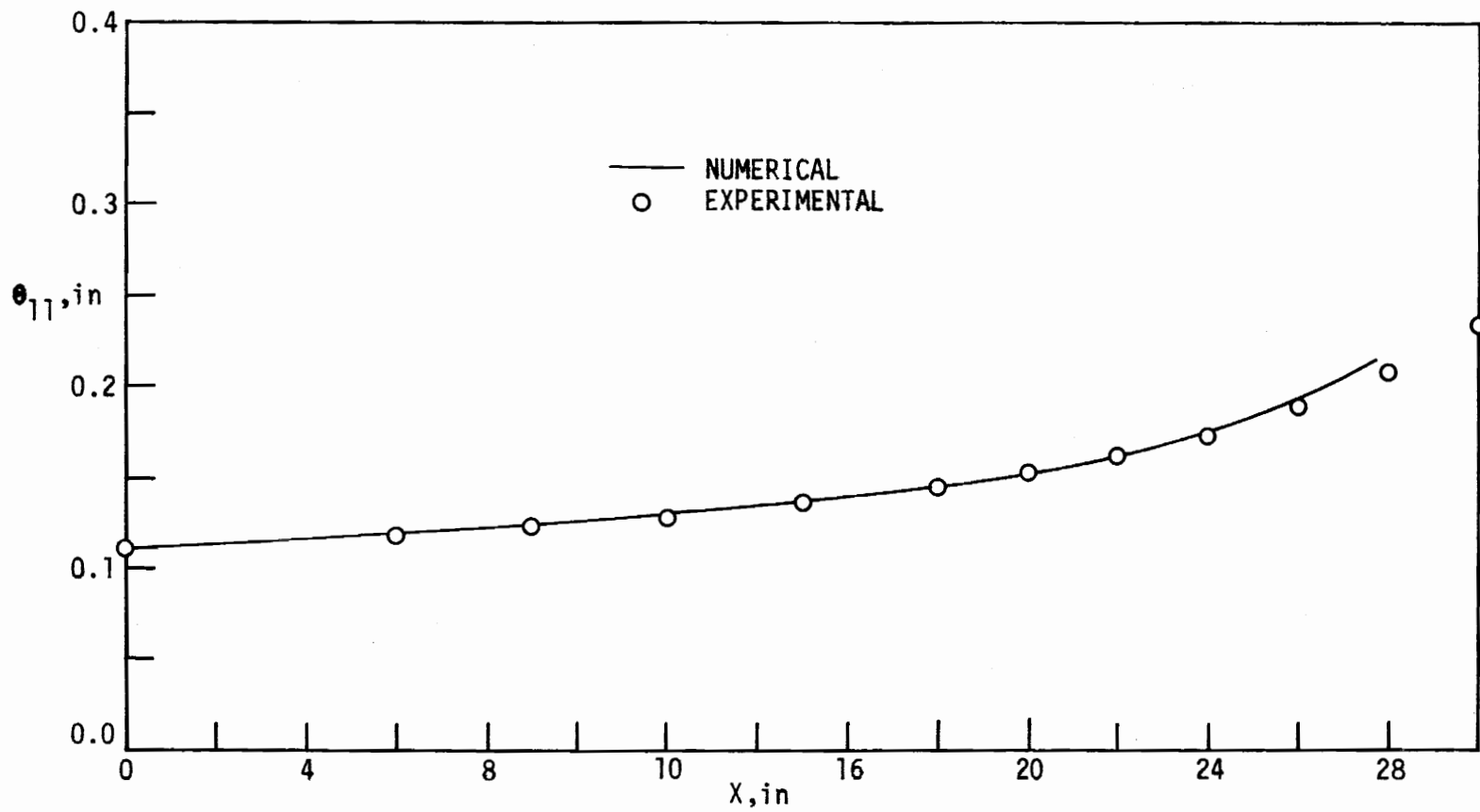


Fig. 4.17 Development of θ_{11} on the Plane of Symmetry Compared with Johnston's Experimental Data.

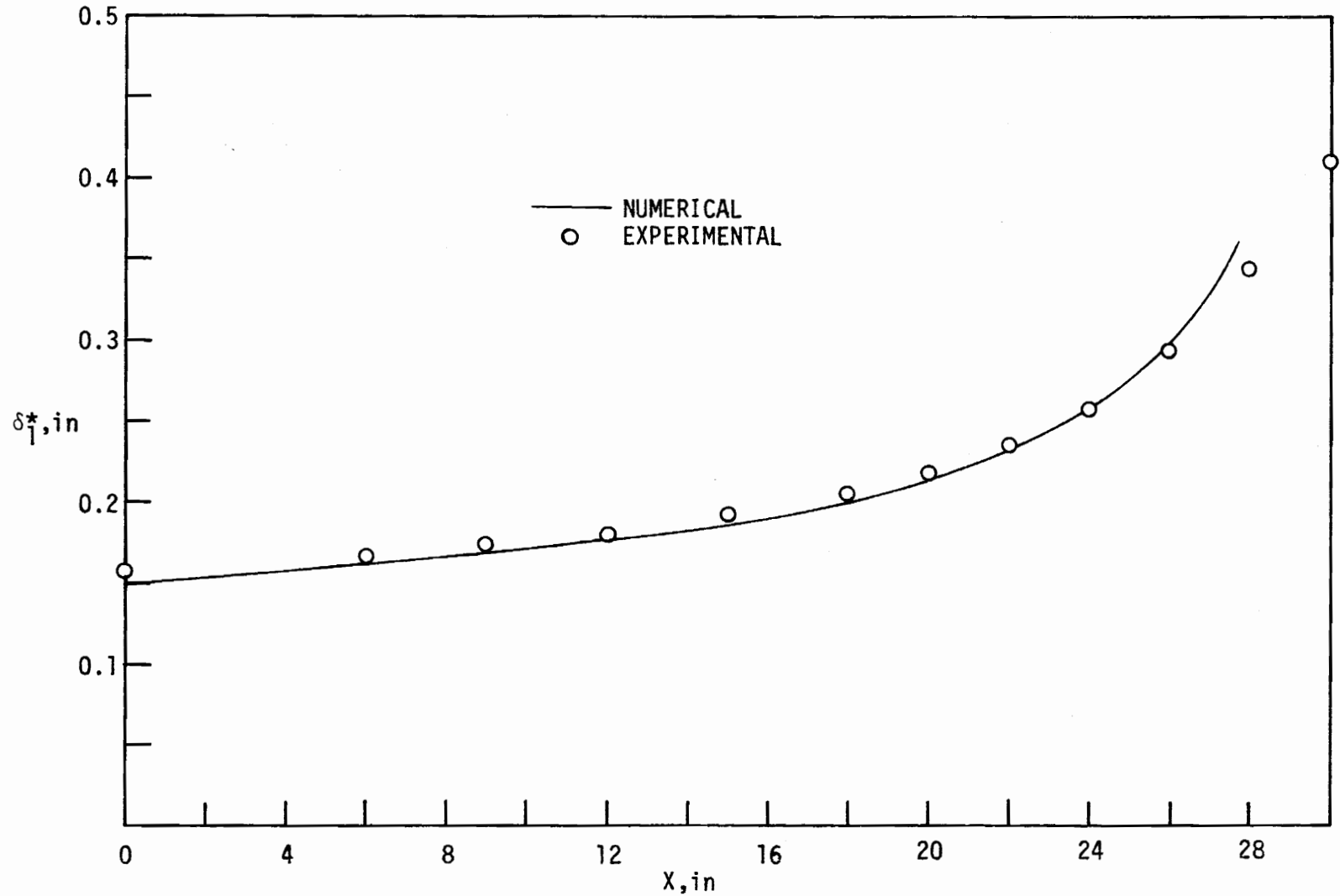


Fig. 4.18 Development of δ_1^* on the Plane of Symmetry Compared with Johnston's Experimental Data.

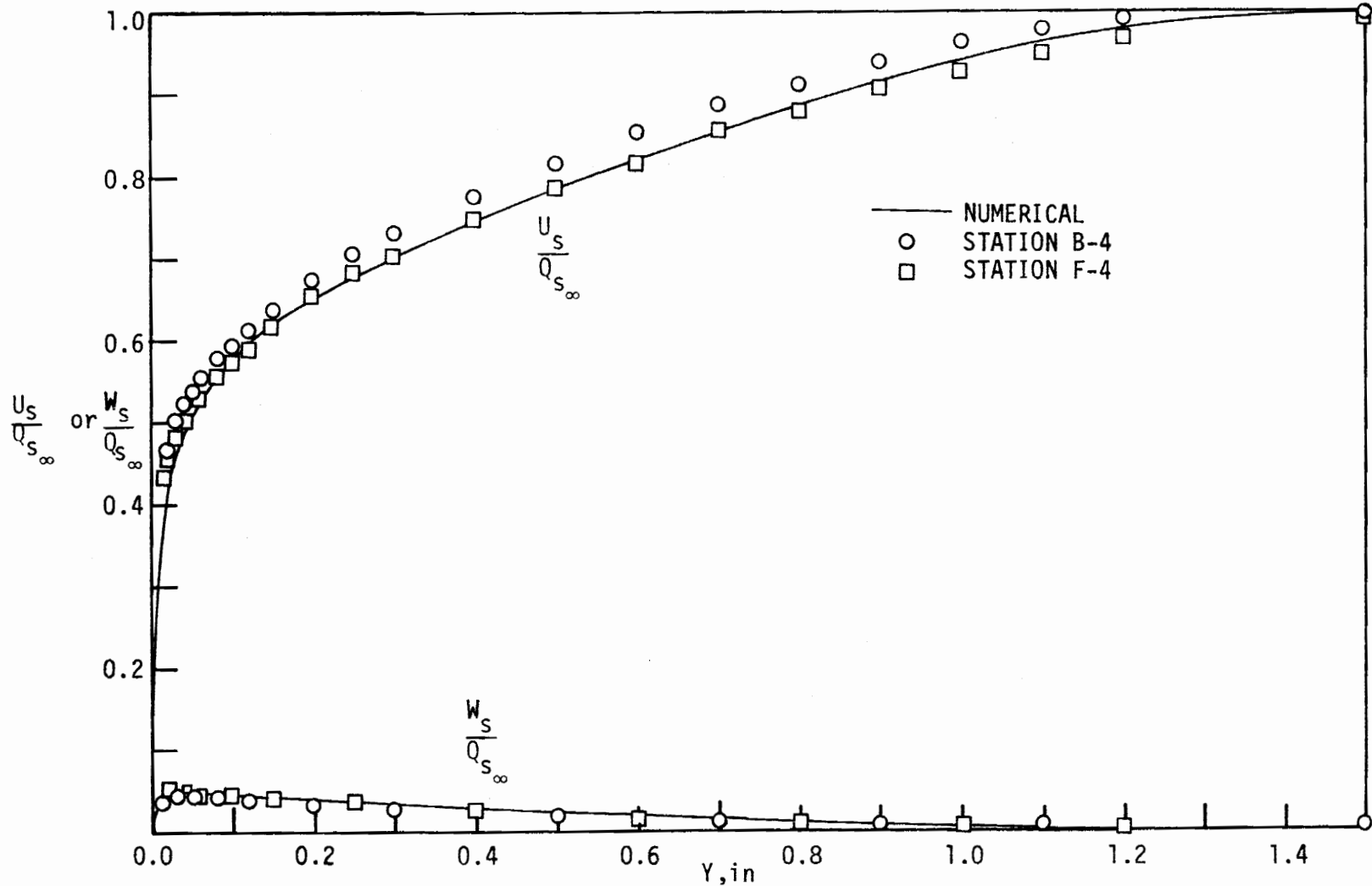


Fig. 4.19a U_s - and W_s -Velocity Profiles Compared with Johnston's Experimental Data at Stations B-4 and F-4.

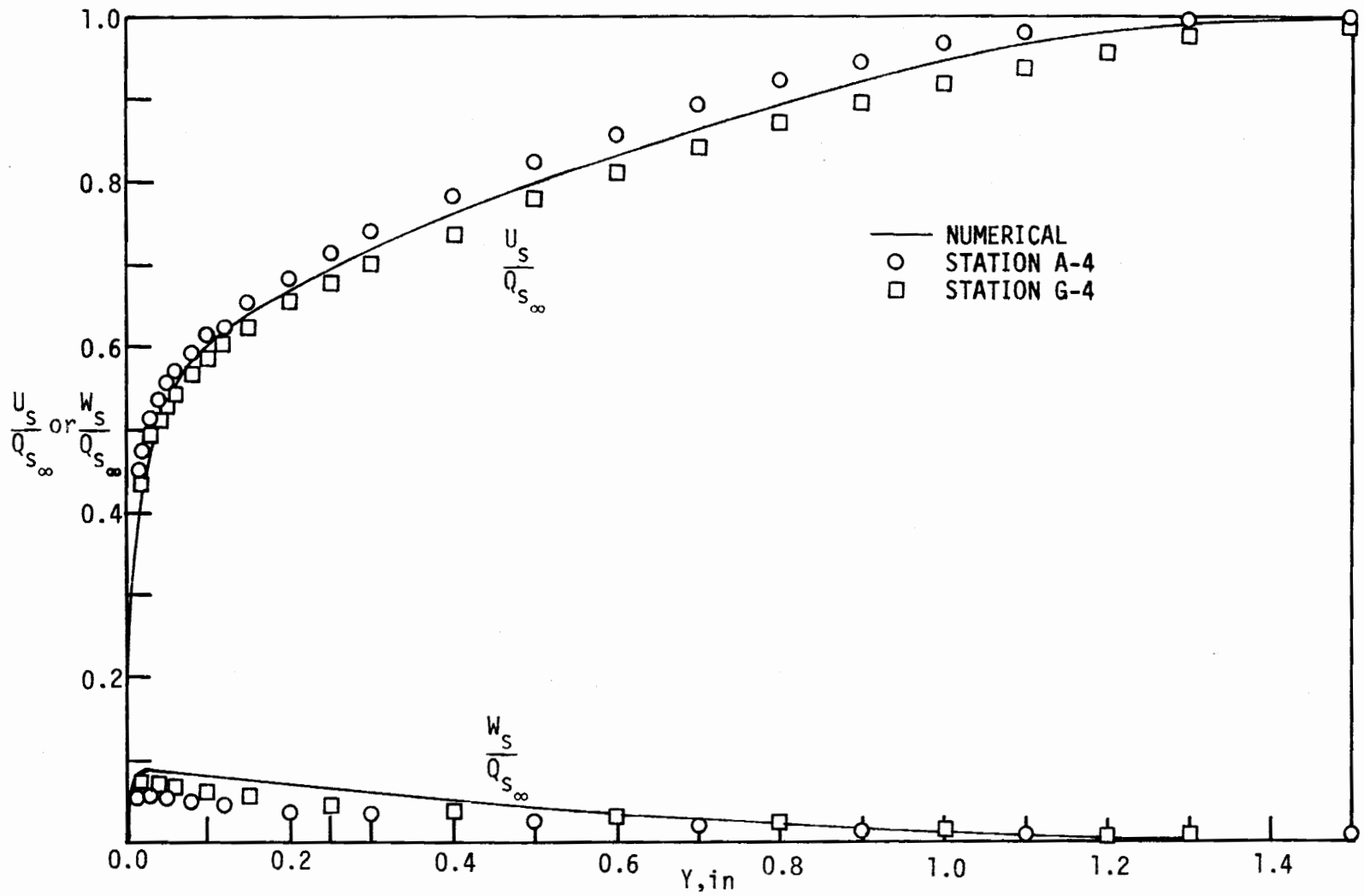


Fig. 4.19b U_s and W_s -Velocity Profiles Compared with Johnston's Experimental Data at Stations A-4 and G-4.

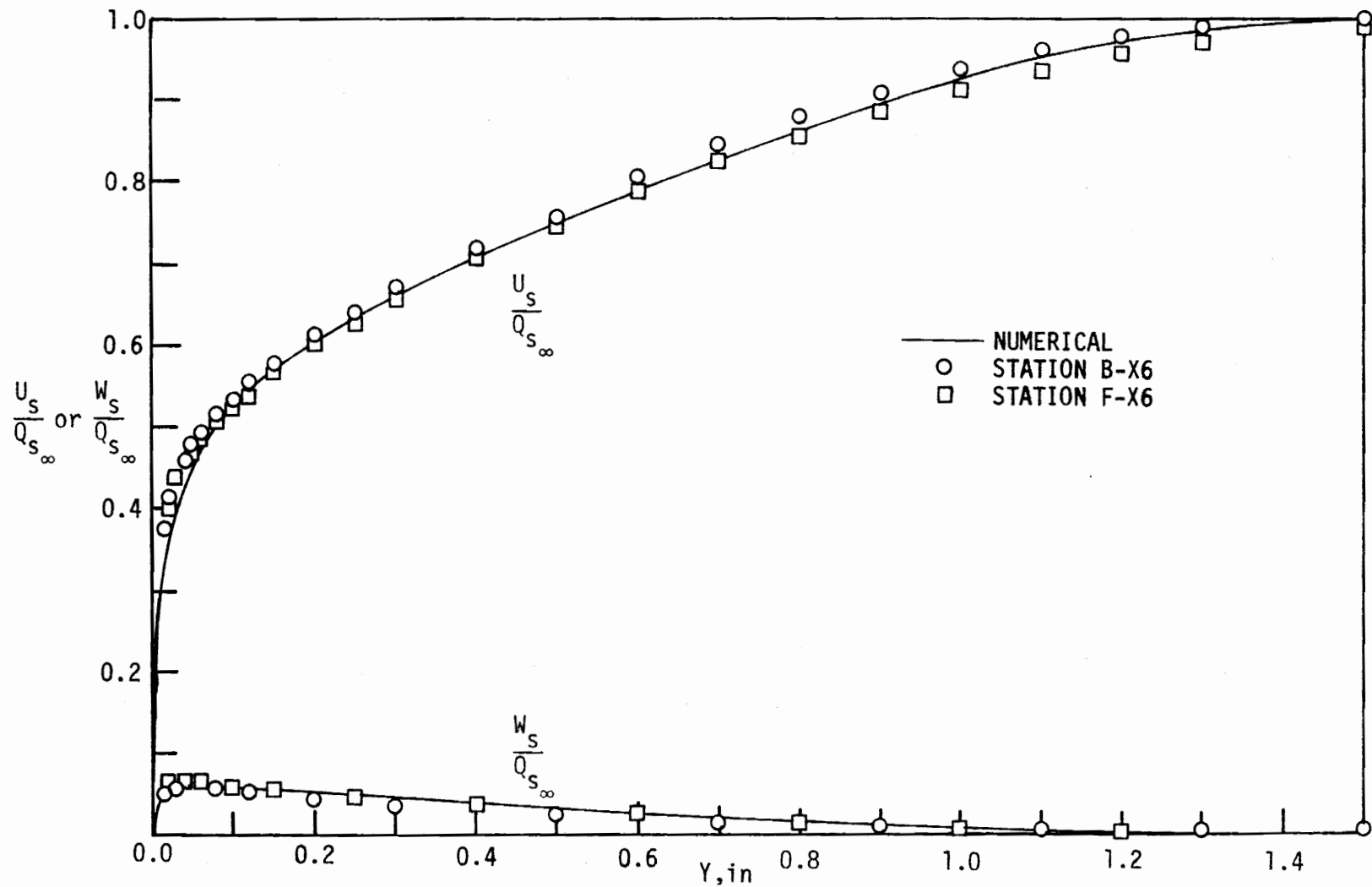


Fig. 4.20a U_s and W_s -Velocity Profiles Compared with Johnston's Experimental Data at Stations B-X6 and F-X6.

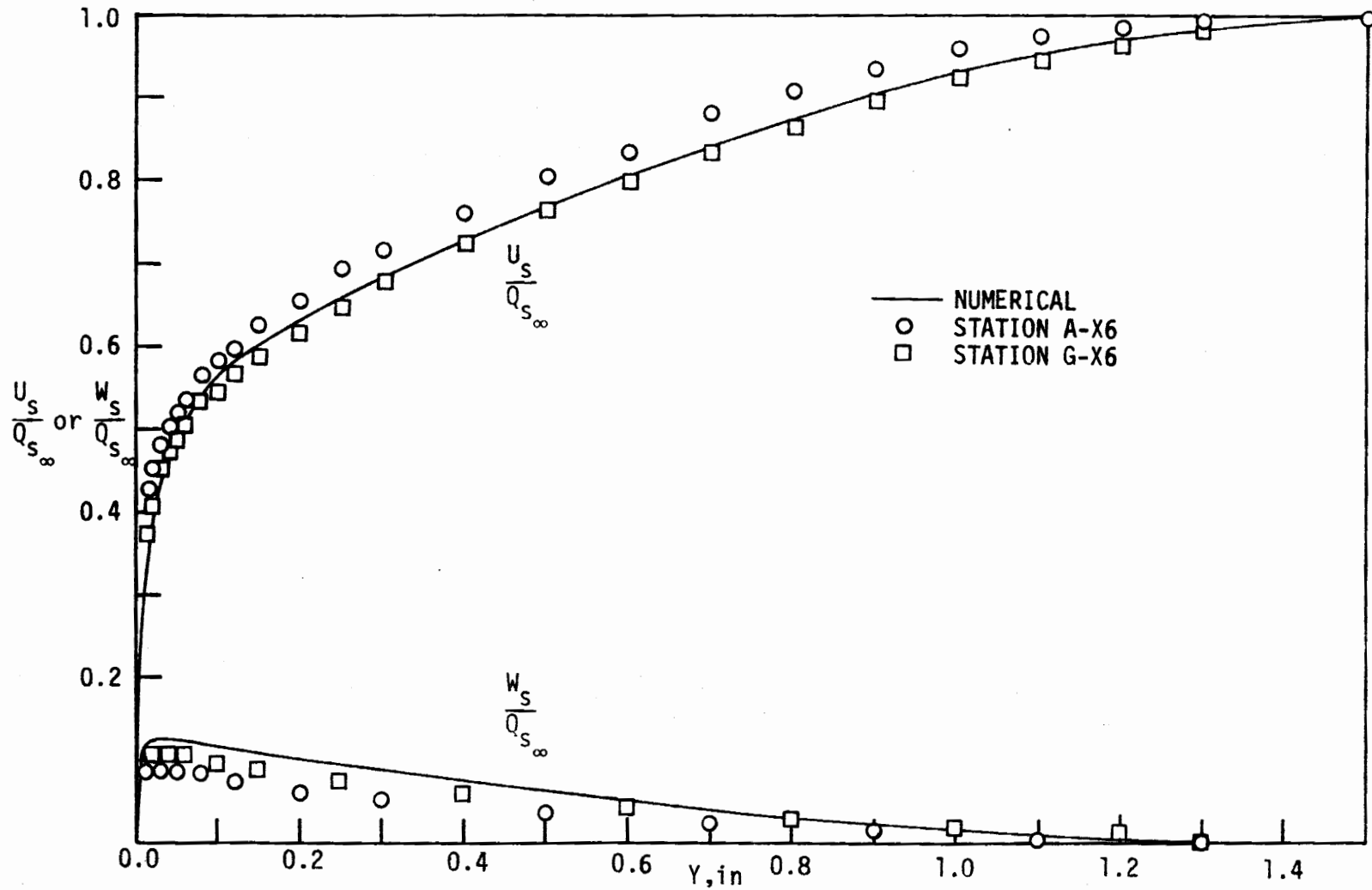


Fig. 4.20b U_s and W_s Velocity Profiles Compared with Johnston's Experimental Data at Stations A-X6 and G-X6.

the results of the present investigation indicated that the local streamline direction monotonically increased as the wall was approached as exhibited in Figs. 4.21 and 4.22 for two typical locations. This behavior was also detected by East. As shown in Fig. 4.23 a significant variation of the flow angle occurs in a very small region close to the wall and generally much closer to the wall than is accessible to ordinary experimental techniques. Rogers and Head [54] developed a probe that was especially designed for minimum interference with the fluid and they showed experimentally that the flow angle had a monotonically increasing characteristic in the near wall region.

The momentum thicknesses and the displacement thicknesses, with respect to a local streamline coordinate direction, are shown in Figs. 4.24 through 4.26. Again the predicted results were within the range of the experimental data presented by Johnston. These figures also illustrate the asymmetry of the flow with respect to the $z = 0$ plane.

Several parametric studies were undertaken to observe the dependency of the solution on the size of Δx , Δy , Δz . The Δx step was governed by Eq. 4.3 where σ was taken as the previously determined value of 0.003. Decreasing this value had negligible effect on the results. Increasing this value had negligible effect on the u -profile, but influenced the v -profile and tended to stave off the predicted separation point to a location further downstream. For example, with $\sigma = 0.005$ the point of separation

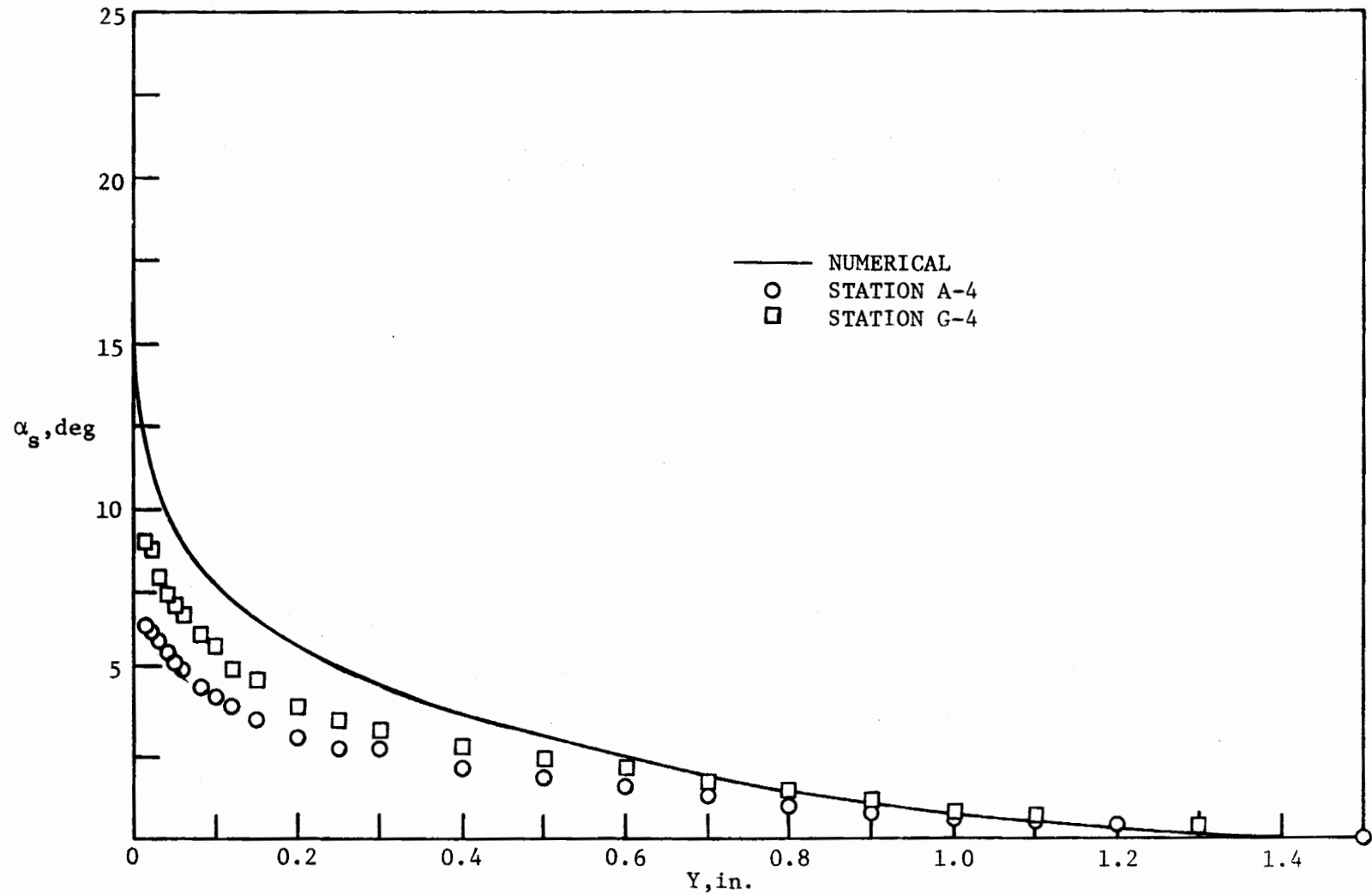


Fig. 4.21 Variation of Angle of Skewing Compared with Johnston's Experimental Data at Stations A-4 and G-4.

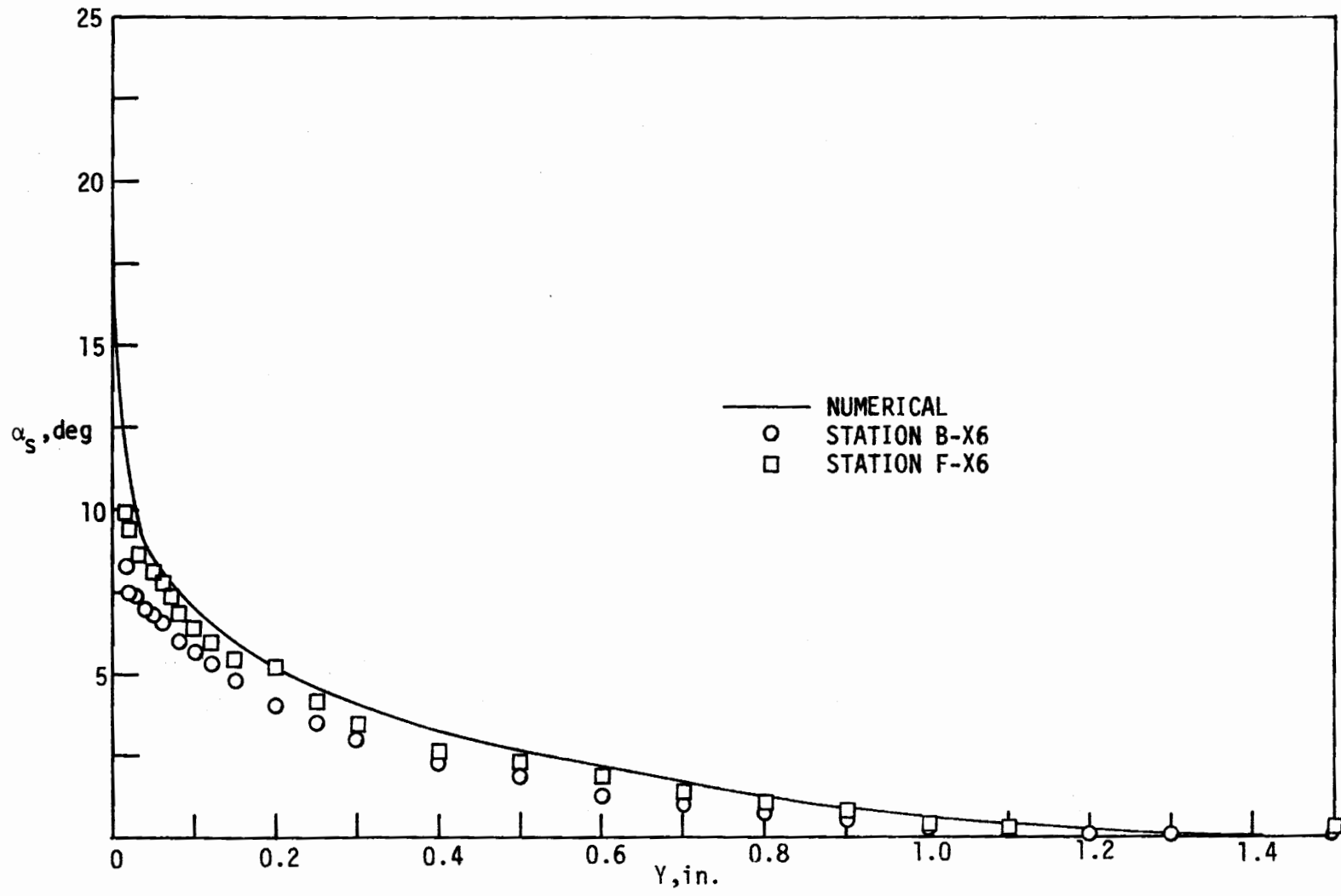


Fig. 4.22 Variation of Angle of Skewing Compared with Johnston's Experimental Data at Stations B-X6 and F-X6.

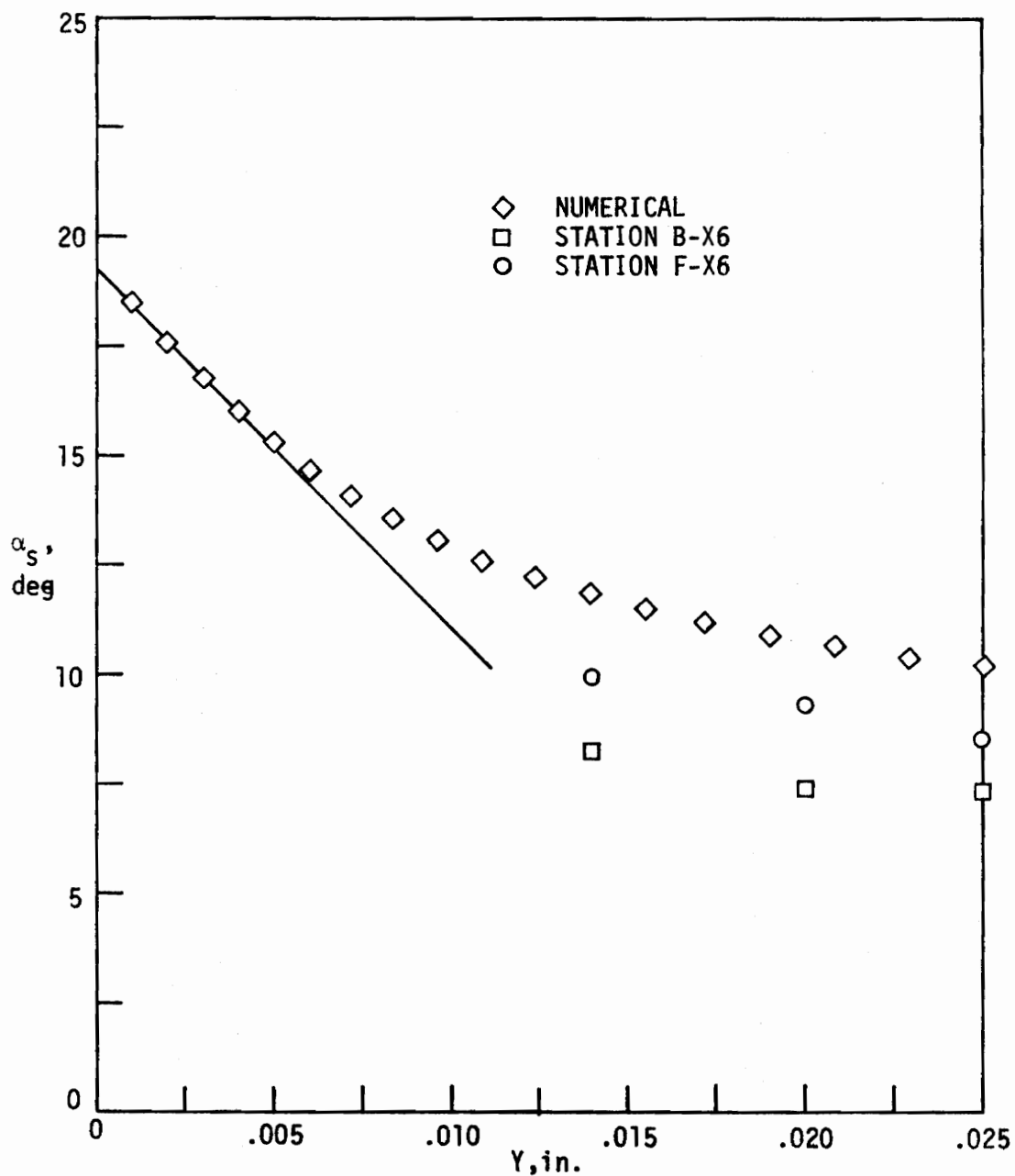


Fig. 4.23 Variation of Angle of Skewing in the Near Wall Region Compared with Johnston's Experimental Data at Stations B-X6 and F-X6.

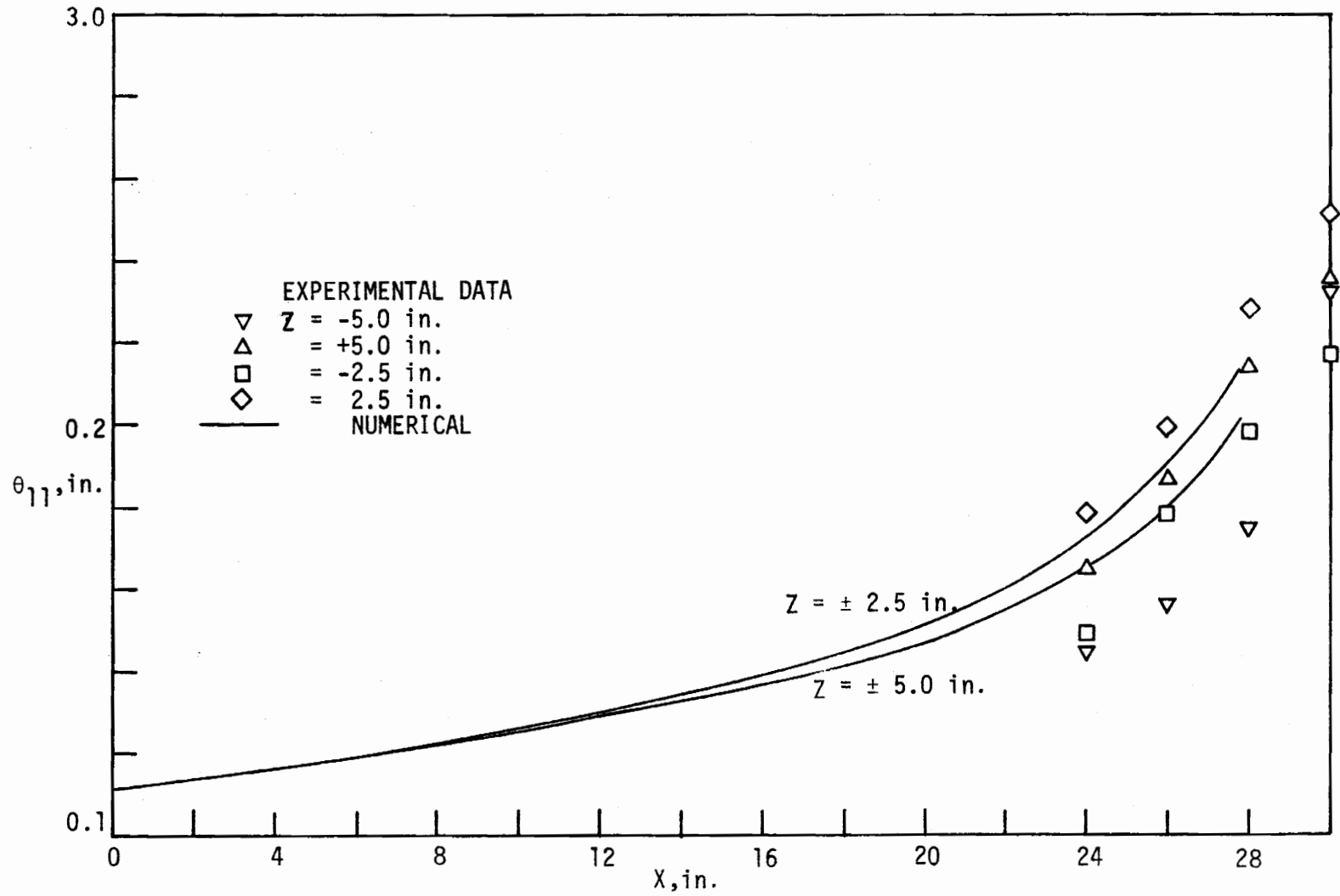


Fig. 4.24 Development of θ_{11} off the Plane of Symmetry Compared with Johnston's Experimental Data.

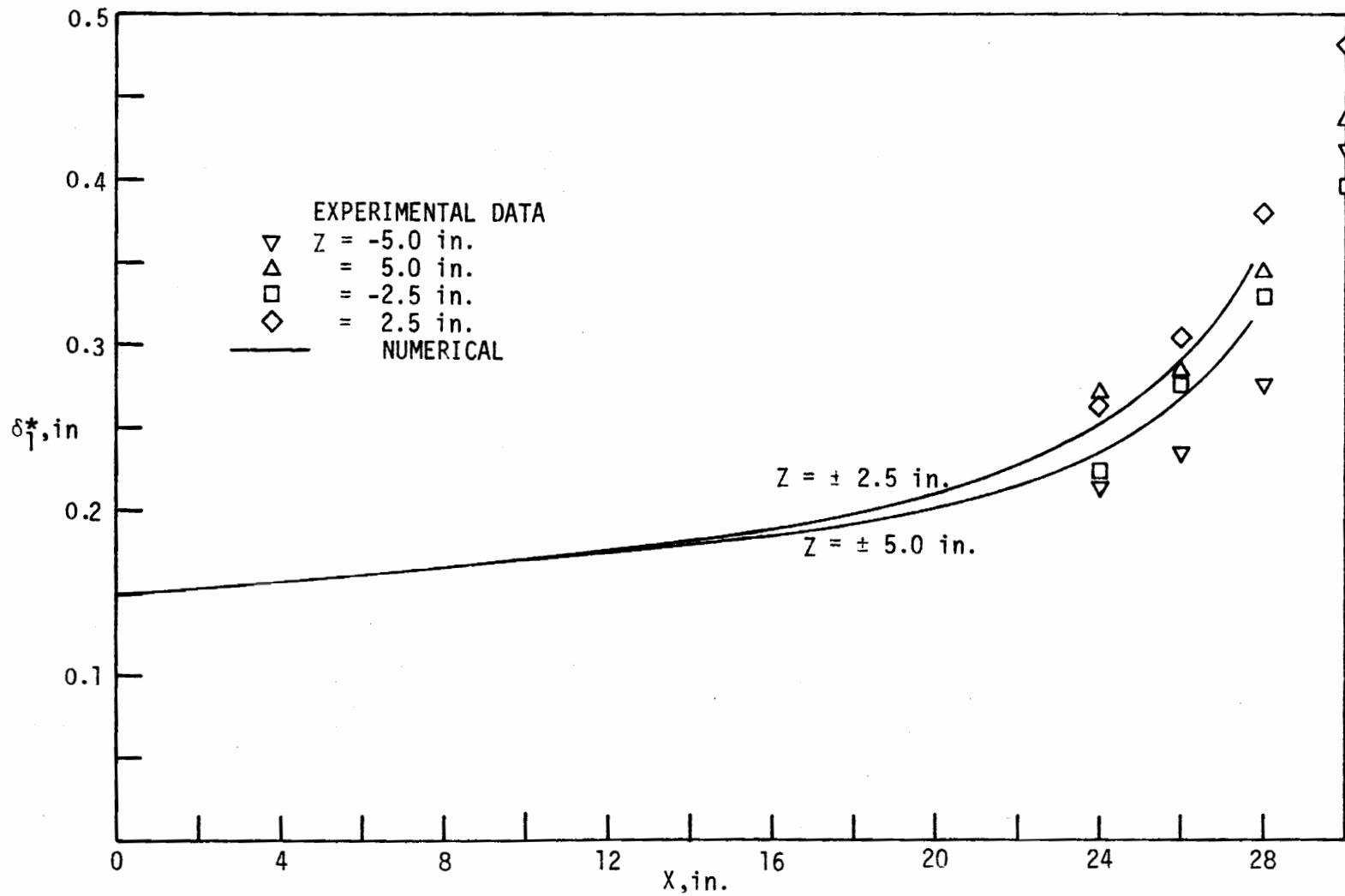


Fig. 4.25 Development of δ_1^* off the Plane of Symmetry Compared with Johnston's Experimental Data.

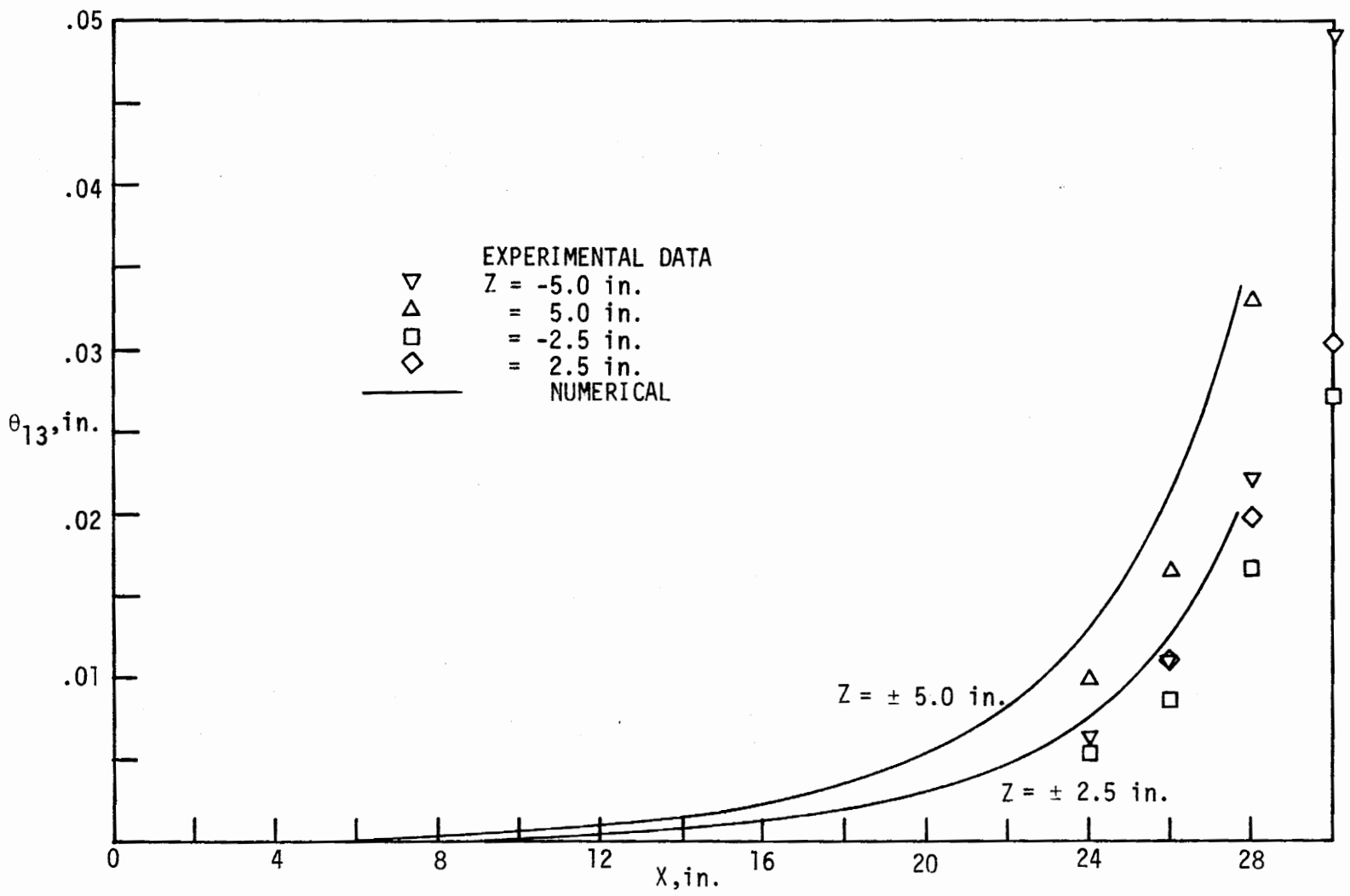


Fig. 4.26 Development of θ_{13} off the Plane of Symmetry Compared with Johnston's Experimental Data.

was located approximately 0.02 in. further downstream and the \bar{V} -velocity component at the free stream exhibited about a 25% decrease at a distance of 26 in. from the match point.

Instead of a successive increase of ΔY of 10% through the boundary layer from an initial ΔY of 0.001 in., a rate of increase of 6% was used. The differences between these two rates of increase were insignificant for the v -profile, but the u and w velocities near the wall changed by as much as 0.5% as separation was approached.

Halving the step size of ΔZ from 0.75 in. to 0.375 in. resulted in a small change (third significant digit changed by about one unit) and thus did not merit the increase of computer time.

To summarize, the values of the increments used were:

- i) $\Delta x = 0.003 u_{\infty} \left(\frac{du_{\infty}}{dx} \right)^{-1}$
- ii) $\Delta Y = 0.001$ in, until $Y = 0.005$ in.; then ΔY was successively increased by 6%
- iii) $\Delta Z = 0.75$ in.

The total run time for this solution including a 62 in. two-dimensional lead-in section was approximately 16 min and 30 sec on an IBM 360-65. This time does not include the 32 sec necessary for compiling when the object deck is unavailable.

To further substantiate the results of this program for three-dimensional turbulent boundary-layer flows, the Hornung and Joubert [29] geometry was investigated.

To match the profile at station 10, a two-dimensional turbulent boundary layer was developed from a distance of 22 ft from the

center of the cylinder to 4 ft from the center of the cylinder at which point the three-dimensional solution was initiated. The actual centerline of the cylinder was 17 ft down stream of the leading edge which was some 5 ft shorter than the necessary length to generate an adequate fit at station 10. The reason for this additional length was the presence of a slightly divergent inlet channel, which possibly imposed a small adverse pressure gradient, and resulted in an increased rate of boundary layer growth in this test section. The final match, shown in Fig. 4.27, was the result of several trial runs in which the inlet length was varied to allow the computed boundary layer thickness at station 10 to be approximately the same as the experimental value.

Figures 14.28 and 14.29 show the results of the Hornung and Joubert geometry at stations 12 ($Z = 6$ in.) and station 14 ($Z = 12$ in.), respectively. The results were in even better agreement with experiment than previously experienced in the Johnston geometry. The probable reason for this better agreement was the lesser influence of the confining boundaries. In the Hornung and Joubert geometry the test section dimensions were large compared to boundary layer thicknesses on the walls, the latter having a negligible influence on the potential flow in the center portions of the channel. For Johnston's apparatus the distance between the top and bottom surfaces was 8 in. and the boundary layer thickness was of order 1.5 in., and this close spacing caused the experimental velocities to deviate from the theoretical values due to the

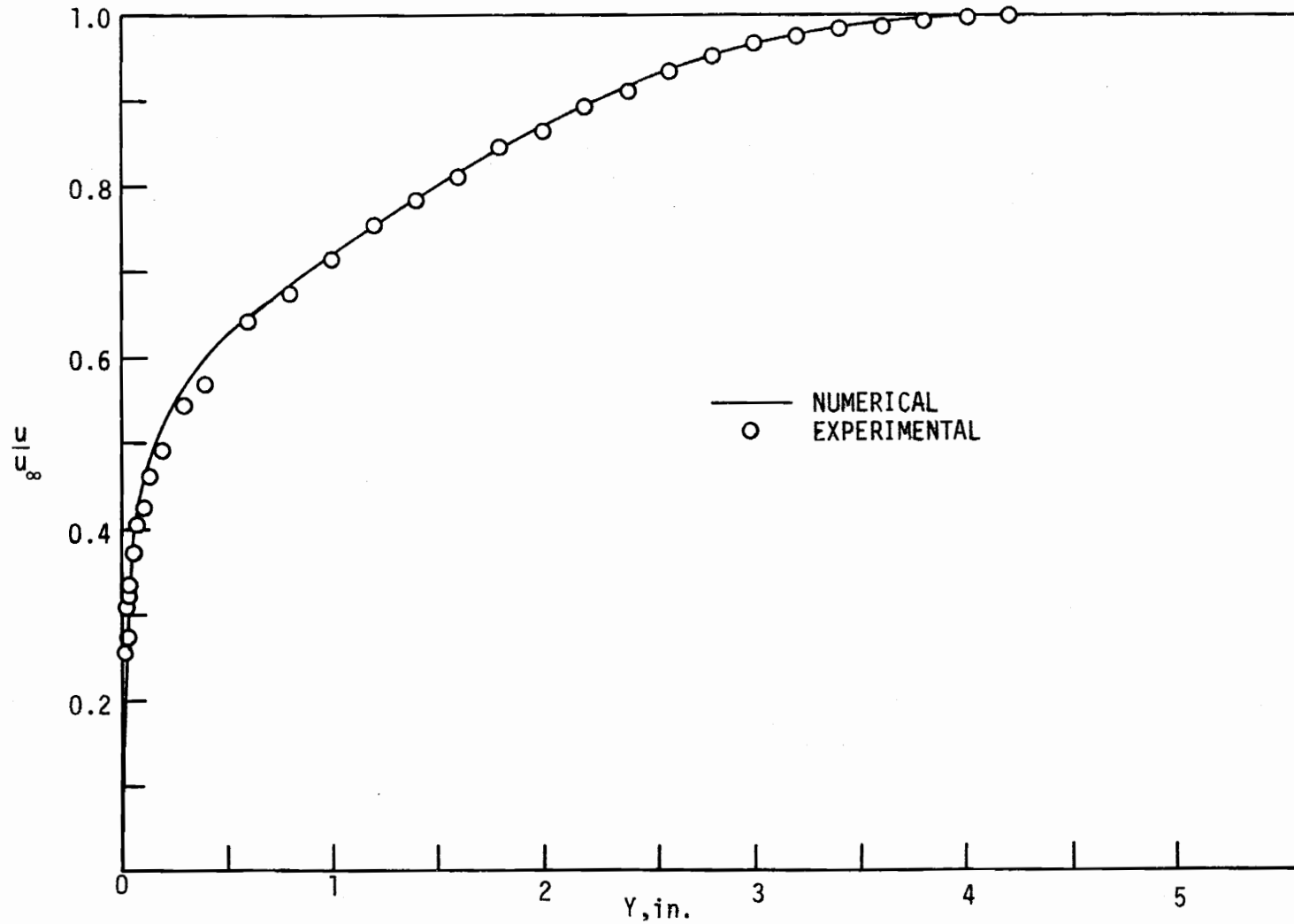


Fig. 4.27 \bar{u} -Velocity Profile Compared with Hornung and Joubert's Experimental Data at Station 10.

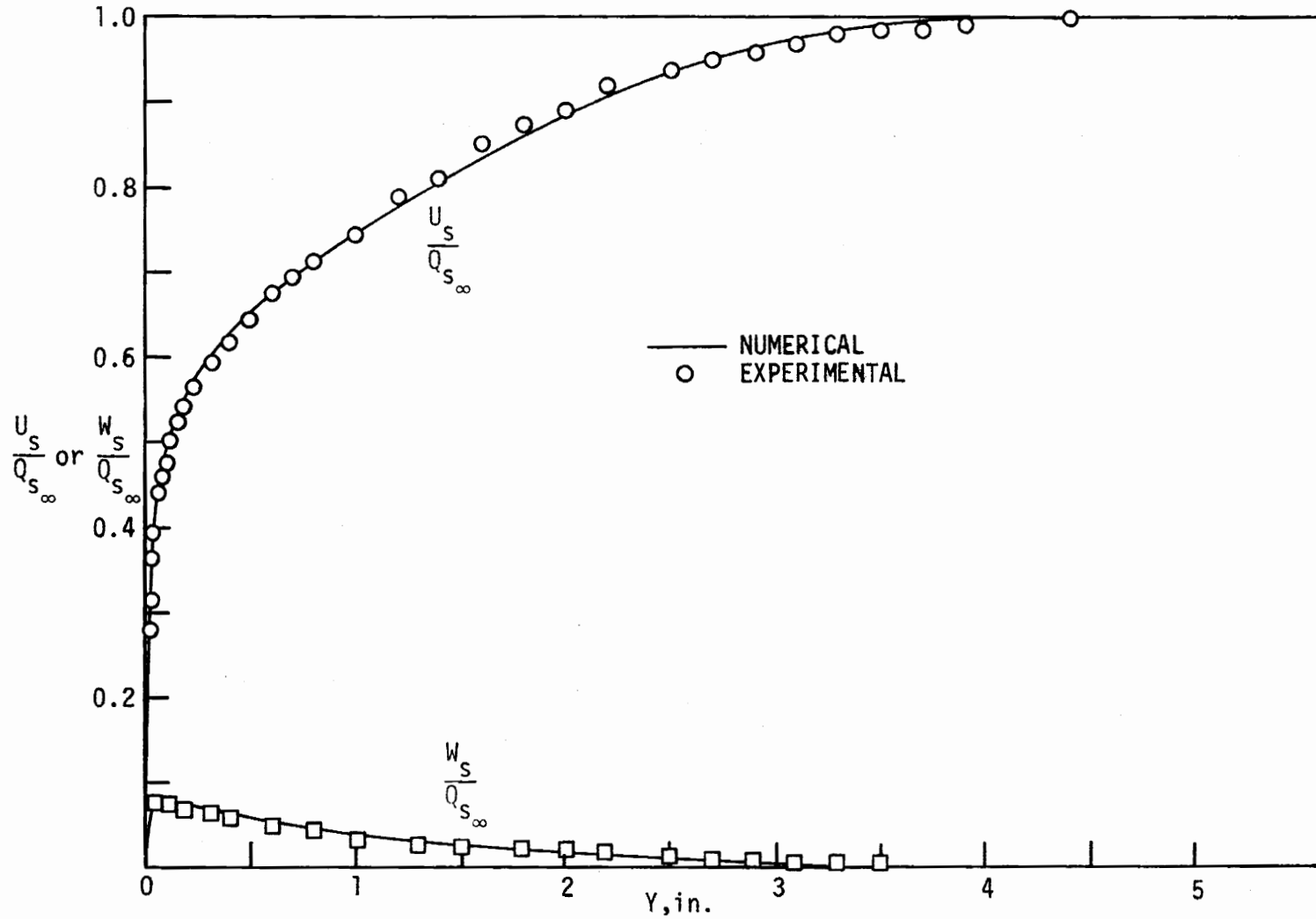


Fig. 4.28 U_s - and W_s -Velocity Profiles Compared with Hornung and Joubert's Experimental Data at Station 12.

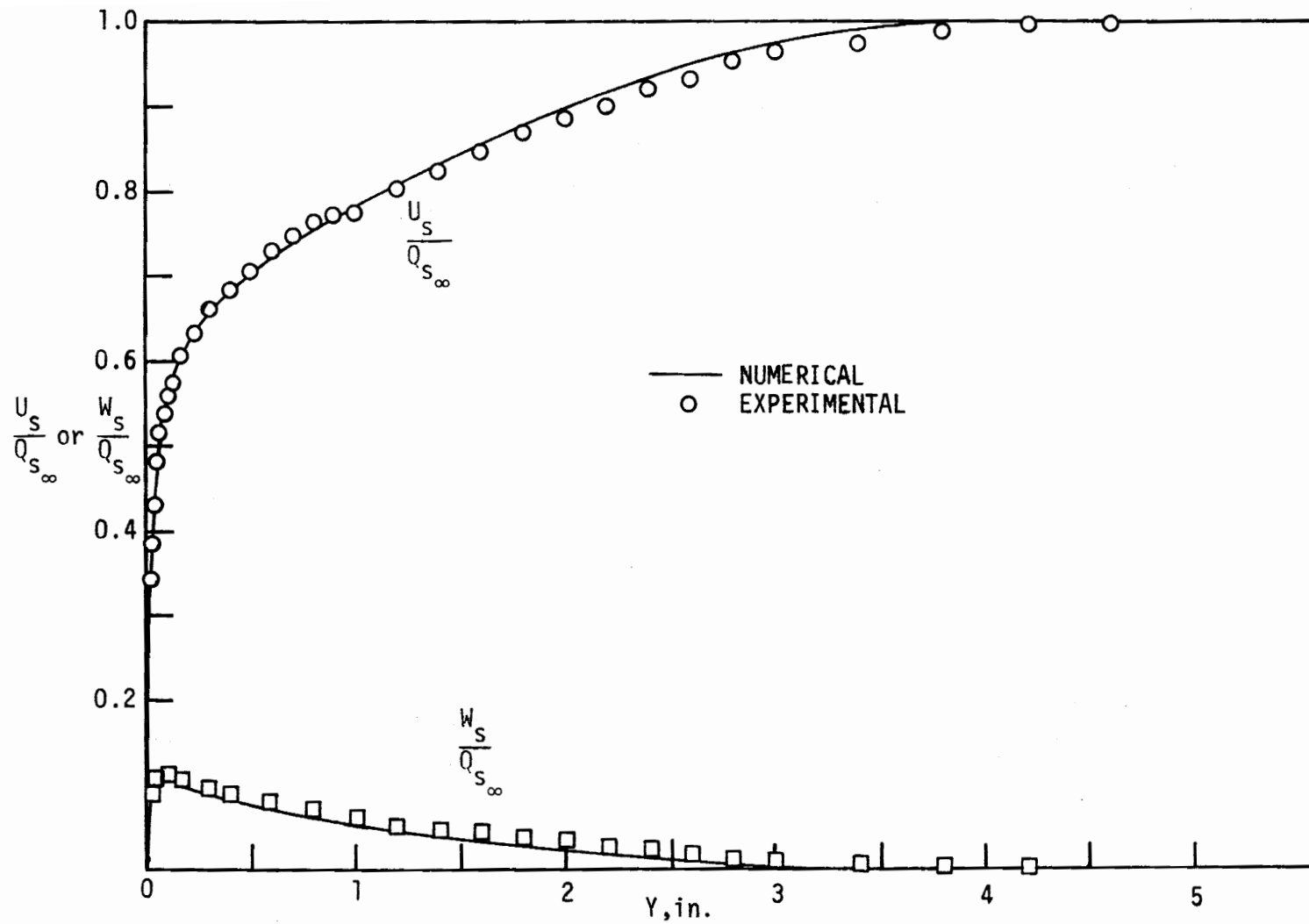


Fig. 4.29 U_s and W_s -Velocity Profiles Compared with Hornung and Joubert's Experimental Data at Station 14.

displacement effects of the boundary layers.

The solution was continued until the separation point was reached. Hornung and Joubert did not state explicitly at what position separation occurred. However, they did show a profile at station 9 for which back flow was not noted. The present program predicted separation on the plane of symmetry to occur at 2 in. before this experimental station. Again separation was determined by the boundary layer velocity near the surface being equal to or less than zero.

A parametric study was made to determine the step sizes necessary to insure their negligible influence on the results. Again, the x step size was governed by Eq. 4.3 with $\sigma = 0.003$ with insignificant change for smaller values of σ . Because of the greater thickness of the boundary layer for this geometry the Y increment near the wall was 0.002 in. for five locations and subsequently was increased by 6% as determined by the Johnston geometry. The value for ΔZ was 1.5 in. and a reduction of this value to 1 in. affected the \bar{U} and \bar{W} profiles by less than 0.05% at location 12.

The total computer time required for the solution for the Hornung and Joubert geometry was about 13 min. This time also included the 18 ft distance required to develop the two-dimensional boundary-layer in the lead-in sections. Again, compiling time is not given since for production runs an object deck would be used to obviate the necessity of repeated compilations of the program.

Since the shear stress profiles were not measured in either the Johnston or the Hornung and Joubert experiments, direct comparison with measured data was impossible. However, the shape of these profiles are of general interest in three-dimensional flows since they were determined from a scalar mixing length hypothesis. Figures 4.30 and 4.31 show typical shear stress profiles in both the X and Z directions, respectively.

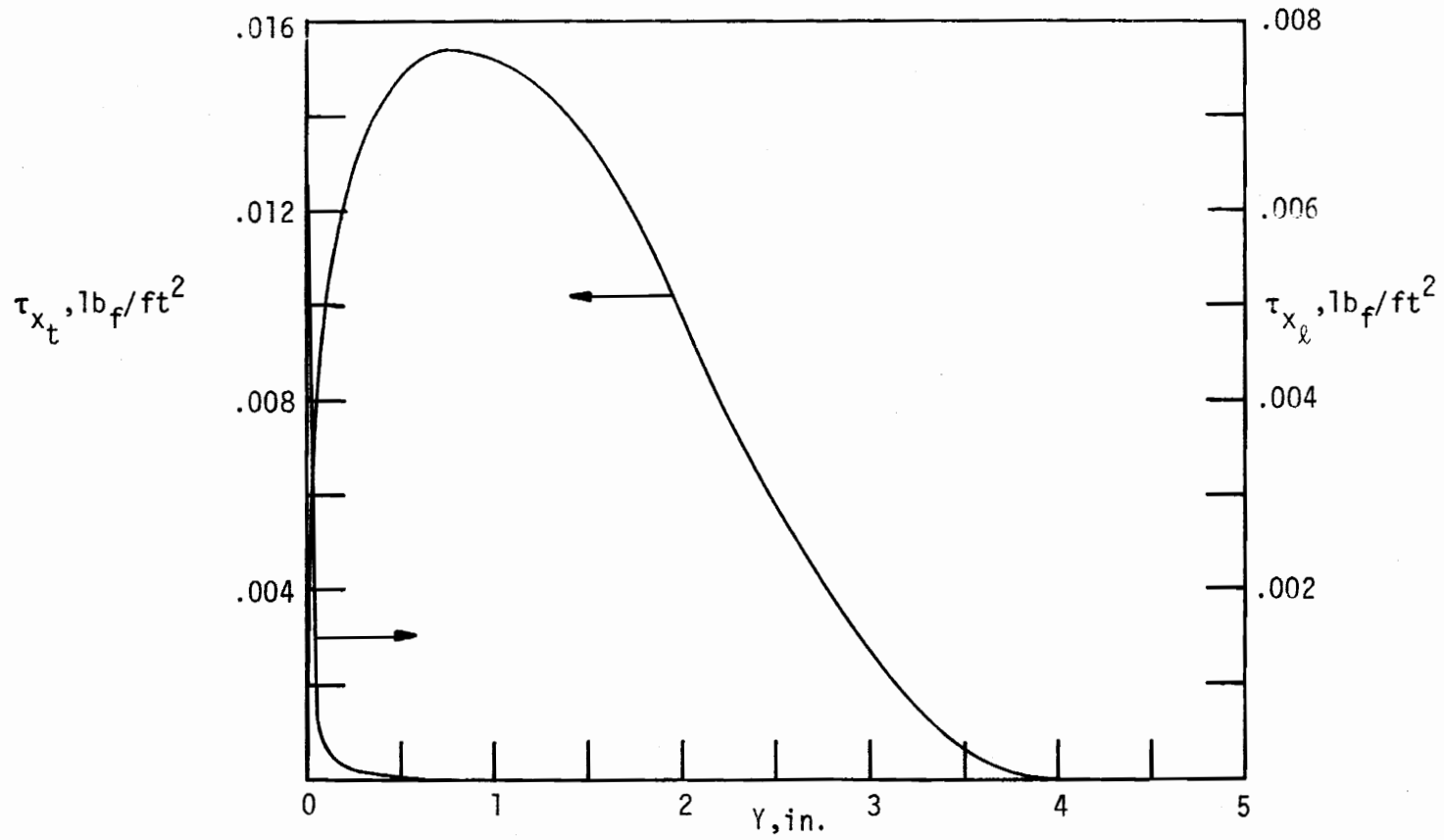


Fig. 4.30 Variation of the X Component of the Laminar and Turbulent Shear Stress, Hornung and Joubert Station 12.

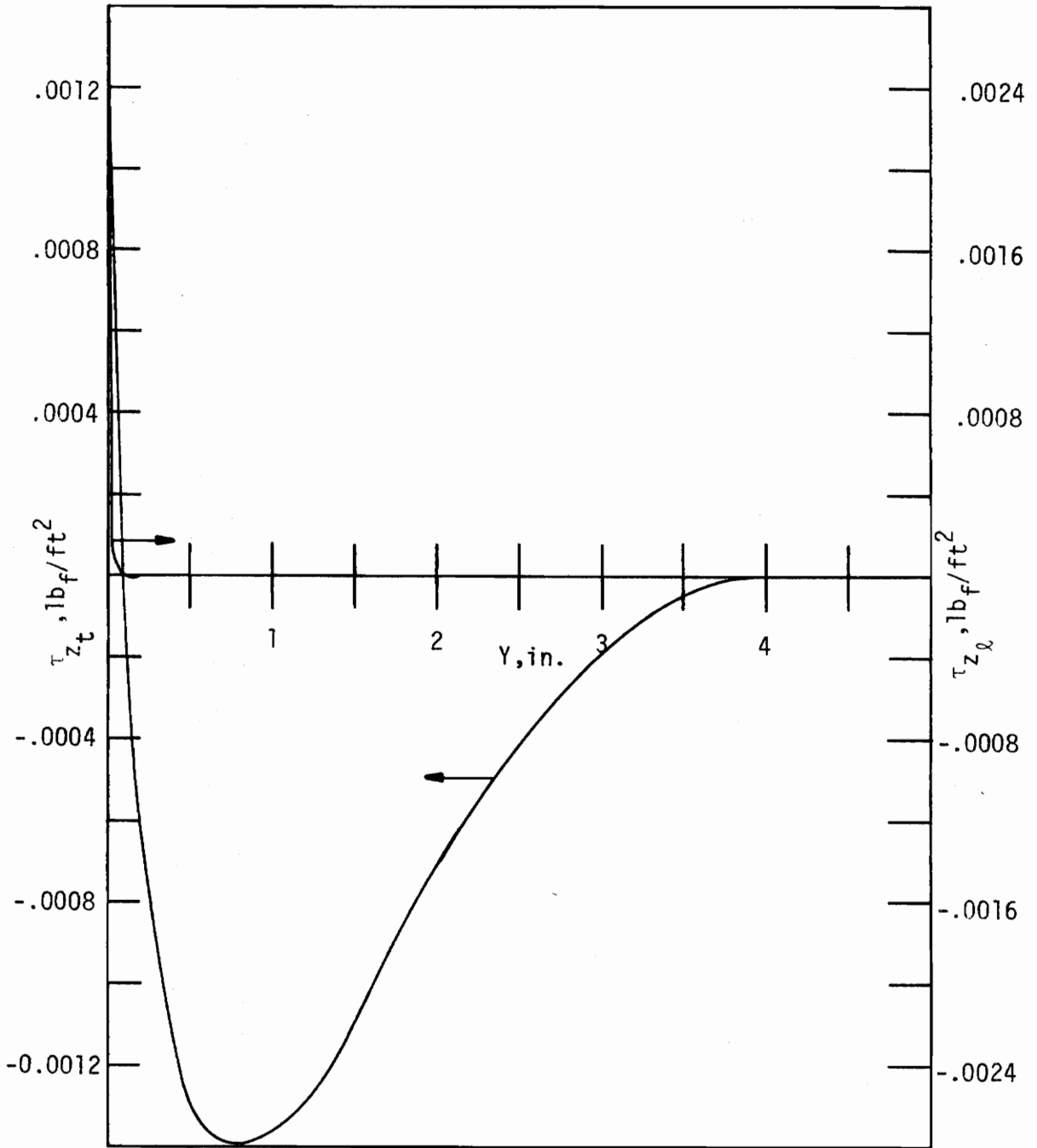


Fig. 4.31 Variation of the Z Component of the Laminar and Turbulent Shear Stress, Hornung and Joubert Station 12.

V. SUMMARY AND CONCLUSIONS

A technique is presented to solve the equations of motion for a broad class of both two-dimensional and three-dimensional turbulent boundary-layer flows. An extension of the implicit numerical finite difference technique, presented by Crank and Nicholson [37] for unsteady heat conduction, to the three-dimensional equations of motion was introduced to cast the partial differential equations in a finite difference form.

The method assumed that an eddy viscosity model expressed in terms of a mixing length was known and the program was sufficiently generalized to allow the adaptation and subsequent introduction of other experimental correlations as they become available. The mixing length model chosen for this investigation is given by Pletcher [11]. The model was generalized to three-dimensional flows as given by Prandtl (see Goldstein [34]) and the mixing length was treated as a scalar function.

The final finite-difference equations were cast into a form such that the corresponding matrix of coefficients to be solved were in a tridiagonal form and were easily solved using the Thomas algorithm [31].

This numerical technique was applied to two-dimensional laminar and turbulent boundary-layer flows and three-dimensional turbulent boundary-layer flows from which the following observations and conclusions were obtained:

1. The Crank-Nicholson finite-difference scheme for writing finite-difference equations yielded a stable and convergent method for all the cases tested.
2. The Blasius profile for laminar two-dimensional zero pressure gradient flows was predicted and good agreement with the theoretical profile was obtained.
3. The form of the continuity equation was critical when the \bar{V} - velocity profile was unknown as an initial condition.
4. The mixing length hypothesis model yielded good results for two-dimensional turbulent flows in both zero and adverse external pressure gradient flows. For three-dimensional turbulent boundary-layer flows the results were in good agreement when compared to experimental data.
5. The computational time required for the Johnston [28] and the Hornung and Joubert [29] geometries was at least five times faster than the explicit Dufort-Frankel finite difference technique presented by East [27], for the same flow circumstances.
6. The concept of a collateral near-wall layer for a three-dimensional turbulent boundary layer was not substantiated by the present analysis.

7. More experimental turbulence data in three-dimensional turbulent boundary layer flow circumstances are required to further validate and improve the turbulent-shear stress model.

VI. BIBLIOGRAPHY

1. Spalding, D. B., "Theories of the Turbulent Boundary Layer," Applied Mechanics Reviews, Vol. 20, No. 8, August 1967.
2. Pierce, F. J., and D. H. Krommenhoek, "Wall Shear Stress Diagnostics in Three-Dimensional Turbulent Boundary Layers," Interim Technical Report No. 2, USARO-D Project No. 6858E, September, 1968, (AD 680 973).
3. Thompson, B. G. J., "A Critical Review of Existing Methods of Calculating the Turbulent Boundary Layer," ARC R&M 3447, Ministry of Supply, Great Britain, 1964.
4. Hinze, J. O., Turbulence, Chapter 1, McGraw-Hill Book Company, Inc., New York, 1959.
5. Prandtl, L., "Über die ausgebildete Turbulenz," a lecture delivered at Zurich in September, 1926, before the International Congress for Applied Mechanics, (translated as "Turbulent Flow"), NACA TM 435, 1927.
6. Townsend, A. A., "Equilibrium Layers and Wall Turbulence," Journal of Fluid Mechanics, Vol. II, pp. 97-120, August 1961.
7. van Driest, E. R., "On Turbulent Flow Near a Wall," Journal of the Aeronautical Sciences, pp. 1007-1011, November 1956.
8. Cebeci, T., "Calculation of Compressible Turbulent Boundary Layers with Heat and Mass Transfer," AIAA Paper NO. 70-741 presented at the AIAA 3rd Fluid and Plasma Dynamics Conference, June 1970.
9. Mellor, G. L., "The Effects of Pressure Gradients on Turbulent Flow Near a Smooth Wall," Journal of Fluid Mechanics, Vol. 24, part 2, pp. 255-274, 1966.
10. Mellor, G. L., and D. M. Gibson, "Equilibrium Turbulent Boundary Layers," Journal of Fluid Mechanics, Vol. 24, part 2, pp. 225-253, 1966.
11. Pletcher, R. H., "On a Finite-Difference Solution for the Constant-Property Turbulent Boundary Layer," AIAA Journal, Vol. 7, No. 2, pp. 305-311, 1969.
12. Maise, G., and H. McDonald, "Mixing Length and Kinematic Eddy Viscosity in a Compressible Boundary Layer," AIAA Journal, Volume 6, No. 1, pp. 73-80, 1968.

13. Bradshaw, P., D. H. Ferris, and N. P. Atwell, "Calculation of Boundary-Layer Development Using the Turbulent Energy Equation," *Journal of Fluid Mechanics*, Vol. 28, part 3, pp. 593-616, 1967.
14. Bradshaw, P., "Calculation of Boundary-Layer Development Using the Turbulent Energy Equation, VII: Three-Dimensional Flow," National Physical Laboratory, AERO Report 1286, 1969.
15. Nash, J. F., "The Calculation of Three-Dimensional Turbulent Boundary Layers in Incompressible Flow," *Journal of Fluid Mechanics*, Vol. 37, part 4, pp. 625-642, 1969.
16. Donaldson, C. duP., and H. Rosenbaum, "Calculation of Turbulent Shear Flows Through Closure of the Reynolds Equations by Invariant Modeling," Compilation of Papers Presented at Symposium on Compressible Turbulent Boundary Layers, Sponsored by Langley Research Center, pp. 10.1-10.23, December 1968.
17. Smith, A. M. O., and T. Cebeci, "Numerical Solution of the Turbulent Boundary-Layer Equations," McDonnell Douglas, Report No. DAC 33735, May 1967.
18. Hartree, D. R., and J. R. Womersley, "A Method for the Numerical or Mechanical Solution of Certain Types of Partial Differential Equations," *Proc. Roy. Soc. (London)*, p. 353, 1937.
19. Smith, A. M. O., and D. W. Clutter, "Machine Calculation of Compressible Laminar Boundary Layers," *AIAA Journal*, Vol. 3, No. 4, pp. 639-647, 1965.
20. Smith, A. M. O., N. A. Jaffe, and R. C. Lind, "Study of a General Method of Solution of the Incompressible Turbulent Boundary Layer Equations," Douglas Aircraft Division, Report No. LB-52949, November 1965.
21. Mellor, G. L., "Incompressible, Turbulent Boundary Layers with Arbitrary Pressure Gradients and Divergent or Convergent Cross Flows," *AIAA Journal*, Vol. 5, No. 9, pp. 1570-1579, 1967.
22. Der, J., and G. S. Raetz, "Solution of General Three-Dimensional Laminar Boundary-Layer Problems by an Exact Numerical Method," IAS Paper No. 62-70, January 1962.
23. Dwyer, H. A., "Solution of a Three-Dimensional Boundary-Layer Flow with Separation," *AIAA Journal*, Vol. 6, No. 7, pp. 1336-1342, 1968.
24. Sowerby, L., "The Three-Dimensional Laminar Boundary Layer on a Flat Plate," *Journal of Fluid Mechanics*, Vol. 22, part 3, pp. 587-598, 1965.

25. Flügge-Lotz, I., and F. G. Blottner, Technical Report Number 131, 1962, Division of Engineering Mechanics, Stanford University, California. See also Applied Mechanics Reviews, Vol. 15, 1962.
26. Fussell, D. D., "The Study of Numerical Methods for Solving the Laminar Boundary Layer Equations," Doctoral Dissertation, Rice University, Houston, Texas, 1965.
27. East, J. L., "An Exact Numerical Solution of the Three-Dimensional Incompressible Turbulent Boundary Layer Equations," Doctoral Dissertation, Virginia Polytechnic Institute and State University, Blacksburg, Virginia, 1970.
28. Johnston, J. P., "Three-Dimensional Turbulent Boundary Layer," MIT Gas Turbine Lab. Report No. 39, 1957.
29. Hornung, H. G., and P. N. Joubert, "The Mean Velocity Profile in Three-Dimensional Turbulent Boundary Layers," Journal of Fluid Mechanics, Vol. 15, part 3, pp. 368-384, 1962.
30. Hunt, J. L., D. M. Bushnell, and I. E. Beckwith, "Finite-Difference Analysis of the Compressible Turbulent Boundary Layer on a Blunt Swept Slab with Leading-Edge Blowing," Analytical Methods in Aircraft Aerodynamics, NASA SP-228, pp. 417-472, Oct. 1969.
31. Ames, W. F., Numerical Methods for Partial Differential Equations, Barnes and Noble, Inc., New York, 1969.
32. Schlichting, H., Boundary Layer Theory, Chapters 7, 18 and 19, Fourth Edition, McGraw-Hill Book Company, Inc., New York, 1960.
33. Frederick, D., and T. S. Chang, Continuum Mechanics, chapter 3, Allyn and Bacon, Inc., Boston, 1965.
34. Goldstein, S., Modern Developments in Fluid Dynamics, Vol. 1, Dover Publications, Inc., pp. 205-210, 1965.
35. Laufer, J., "The Structure of Turbulence in Fully Developed Pipe Flow," NACA TN 2954, June 1953.
36. Coles, D., "The Turbulent Boundary Layer in a Compressible Fluid," RAND Corp. Report No. R-403-PR, September 1962.
37. Crank, J., and P. Nicholson, "A Practical Method for Numerical Evaluation of Solutions of Partial Differential Equations of the Heat Conduction Type," Proc. Cambridge Philos. Soc., Vol. 43, pp. 50-67, 1947.

38. Wu, J. C., "The Solution of Laminar Boundary-Layer Equations by the Finite Difference Method," Douglas Aircraft Company, Inc., Report No. SM-37484, June 1960.
39. Coles, D., "The Law of the Wake in the Turbulent Boundary Layer," *Journal of Fluid Mechanics*, Vol. I, Part 2, pp. 191-226, 1956.
40. Milne-Thompson, L. M., Theoretical Hydrodynamics, The MacMillan Company, New York, 1960.
41. Pai, Shih-I, Fluid Dynamics of Jets, D. Van Nostrand Company, Inc., New York, pp. 9-13, 1954.
42. Traub, J. F., "The Solution of Transcendental Equations," Mathematical Methods for Digital Computers, John Wiley and Sons, Inc., New York, Vol. 2, pp. 171-184, 1967.
43. Richtmyer, R. D., and K. W. Morton, Difference Methods for Initial-Value Problems, Interscience Publishers, New York, second ed., 1967.
44. Ludwig, H., and W. Tillmann, "Investigations of the Wall Shearing Stress in Turbulent Boundary Layers," NACA TM 1285, 1950.
45. Schubauer, G. B., and P. S. Klebanoff, "Investigation of Separation of the Turbulent Boundary Layer," NACA TM 2133.
46. Coles, D. E., and E. A. Hirst, Proceedings: Computation of Turbulent Boundary Layers - 1968 AFOSR - IFP - Stanford Conference, Stanford University, 1969.
47. Johnston, J. P., "Measurements in a Three-Dimensional Turbulent Boundary Layer Induced by a Swept, Forward-Facing Step," *Journal of Fluid Mechanics*, Vol. 42, part 4, pp. 823-844, 1970.
48. Francis, G. P., and F. J. Pierce, "An Experimental Study of Skewed Turbulent Boundary Layers in Low Speed Flows," *Trans. ASME, Journal of Basic Engineering*, Vol. 89, Series D, 1967.
49. Klinksiek, W. F., and F. J. Pierce, "Simultaneous Lateral Skewing in a Three-Dimensional Turbulent Boundary Layer Flow," *Trans. ASME, Journal of Basic Engineering*, Vol. 92, Series D, 1970.
50. Gardow, E., "The Three-Dimensional Turbulent Boundary Layer in a Free Vortex Diffuser," MIT Gas Turbine Laboratory Report No. 42, 1958.

51. Smith, M., "Incompressible Skewed Turbulent Boundary Layer on an End Wall of a Curved Two-Dimensional Diffuser," Doctoral Dissertation, Iowa State University of Science and Technology, Ames, Iowa, 1970.
52. Smith, P. D., "An Investigation into Three-Dimensional Boundary Layers," Doctoral Dissertation, University of London, London, England, 1965.
53. Lewkowicz, A., "Two and Three-Dimensional Incompressible Turbulent Boundary Layers," Doctoral Dissertation, University of Liverpool, Liverpool, England, 1965.
54. Rogers, B. K., and M. R. Head, "Measurements of Three-Dimensional Boundary Layers," *Aero. Journ. of the Royal Aeronautical Society*, Vol. 73, pp. 796-798, 1969.

VII. APPENDIX A

COMPUTER PROGRAM

Appendix A contains the general three-dimensional computer program for the Johnston geometry. Included at the end of the appendix is subroutine POT for the Hornung and Joubert geometry which would be used in place of subroutine POT presented for the Johnston geometry. The input parameters are defined at the beginning of the main program to indicate the appropriate data cards necessary to generate two- or three-dimensional, laminar or turbulent flow solutions.

```

C                               DATA CARD INFORMATION
C   DATA CARD NUMBER 1 READS Q0,Q,B,DEN,VISQ,XX,DZ ON THE FORMAT
C       3F10.4,2F11.9,2F10.6
C   DATA CARD 2 READS STSEL ON THE FORMAT
C       D20.7
C   DATA CARD 3 READS N(1),KK,LL,MM,NN ON THE FORMAT
C       5I5
C   DATA CARD 4 READS X(1) ON THE FORMAT
C       D20.7
C   DATA SET 5 (ONLY IF INITIAL PROFILE IS TO BE READ IN) READS
C   Y(1,J),U(1,J,1),V(1,J,1) ON THE FORMAT
C       3D20.7
C   DATA CARD 6 READS MOTI,MOTJ ON THE FORMAT
C       2I5
C   DATA SET 7 (ONLY IF OUTPUT IS DESIRED AT SPECIFIED X LOCATIONS)
C   READS XOUT(J) ON THE FORMAT
C       6F10.6
C   DATA CARD 8 READS NS,CHANGE ON THE FORMAT
C       I5,F10.7

```

```

C                               DEFINITION OF INPUT PARAMETERS
C   U     REFERENCE VELOCITY, FT/SEC.
C   U     VELOCITY AT FIRST X LOCATION, FT/SEC.
C   B     REFERENCE LENGTH, IN.
C   DEN   DENSITY, LBM/FT**3.
C   VISQ  DYNAMIC VISCOSITY, LBM/FT/SEC.
C   XX    DISTANCE FOR THE TWO-DIMENSIONAL SOLUTION, IN.
C   DL    X-INCREMENT SIZE, IN.
C   STSEL DISTANCE FOR ONLY THE THREE-DIMENSIONAL SOLUTION, IN.
C   N(1)  NUMBER OF Y LOCATIONS MINUS ONE.
C   KF    =1 LEADING EDGE SOLUTION.
C         =2 GIVEN INPUT TWO-DIMENSIONAL PROFILE ON THE PLANE OF

```

```

C          SYMMETRY.
C  LL      =1  LAMINAR FLOW ONLY.
C          =2  TURBULENT FLOW ONLY.
C  NN      =1  TWO-DIMENSIONAL FLOW ONLY.
C          =2  TWO-DIMENSIONAL FLOW TO PLANE OF SYMMETRY FLOW.
C          =3  TWO-DIMENSIONAL FLOW TO PLANE OF SYMMETRY FLOW AND
C          THREE-DIMENSIONAL FLOW.
C          =4  PLANE OF SYMMETRY AND THREE-DIMENSIONAL FLOW OR
C          TWO-DIMENSIONAL PRESSURE GRADIENT FLOW.
C  NZ      NUMBER OF Z LOCATIONS.
C  X(1)    INITIAL VALUE OF X, IN.
C  Y(1,J)  VALUES OF Y AT EACH NODE LOCATION EXCLUDING TH SURFACE
C          CONDITIONS, IN.
C  U(1,J,1) INITIAL VALUES OF THE U COMPONENT OF VELOCITY AT EACH
C          NODE LOCATION EXCLUDING THE SURFACE CONDITIONS, FT/SEC.
C  V(1,J,1) INITIAL VALUES OF THE V COMPONENT OF VELOCITY AT EACH
C          NODE LOCATION EXCLUDING THE SURFACE CONDITION, FT/SEC.
C  MDTI    THE FREQUENCY AT WHICH OUTPUT IS DESIRED IF NO SPECIFIC
C          OUTPUT LOCATION IS NAMED.
C  MDTJ    THE NUMBER OF SPECIFIC X LOCATIONS THAT THE OUTPUT IS
C          DESIRED. IF MDTJ IS NOT EQUAL TO ZERO THIS PARAMETER
C          OVER RIDES THE MDTI OUTPUT PARAMETER.
C  XDTJ    THE OUTPUT X LOCATIONS REFERRED TO BY MDTJ, IN.
C  NS      THE NUMBER OF SMALL X STEPS TO BE TAKEN BEFORE THE
C          X-INCREMENT SIZE IS INCREASED.
C  CHANGE  THE VALUE OF SIGMA DESIRED TO GOVERN THE X-DIRECTION
C          INCREMENT SIZE.
C  WITHIN THE PROGRAM THESE SEQUENCING VARIABLES ARE USE TO DIRECT THE
C  SOLUTION TO VARIOUS SEGMENTS OF THE PROGRAM.
C          LLX =1 LAMINAR, =2 TURBULENT
C          MXX =1 TWO-DIMENSIONAL
C          =2 PLANE OF SYMMETRY

```



```

C           =3 PLANE OF SYMMETRY AND THREE-DIMENSIONAL OR PRESSURE
C           GRADIENT
C           KKK - NUMBER OF LOCAL Z-LOCATIONS
C
      IMPLICIT REAL*8(A-H,O-Z)
      COMMON U(2,100,10),V(2,100,10),W(2,100,10),WZ(2,100,2),EM(2,100,10
1),Y(2,100),X(2),Z(10),DPYX(2),VALUE(100),CC,0,8,VISK,VISC,DEN,XX,R
2EYS,DX1,STSDU
      COMMON N(2),KK,LL,MM,NN,KKK,RNX,LLX,NUMBER
      DIMENSION A(100),S(100),C(100),BP(100),D(2,100),DD(100),XOUT(20)
C INITIALIZATION OF THE VARIOUS PARAMETERS
      MCOUNT=0
      NUMBER=0
      CALL INPRO
      READ(5,400) MDT1,MDTJ
400 FORMAT(2I5)
      IF(MDTJ.EQ.0) GO TO 402
      READ(5,401) (XOUT(I),I=1,MDTJ)
401 FORMAT(6F10.6)
402 IX=1
      N(2)=N(1)
      CALL OUTONE(IX)
17 CALL DELTAX
      IF(MDTJ.EQ.0) GO TO 404
      DO 403 JJ=1,MDTJ
      XTTT=XOUT(JJ)/1E./0
      IF(X(2).GT.XTTT.AND.X(1).LT.XTTT) X(2)=XTTT
403 CONTINUE
404 CALL NUSTEP
175 MCOUNT=MCOUNT+1
      NUMBER=NUMBER+1
      NX=N(2)+1

```

```

C START SOLUTION
DO 14 K=1,KKK
NCCOUNT=C
13 CALL COEFF(A,S,SP,C,D,K)
NF=N(2)
DO 1 J=2,NP
1 DD(J)=D(1,J)
DO(N(2))=-C(N(2))*U(2,N(2)+1,K)+DD(N(2))
CALL ANSWER(A,S,C,DD)
DO 2 J=2,NP
U(2,J,K)=VALUE(J)
2 CONTINUE
IF(MMX-2) 11,3,5
3 DO 4 J=2,NP
4 DD(J)=D(2,J)
DO(N(2))=-C(N(2))*WZ(2,N(2)+1,K)+DD(N(2))
CALL ANSWER(A,SP,C,DD)
DO 5 J=2,NP
5 WZ(2,J,K)=VALUE(J)
GO TO 11
6 IF(K-20.1) GO TO 3
DO 7 J=2,NP
7 DD(J)=D(2,J)
DO(N(2))=-C(N(2))*W(2,N(2)+1,K)+DD(N(2))
CALL ANSWER(A,S,C,DD)
DO 8 J=2,NP
8 W(2,J,K)=VALUE(J)
11 CALL CONT(K)
IX=2
CALL SHEAR(IX,K)
C CONVERGENCE CRITERION
NCCOUNT=NCCOUNT+1

```

```

        IF(NCOUNT.GT.1) GO TO 14
        GO TO 13
    14 CONTINUE
C SOLUTION THICKNESS CRITERION
    DO 121 K=1,KKK
        IF(DSQRT((U(2,N(2),K)**2+W(2,N(2),K)**2)/(U(2,NX,K)**2+W(2,NX,K)
        1**2)).GT.5.99999) GO TO 1000
    121 CONTINUE
C EXPANSION OF SOLUTION THICKNESS
    YMAX=1.30*Y(2,NX)
    DO 122 J=NX,100
        Y(1,J)=Y(1,J-1)+(Y(1,J-1)-Y(1,J-2))*1.060
        Y(2,J)=Y(1,J)
        WZ(2,J,1)=WZ(2,NX,1)
        WZ(1,J,1)=WZ(1,NX,1)
        JT=J
        IF(YMAX.LT.Y(1,J)) GO TO 123
    122 CONTINUE
        WRITE(6,600)
    600 FORMAT(1X,' SOLUTION THICKNESS TOO LARGE')
        GO TO 18
    123 N(2)=JT-1
        NP=N(2)
        NX=JT
        NQ=N(1)+1
        DO 124 IP=1,2
            DO 124 KP=1,KKK
                DO 124 JP=NQ,NX
                    EM(IP,JP+1,KP)=EM(IP,NQ+1,KP)
                    U(IP,JP,KP)=U(IP,NQ,KP)
                    V(IP,JP,KP)=V(IP,NQ,KP)
                    W(IP,JP,KP)=W(IP,NQ,KP)

```

```

124 CONTINUE
    N(1)=N(2)
1000 IF(MOTJ.EQ.3) GO TO 1002
    IX=2
    GO 1001 JJ=1,NOTJ
    XTTT=XOUT(JJ)/12.75
    IF(X(2).NE.XTTT) GO TO 1001
    CALL OUTONE(IX)
    WRITE(6,141) MDCOUNT,MDCOUNT,NUMBER
    MDCOUNT=0
1001 CONTINUE
    GO TO 142
1002 IF(MDCOUNT.LT.MOT1) GO TO 142
    IX=2
    CALL OUTONE(IX)
    WRITE(6,141) MDCOUNT,MDCOUNT,NUMBER
141 FORMAT(1X,'MDCOUNT=',I5,'      MDCOUNT=',I5,'      NUMBER=',I5)
    MDCOUNT=0
C SEQUENCING LOGIC
142 IF(MMX.GT.1) GO TO 16
    IF(MM.EQ.1.AND.X(2).GE.XX) GO TO 18
    IF(X(2).LT.XX) GO TO 161
    IF(MM.EQ.2) MMX=2
    IF(MM.EQ.3) MMX=3
C CHANGE OF SOLUTION FROM TWO-DIMENSIONAL TO THREE DIMENSIONAL
    KKK=NN
    IX=2
    CALL POT(IX)
    DO 15 K=1,KKK
    U(2,1,K)=0.0
    V(2,1,K)=0.0
    W(2,1,K)=0.0

```

```

U(1,1,K)=0.0
V(1,1,K)=0.0
W(1,1,K)=0.0
IF(K.GT.1) GO TO 151
WZ(2,1,K)=0.0
WZ(1,1,K)=0.0
151 DO 15 J=2,NX
U(2,J,K)=U(2,J,1)+U(2,NX,K)/U(2,NX,1)
V(2,J,K)=V(2,J,1)+U(2,NX,K)/U(2,NX,1)
W(2,J,K)=W(2,NX,K)
U(1,J,K)=U(2,J,K)
V(1,J,K)=V(2,J,K)
W(1,J,K)=W(2,J,K)
IF(K.GT.1) GO TO 15
WZ(2,J,K)=WZ(2,NX,K)
WZ(1,J,K)=WZ(2,J,K)
15 CONTINUE
NUMBER=1
DO 152 IP=1,2
DO 152 K=2,KKK
CALL SHEAR(IP,K)
152 CONTINUE
C STOPPING CRITERION
16 IF(XX+STSQL.LE.X(2)) GO TO 18
161 IF(U(2,2,1).LT.0.0) GO TO 18
GO TO 17
18 IX=2
IF(U(2,2,1).LT.0.0) IX=1
CALL OUTONE(IX)
WRITE(6,141) NCOUNT,MCOUNT,NUMBER
STOP
END

```

```

SUBROUTINE IMPRO
  IMPLICIT REAL*8(A-H, O-Z)
  COMMON U(2,100,10),V(2,100,10),W(2,100,10),WZ(2,100,2),UW(2,100,10
1),Y(2,100),X(2),Z(10),REYX(2),VALUE(100),Q0,Q,B,VISK,VISD,DEN,XX,B
2EYB,DX1,STSOL
  COMMON N(2),KK,LL,MM,NN,KKK,MMX,LLX,NUMBER
C THIS SUBROUTINE EITHER READS IN A STARTING PROFILE OR GENERATES A
C BLOCK PROFILE FOR THE LEADING EDGE SOLUTION.
  READ(5,600) Q0,Q,B,DEN,VISD,XX,DZ
  WRITE(6,600) Q0,Q,B,DEN,VISD,XX,DZ
600  FORMAT(3F10.4,2F11.8,2F10.6)
  READ(5,6000) STSOL
6000 FORMAT(D20.7)
  READ(5,601) N(1),KK,LL,MM,NN
  WRITE(6,601) N(1),KK,LL,MM,NN
601  FORMAT(5I5)
  LLX=1
  MMX=1
  KKK=1
  IF(LL.EQ.2) LLX=2
  IF(MM.EQ.4) MMX=3
  IF(MMX.EQ.3) KKK=NN
  B=B/12.
  STSOL=STSOL/B/12.
  XX=XX/B/12.
  DZ=DZ/(12.*B)
  VISK=VISD/DEN
  REYB=Q0*B/VISK
  WRITE(6,603) VISK,REYB
603  FORMAT(2D20.7)
  NX=N(1)+1
  IX=1

```

```

      READ(5,604) X(1)
604  FORMAT(D20.7)
      REYX(1)=Q*X(1)/VISK/12.
      X(1)=X(1)/5/12.
      Y(1,1)=0.0
      Y(2,1)=0.0
      Z(1)=0.0
      DO 1 K=2,NN
1     Z(K)=Z(K-1)+DZ
      KKK=1
      IF(MM.EQ.4) KKK=NN
C BLOCK PROFILE
      DO 2 K=1,KKK
      U(1,1,K)=0.0
      V(1,1,K)=0.0
      W(1,1,K)=0.0
      U(1,NX,K)=0/00
      V(1,NX,K)=0.0
      W(1,NX,K)=0.0
      IF(K.GT.1) GO TO 2
      WZ(1,1,K)=0.0
      WZ(1,NX,K)=0.0
2     CONTINUE
      IF(MM.EQ.4) CALL POT(IX)
      IF(KK.EQ.2) GO TO 7
      NQ=N(1)
      DO 3 K=1,KKK
      DO 3 J=2,NQ
      U(1,J,K)=U(1,NX,K)
21  V(1,J,K)=0.0
      W(1,J,K)=W(1,NX,K)
      IF(K.LT.2) WZ(1,J,K)=WZ(1,NX,K)

```

```

3 CONTINUE
  DY=0.001/(B*12.)*DSQRT(REYB)
  DO 6 J=2,NX
    IF(J.GT. 6) GO TO 5
    Y(1,J)=Y(1,J-1)+DY
    Y(2,J)=Y(1,J)
    GO TO 6
  5 DY=DY*1.06
    Y(1,J)=Y(1,J-1)+DY
    Y(2,J)=Y(1,J)
  6 CONTINUE
  GO TO 10
C INPUT PROFILE
  7 DO 8 J=2,NX
C U(1,NX,1) MUST BE CONSISTANT WITH POTENTIAL FLOW AND Y(1,J) GIVEN IN
C INCHES WITH THE VELOCITIES GIVEN IN FT/SEC.
    READ(5,602) Y(1,J),U(1,J,1),V(1,J,1)
  602 FORMAT(3D20.7)
    W(1,J,1)=W(1,NX,1)
    Y(1,J)=Y(1,J)/(B*12.)*DSQRT(REYB)
    Y(2,J)=Y(1,J)
    U(1,J,1)=U(1,J,1)/Q1
    V(1,J,1)=V(1,J,1)*DSQRT(B/(Q0*VISK))
  8 CONTINUE
  DO 9 K=1,KKK
    DO 9 J=2,NX
      U(1,J,K)=U(1,J,1)*U(1,NX,K)/U(1,NX,1)
      V(1,J,K)=V(1,J,1)*U(1,NX,K)/U(1,NX,1)
      W(1,J,K)=W(1,NX,K)
      IF(K.GT.1) GO TO 9
      WZ(1,J,1)=WZ(1,NX,1)
    9 CONTINUE

```



```
10 IX=1  
   DO 11 K=1,KKK  
     CALL SHEAR(IX,K)  
   11 CONTINUE  
     RETURN  
     END
```

```

SUBROUTINE POT(JX)
  IMPLICIT REAL*8(A-H,U-Z)
  COMMON U(2,100,10),V(2,100,10),W(2,100,10),WZ(2,100,2),PM(2,100,10
1),Y(2,100),X(2),Z(10),SEYX(2),VALUE(100),QC,Q,R,VI SK,VISU,DEN,XX,R
2EYB,DX1,STSOL
  COMMON N(2),KK,LL,MM,NN,KKK,MMX,ILX,NIMBER

```

C THIS SUBROUTINE CALCULATES THE POTENTIAL FLOW FOR AN IMPINGING JET AT
C ANY X-LOCATION ALONG THE Z-AXIS

```

  NX=N(IY)+1
  NX=N(IX)+1
  WW=0.0
  UU=U(1,NX,1)
  PI=3.1415926536
  A=2.75/B+XX
  U2=UU**2
  W2=WW**2
  ERROR=0.1D-08
  DO 3 K=1,KKK
1  F=-PI*(X(IX)-A)-0.5*DLOG(((1.+UU)**2+W2)/((1.-UU)**2+W2))-DATAN(2.
1*UU/(1.-U2-W2))
  G=-PI*(Z(K))-0.5*DLOG(((1.-WW)**2+U2)/((1.+WW)**2+U2))+DATAN(2.*WW
1/(1.-U2-W2))
  FU=-2.*(1.-U2+W2)/(((1.-UU)**2+W2)*((1.+UU)**2+W2))-2.*(1.-W2+
1U2)/(((1.-U2-W2)**2+4.*U2))
  GW= 2.*(1.-W2+U2)/(((1.-WW)**2+U2)*((1.+WW)**2+U2))+2.*(1.-U2+
1W2)/(((1.-U2-W2)**2+4.*W2))
  FW=4.*UU*WW*(1./(((1.-UU)**2+W2)*((1.+UU)**2+W2))-1./((1.-U2-W2)**
12+4.*U2))
  GU=4.*UU*WW*(1./(((1.-WW)**2+U2)*((1.+WW)**2+U2))-1./((1.-U2-W2)**
12+4.*W2))
  GU=-GU
  BOTTOM=FU*GW-FW*GU

```

```

DHW=(F#SU-G*FU)/D*BTOM
DUU=(S*FX-F#GW)/D*BTOM
UU=UU+DUU
WW=WW+D*WW
WZ=HW**2
U2=UU**2
IF(DABS(F).LT.F*KKR.AND.DABS(G).LT.EPDR) GO TO 2
GO TO 1
2 U(IX,NX,K)=UU
  W(IX,NX,K)=WW
  IF(IX.EQ.1.OR.K.GE.KKK.OR.X(2).FQ.XX) GO TO 3
  UU=U(IX-1,NX,K+1)
  WW=W(IX-1,NX,K+1)
  U2=UU*UU
  WZ=WW*WW
3 CONTINUE
WZ(IX,NX,1)=PI/4.*(1.-U(IX,NX,1)**4)
251 RETURN
    END

```

```

SUBROUTINE DELTAX
IMPLICIT REAL*(A-H,O-Z)
COMMON U(2,100,17),V(2,100,17),W(2,100,17),X(2,100,17),Y(2,100,17),Z(2,100,17),REX(2),VALU(100),DPR(2),VISC,VISX,VISY,
1),Y(2,100),X(2),Z(10),REX(2),VALU(100),DPR(2),VISC,VISX,VISY,
ZEYB,DX1,STSOL
COMMON N(2),KK,LI,MM,NN,KKK,MMX,LLX,NUMBER
C THIS SUBROUTINE CALCULATES A NEW STEP SIZE IN THE X DIRECTION
PPP=0
IF(NUMBER.GT.0) GO TO 1
READ(5,1000) MS,CHANGE
1000 FORMAT(I5,F10.7)
C FIRST STEP SIZE
DX=0.0010/(6*12.)
X(1)=X(1)+DX
GO TO 5
C SUBSEQUENT STEP SIZES
1 MX=N(2)+1
GO 2 J=1,NX
IF(J(2,J,1)/U(2,IX,1).LT.0.95) GO TO 2
II=J
GO TO 3
2 CONTINUE
3 DX=Y(2,II-1)/DSQRT(REXB)
IF(NUMBER.LT.MS) DX=0.0010/(6*12.)
DX1=X(2)-X(1)
IF(KK.EQ.2) GO TO 4
IF(NUMBER.GE.MS.AND.X(1).GT.XX.AND.MM.GT.1.AND.MM.LI.4) GO TO 4
MP=MS-1
IF(NUMBER.GT.MP) PPP=DX1*1.1
IF(NUMBER.GT.MP.AND.OX.GT.PPP) DX=PPP
4 X(1)=X(2)
X(2)=X(1)+DX

```

```
PCENT=DABS(1.-U(1, NX, 1)/U(2, NX, 1))*IX/DX1  
IF(PCENT.GT.CHANGE) X(2)=X(1)+CHANGE/PCENT*DX  
5 IF(MX.EQ.1.AND.X(2).GT.XX) X(2)=XX  
6 IF(MX.GT.1.AND.X(2).GT.XX+STSDI) X(2)=XX+STSDI  
RETURN  
END
```

```

SUBROUTINE MUSTEP
IMPLICIT REAL*8(A-H,O-Z)
COMMON U(2,100,10),V(2,100,10),W(2,100,10),WZ(2,100,2),PM(2,100,10
1),Y(2,100),X(2),Z(10),REYX(2),VALUE(100),Q0,Q,R,VISK,VISD,DEN,XX,Z
ZEY0,DX1,STSOL

```

```

COMMON N(2),KK,LL,MM,NN,KKK,MMX,ILX,NUMBER

```

C THIS SUBROUTINE PROJECTS NEW VELOCITY PROFILES ALONG THE NEXT X-STEP
C FOR USE IN THE CALCULATIONS ALONG THIS NEW LOCATION

```

NX=N(1)+1

```

```

N(2)=N(1)

```

```

NP=N(2)

```

```

LIVE=1

```

```

LIVE=2

```

```

IF (NUMBER.EQ.0) LIVE=2

```

```

IF (NUMBER.EQ.0) LIVE=1

```

```

DO 10 K=1,KKY

```

```

DO 10 J=1,NX

```

```

PM(LIVE,J,K)=PM(LIVE,J,K)

```

```

U(LIVE,J,K)=U(LIVE,J,K)

```

```

V(LIVE,J,K)=V(LIVE,J,K)

```

```

W(LIVE,J,K)=W(LIVE,J,K)

```

```

IF(K.EQ.1) WZ(LIVE,J,K)=WZ(LIVE,J,K)

```

```

10 CONTINUE

```

```

IF(MMX.EQ.1) GO TO 12

```

```

IX=2

```

```

CALL POT(IX)

```

```

DO 11 K=1,KKK

```

```

DO 11 J=1,NP

```

```

U(2,J,K)=U(2,J,K)+U(2,NX,K)/U(1,NX,K)

```

```

IF(W(1,NX,K).EQ.0.0) GO TO 111

```

```

W(2,J,K)=W(2,J,K)*W(2,NX,K)/W(1,NX,K)

```

```

111 IF(WZ(1,NX,K).EQ.0.0.OR.K.GT.1) GO TO 11

```

```
WZ(2,J,K)=WZ(2,J,K)*MZ(2,NX,K)/WZ(1,NX,K)
11 CONTINUE
12 RYX(1)=U(1,NX,1)*Q)*U*X(1)/VISK
   RYX(2)=U(2,NX,1)*Q)*U*X(2)/VISK
5 RETURN
END
```

```

SUBROUTINE COEFF(A,S,SP,C,D,K)
IMPLICIT REAL*8(A-H,O-Z)
COMMON U(2,100,10),V(2,100,10),W(2,100,10),WZ(2,100,2),EM(2,100,10)
1),Y(2,100),X(2),Z(10),REYX(2),VALUE(100),Q0,Q,B,VISK,VISD,DEN,XX,R
ZEYS,OX1,STSOL
COMMON N(2),KK,LL,KM,NN,KKK,MMX,LLX,NUMBER
DIMENSION A(100),S(100),SP(100),C(100),D(2,100)
C THIS SUBROUTINE FILLS UP THE TRI-DIAGONAL MATRIX FOR EACH OF THE
C UNKNOWNS.
  NP=N(2)
  NX=N(2)+1
  L=1
  IF(K.GT.1) L=L-1
C EACH STREAM GRADIENTS
  DUMX=(U(2,NX,K)+U(2,NX,K-L)+U(1,NX,K)+U(1,NX,K-L))/4.
  WPMX=(W(2,NX,K)+W(2,NX,K-L)+W(1,NX,K)+W(1,NX,K-L))/4.
  FUMX=0.5*(U(2,NX,K)-U(1,NX,K)+U(2,NX,K-L)-U(1,NX,K-L))/(X(2)-X(1))
  FWMX=0.5*(W(2,NX,K)-W(1,NX,K)+W(2,NX,K-L)-W(1,NX,K-L))/(X(2)-X(1))
  IF(K.GT.1) GO TO 200
  DUMZ=.0
  FUMZ=.0
  FWMZ=(WZ(2,NX,K)-WZ(1,NX,K))/(X(2)-X(1))
  DPMZ=(W(1,NX,K)+W(2,NX,K))/2.
  GO TO 201
200 DUMZ=0.5*(U(2,NX,K)-U(2,NX,K-1)+U(1,NX,K)-U(1,NX,K-1))/(Z(K)-Z(K-1))
  FUMZ=0.5*(U(2,NX,K)-U(2,NX,K-1)+U(1,NX,K)-U(1,NX,K-1))/(Z(K)-Z(K-1))
  FWMZ=0.5*(W(2,NX,K)-W(2,NX,K-1)+W(1,NX,K)-W(1,NX,K-1))/(Z(K)-Z(K-1))
  GO TO 201
C CONTINUE
C FINITE DIFFERENCE EQUATION FUNCTIONS
  D=SP(1)-2*SP
  DX=X(2)-X(1)

```



```

DYP=Y(2,J+1)-Y(2,J)
DYM=Y(2,J)-Y(2,J-1)
UP=(U(2,J,K)+U(2,J,K-1)+U(1,J,K)+U(1,J,K-1))/4.
VP=(V(2,J,K)+V(2,J,K-1)+V(1,J,K)+V(1,J,K-1))/4.
IF(V(1,J,K).EQ.0.0) VB=2.0*VB
WF=(W(2,J,K)+W(2,J,K-1)+W(1,J,K)+W(1,J,K-1))/4.
IF(K.EQ.1) GO TO 51
DZ=Z(K)-Z(K-1)
GUX=0.5*(U(2,J,K-1)-U(1,J,K-1)-U(1,J,K))/DX
GRX=0.5*(W(2,J,K-1)-W(1,J,K-1)-W(1,J,K))/DX
GUZ=0.5/DZ*(U(1,J,K)-U(1,J,K-1)-U(2,J,K-1))
GWZ=0.5/DZ*(W(1,J,K)-W(1,J,K-1)-W(2,J,K-1))
GUY=(DYM/DYP*(U(2,J+1,K-1)-U(2,J,K-1)+U(1,J+1,K-1)-U(1,J,K-1)
1+U(1,J+1,K)-U(1,J,K))+DYP/DYM*(U(2,J,K-1)-U(2,J-1,K-1)+U(1,J,K-1)
2-U(1,J-1,K-1)+U(1,J,K)-U(1,J-1,K)))/(4.*(DYP+DYM))
GWY=(DYM/DYP*(W(2,J+1,K-1)-W(2,J,K-1)+W(1,J+1,K-1)-W(1,J,K-1)
1+W(1,J+1,K)-W(1,J,K))+DYP/DYM*(W(2,J,K-1)-W(2,J-1,K-1)+W(1,J,K-1)
2-W(1,J-1,K-1)+W(1,J,K)-W(1,J-1,K)))/(4.*(DYP+DYM))
GEMUY=(1.+EM(2,J+1,K-1))*(U(2,J+1,K-1)-U(2,J,K-1))/DYP
1-(1.+EM(2,J,K-1))*(U(2,J,K-1)-U(2,J-1,K-1))/DYM+(1.+EM(1,J+1,K-1))
2*(U(1,J+1,K-1)-U(1,J,K-1))/DYP-(1.+EM(1,J,K-1))*(U(1,J,K-1)-
3U(1,J-1,K-1))/DYM+(1.+EM(1,J+1,K))*(U(1,J+1,K)-U(1,J,K))/DYP
4-(1.+EM(1,J,K))*(U(1,J,K)-U(1,J-1,K))/DYM)/(2.*(DYP+DYM))
GEMWY=(1.+EM(2,J+1,K-1))*(W(2,J+1,K-1)-W(2,J,K-1))/DYP
1-(1.+EM(2,J,K-1))*(W(2,J,K-1)-W(2,J-1,K-1))/DYM+(1.+EM(1,J+1,K-1))
2*(W(1,J+1,K-1)-W(1,J,K-1))/DYP-(1.+EM(1,J,K-1))*(W(1,J,K-1)-
3W(1,J-1,K-1))/DYM+(1.+EM(1,J+1,K))*(W(1,J+1,K)-W(1,J,K))/DYP
4-(1.+EM(1,J,K))*(W(1,J,K)-W(1,J-1,K))/DYM)/(2.*(DYP+DYM))
A(J)=(-(DYP/DYM)*VB/2.-(1.+EM(2,J,K))/DYM)/(DYP+DYM)/2.
S(J)=UB/DX+VB*(DYP-DYM)/(DYP*DYM*2.)+(1.+EM(2,J+1,K))/DYP+(1.+EM(
12,J,K))/DYM)/(DYP+DYM)
S(J)=S(J)/2.+WB/2./DZ

```

```

C(J) = ((DYM/DYP)*VB/2. - (1.+EM(2,J+1,K))/DYP)/(DYP+DYM)/2.
D(1,J) = UBNX*FUNX + WBNX*FUNZ + GEMUYY - UB*GUX - VB*GUY - WB*GUZ
D(2,J) = UBNX*FWNX + WBNX*FWNZ + GEMWYY - UB*GWX - VB*GWY - WB*GWZ
GO TO 4
31 GUX = -U(1,J,K)/DX
GUY = 0.5/(DYP+DYM)*((DYM/DYP*(U(1,J+1,K)-U(1,J,K))+DYP/DYM*(U(1,J,K)
1-U(1,J-1,K)))
GEMUYY = ((1.+EM(1,J+1,K))*(U(1,J+1,K)-U(1,J,K))/DYP - (1.+EM(1,J,K)
1)*(U(1,J,K)-U(1,J-1,K))/DYM)/(DYP+DYM)
A(J) = -(DYP/DYM)*VB/2. - (1.+EM(2,J,K))/DYM)/(DYP+DYM)
S(J) = UA/DX + VB*(DYP-DYM)/(DYP*DYM**2.) + ((1.+EM(2,J+1,K))/DYP + (1.+EM(
12,J,K))/DYM)/(DYP+DYM)
C(J) = ((DYM/DYP)*VB/2. - (1.+EM(2,J+1,K))/DYP)/(DYP+DYM)
D(1,J) = UBNX*FUNK + GEMUYY - VB*GUY - UB*GUX
WZB = (WZ(1,J,K) + WZ(2,J,K))/2.
GWZX = -WZ(1,J,K)/DX
GWZY = (DYM/DYP*(WZ(1,J+1,K) - WZ(1,J,K)) + DYP/DYM*(WZ(1,J,K) - WZ(1,J-1,
1K)))/(2.*(DYP+DYM))
GMKZYY = ((1.+EM(1,J+1,K))*(WZ(1,J+1,K) - WZ(1,J,K))/DYP - (1.+EM(1,J,K)
1)*(WZ(1,J,K) - WZ(1,J-1,K))/DYM)/(DYP+DYM)
RP(J) = S(J) + WZB/2.
D(2,J) = UBNX*FWZNX + WZNB**2 - WZB*WZ(1,J,K)/2. + GMWZYY - UB*GWZX - VB*GWZY
4 CONTINUE
RETURN
END

```

```

SUBROUTINE SHEAR(IX,K)
IMPLICIT REAL*8(A-H,O-Z)
COMMON U(2,100,10),V(2,100,10),W(2,100,10),WZ(2,100,2),EM(2,100,10
1),Y(2,100),X(2),Z(10),AFYX(2),VALUE(100),OO,Q,B,VISK,VISO,DEN,XX,R
ZEYS,DX1,STSGI
COMMON N(2),KK,LL,MM,NN,KKK,MMX,LLX,NUMBER
C THIS SUBROUTINE CALCULATES THE MIXING LENGTH AND THE SUBSEQUENT EDDY
C VISCOSITY
AP=25.0
MAX=N(IX)+2
EM(IX,MAX,K)=0
NX=N(IX)+1
IF(LLX.GT.1) GO TO 2
C LAMINAR FLOW
DO 1 J=1,NX
EM(IX,J,K)=0.0
1 CONTINUE
GO TO 10
C TURBULENT FLOW
2 QN=DSORT(U(IX,NX,K)**2+W(IX,NX,K)**2)
DO 3 J=2,NX
QN=DSORT(U(IX,J,K)**2+W(IX,J,K)**2)/QN
IF(QN.LT.0.005*QN) GO TO 3
JX=J
QNM=DSORT(U(IX,J-1,K)**2+W(IX,J-1,K)**2)/QN
GO TO 4
3 CONTINUE
4 DELTA=Y(1,JX-1)+(0.0050-QNM)/(QN-QNM)*(Y(1,JX)-Y(1,JX-1))
541 FUNCT=DSORT((U(IX,2,K)/Y(IX,2))**2+(W(IX,2,K)/Y(IX,2))**2)
YF1=ST=0.6*DELTA*DSORT(FUNCT)*REYN**0.25
APL=AP
DO 11 J=2,NX

```

```

DYM=Y(1,J)-Y(1,J-1)
FUNC=DSORT((U(IX,J,K)-U(IX,J-1,K))/DY**2+((W(IX,J,K)-W(IX,J-1,K)
1) )/DY**2)
YP=(Y(IX,J)+Y(IX,J-1))/2.*DSORT(FUNC)*REYB**0.25
IF(YP/25..GT.130.) YP=130.*25.
YCD=(Y(IX,J)+Y(IX,J-1))/2./DELTA
IF(YCD.GT.0.6) GO TO 7
IF(YP.GT.0.1) GO TO 5
C VAN ORIENT INNER FORMULATION
41 XMIX=YOB #REYB**0.25*(0.41*(1.-DEXP(-YP/APS)))*DELTA
GO TO 8
C IMMEDIATE FORMULATION
5 IF(YPTEST.GE.130.) GO TO 6
XMIX=YOB #REYB**0.25*(0.41*(1.-DEXP(-YP/APS)))*DELTA
YZ=130.*YCD/0.6
XMAX=DELTA*REYB**0.25*(0.41*YOB*(1.-DEXP(-YZ/APS))-1.53506*(YCD-0.
11)**2+2.75625*(YCD-0.1)**3-1.88425*(YCD-0.1)**4)
IF(XMIX.GT.XMAX) XMIX=XMAX
GO TO 8
6 XMIX=DELTA*REYB**0.25*(0.41*YCD*(1.-DEXP(-YP/APS))-1.53506*(YCD-0.
11)**2+2.75625*(YCD-0.1)**3-1.88425*(YCD-0.1)**4)
GO TO 8
C OUTER REGION FORMULATION
7 XMIX=YCD #REYB**0.25*(0.41*(1.-DEXP(-YP/APS)))*DELTA
XMAX=0.089*DELTA*REYB**0.25
IF(XMIX.GT.XMAX) XMIX=XMAX
C DETERMINATION OF THE EDDY VISCOSITY
8 EM(IX,J,K)=XMIX**2*FUNC
11 CONTINUE
EM(IX,1,K)=0.0
10 RETURN
END

```

```

SUBROUTINE ANSWER(A,S,C,D)
  IMPLICIT REAL*8(A-H,O-Z)
  COMMON U(2,100,10),V(2,100,10),W(2,100,10),WZ(2,100,2),EM(2,100,10
1),Y(2,100),X(2),Z(10),REYX(2),VALUE(100),Q0,Q,B,VISK,VISD,DEN,XX,R
25YB,DX1,STSOL
  COMMON N(2),KK,LL,MM,NN,KKK,MMX,LLX,NUMBER
C THIS SUBROUTINE SOLVES A SET OF SIMULTANEOUS EQUATIONS IN WHICH THE
C MATRIX OF COEFFICIENTS IS IN A TRI-DIAGONAL FORM
  DIMENSION A(100),S(100),C(100),D(100),E(100),F(100),G(100)
  NP=N(2)
  G(2)=S(2)
  F(2)=-C(2)/G(2)
  F(2)=D(2)/G(2)
  DO 1 J=3, NP
  G(J)=A(J)*F(J-1)+S(J)
  F(J)=(D(J)-A(J)*F(J-1))/G(J)
1 F(J)=-C(J)/G(J)
  NX=N(2)-1
  VALUE(N(2))=F(N(2))
  DO 2 J=2, NX
  JJ=(NX-J)+2
C VALUE(J) IS THE SOLUTION SET TO THE SIMULTANEOUS EQUATIONS
  VALUE(JJ)=C(JJ)*VALUE(JJ+1)+F(JJ)
  RETURN
END

```

```

SUBROUTINE CONT(K)
  IMPLICIT REAL*8(A-H,O-Z)
  COMMON U(2,100,10),V(2,100,10),W(2,100,10),WZ(2,100,2),EM(2,100,10
1),Y(2,100),X(2),Z(10),REYX(2),VALUE(100),Q0,Q,B,VISK,VISD,DFN,XX,R
  RLYS,DX1,STSDI
  COMMON N(2),KK,LL,MM,NN,KKK,MMX,LI X,NUMBER
C THIS SUBROUTINE SOLVES THE CONTINUITY EQUATION
  NX=N(2)+1
  IF(K.GT.1) GO TO 21
C TWO-DIMENSIONAL AND PLANE OF SYMMETRY
  DO 1 J=2,NX
    UFX=(U(2,J,K)-U(1,J,K)+U(2,J-1,K)-U(1,J-1,K))/(X(2)-X(1))
    WZF=WZ(2,J,K)+WZ(2,J-1,K)
    V(2,J,K)=V(2,J-1,K)-(Y(2,J)-Y(2,J-1))*(UFX+WZF)/2.0
  1 CONTINUE
  GO TO 3
C THREE-DIMENSIONAL
  21 DO 2 J=2,NX
    UFX=(U(2,J,K)-U(1,J,K)+U(2,J-1,K)-U(1,J-1,K))/(2.*(X(2)-X(1)))
    WFX=(W(2,J,K)-W(2,J,K-1)+W(2,J-1,K)-W(2,J-1,K-1))/(2.*(Z(K)-Z(K-
1)))
    WZF=(W(2,J,K)-W(2,J,K-1)+W(2,J-1,K)-W(2,J-1,K-1))/(2.*(Z(K)-Z(K-1
1)))
    V(2,J,K)=V(2,J-1,K)-(Y(2,J)-Y(2,J-1))*(UFX+WFX+WZF)
  2 CONTINUE
  RETURN
END

```

```

SUBROUTINE OUTONE(IX)
  IMPLICIT REAL*8(A-H,O-Z)
  COMMON U(2,100,10),V(2,100,10),W(2,100,10),WZ(2,100,2),EM(2,100,10
1),Y(2,100),X(2),Z(10),REYX(2),VALUE(100),Q0,Q,8,VISK,VISD,DEN,XX,R
2EYE,DX1,STSDI
  COMMON N(2),KK,LL,MM,NN,KKK,MMX,LLX,NUMBER
  DIMENSION US(2,100),NS(2,100),D1(2),D3(2),T11(2),T31(2),T13(2),T33
1(2),US(100),WB(100),FWY(100),FWY(100)
  C THIS SUBROUTINE IS A GENERAL OUTPUT PROGRAM AND CALCULATES THE
  C VARIOUS BOUNDARY LAYER PARAMETERS.
  NX=N(IX)+1
  DO 10 K=1,KKK,4
    BETA=DATAN2(W(IX,NX,K),U(IX,NX,K))
  C CALCULATION OF THE BOUNDARY LAYER THICKNESSES
  DO 1 I=1,2
    D1(I)=0.0
    D3(I)=0.0
    T11(I)=0.0
    T31(I)=0.0
    T13(I)=0.0
    T33(I)=0.0
    US(I,1)=0.0
    WB(I,1)=0.0
  DO 2 J=2,NX
    US(1,J)=U(IX,J,K)
    WB(1,J)=W(IX,J,K)
    US(2,J)=U(IX,J,K)*COS(BETA)+W(IX,J,K)*SIN(BETA)
    WB(2,J)=W(IX,J,K)*COS(BETA)-U(IX,J,K)*SIN(BETA)
  DO 3 I=1,2
  DO 3 J=2,NX
    DI=(US(I,J)+US(I,J-1))/2.
    WI=(WB(I,J)+WB(I,J-1))/2.

```

```

F3=(US(I,NX)-F1)*(Y(IX,J)-Y(IX,J-1))*B*12./DSQRT(REY3)
F4=(WS(I,NX)-F2)*(Y(IX,J)-Y(IX,J-1))*B*12./DSQRT(REY5)
D1(I)=D1(I)+F3/US(2,NX)
D2(I)=D2(I)+F4/US(2,NX)
T11(I)=T11(I)+F1*F3/US(2,NX)**2
T31(I)=T31(I)+F1*F4/US(2,NX)**2
T13(I)=T13(I)+F2*F3/US(2,NX)**2
3 T33(I)=T33(I)+F2*F4/US(2,NX)**2
F1=X(IX)*B*12.
F2=Z(K)*B*12.
WRITE(6,600) F1,F2,REYX(IX),REYF
600 FORMAT(1H1,35X,'RESULTS AT X=',D13.6,'IN. AND Z=',D13.6,'IN.'/43X
1,'REYX=',D13.6,' AND REYB=',D13.6//)
WRITE(5,601)
601 FORMAT(8X,'D1,IN',11X,'D2,IN',10X,'T11,IN',10X,'T31,IN',10X,'T13,I
IN',10X,'T33,IN')
DO 4 J=1,2
WRITE(5,602) D1(J),D2(J),T11(J),T31(J),T13(J),T33(J)
602 FORMAT(6D16.6)
4 CONTINUE
C OUTPUT FOR VELOCITIES WHERE WS(2,J) AND US(2,J) BECOME THE POLAR PLOT
C PARAMETERS.
WRITE(6,603)
603 FORMAT(55X,'DIMENSIONLESS VARIABLES'/14X,'Y',19X,'U',19X,'V',19X,'
1W',15X,'US/USN',15X,'WS/USN'//)
DO 7 J=1,NX
US(2,J)=US(2,J)/US(2,NX)
WS(2,J)=WS(2,J)/US(2,NX)
WRITE(6,604) Y(IX,J),U(IX,J,K),V(IX,J,K),W(IX,J,K),US(2,J),WS(2,J)
* 1,J
604 FORMAT(6D20.7,16)
7 CONTINUE

```



```

WRITE(6,605)
605 FORMAT(1H1,14X,'Y, IN',12X,'U, FT/SEC',12X,'V, FT/SEC',12X,'W, FT/SEC'
1,11X,'ALPHA, DEG',12X,'ETA'/)
DO 8 J=1,NX
ETA=0.0
IF(X(IX).GT.0.0) ETA=Y(IX,J)/DSQRT(K(IX))
YP=Y(IX,J)*90./R(Y)**0.5
UP=U(IX,J,K)*90
VP=V(IX,J,K)*90/R(Y)**0.5
WP=W(IX,J,K)*90
ALPHA=0.0
IF(J.GT.1.AND.US(2,J).GT.0.0) ALPHA= DATAN2(WS(2,J),US(2,J))
ALPHA=ALPHA*180./3.1415926536
WRITE(6,606) YP,UP,VP,WP,ALPHA,ETA,J
606 FORMAT(6D20.7,16)
8 CONTINUE
WRITE(6,6061) BETA
6061 FORMAT(8F20.7,'BETA=',015.7)
C OUTPUT FOR SHEAR STRESS
WRITE(6,607)
607 FORMAT(1H1,6X,'Y, IN',10X,'TAUXL',10X,'TAUXT',10X,'TAUZL',10X,'TAUZ'
1F',9X,'TAU(0)',11X,'YPLUS',10X,'UPLUS'/)
DO 6 J=1,NX
UC(J)=US(1,J)
WC(J)=WS(1,J)
6 CONTINUE
EXY(1)=U(IX,2,K)/Y(IX,2)
EYX(1)=V(IX,2,K)/Y(IX,2)
EXY(NX)=0.0
EYX(NX)=0.0
UP=W(1)
DO 6 J=2,NX

```

```

DYP=Y(IX,J+1)-Y(IX,J)
DYP=Y(IX,J)-Y(IX,J-1)
FUJ(J)=(DYE/DYP*(UR(J+1)-UR(J))+DYP/DYM*(UR(J)-UR(J-1)))/(EYP+DYM)
FWY(J)=(DYM/DYP*(WD(J+1)-WD(J))+DYP/DYM*(WD(J)-WD(J-1)))/(EYP+DYM)
6 CONTINUE
GG=32.176
DO 9 J=1,NX
DYP=0.0
DYM=0.0
IF(J.GT.1) DYM=Y(IX,J)-Y(IX,J-1)
IF(J.LT.NX) DYP=Y(IX,J+1)-Y(IX,J)
TAUXL=VISO*FUJ(J)*GG/D*DSQRT(REYB)/32.176
TAUZL=VISO*FWY(J)*GG/B*DSQRT(REYB)/32.176
TAUXT=DEN*GG**2/DSQRT(REYB)*(EM(IX,J,K)*DYP+EM(IX,J+1,K)*DYM)/
1(DYP+DYM)*FUJ(J)/GG
TAUZT=DEN*GG**2/DSQRT(REYB)*(EM(IX,J,K)*DYP+EM(IX,J+1,K)*DYM)/
1(DYP+DYM)*FWY(J)/GG
IF(J.EQ.1) TAUXT=0.0
IF(J.EQ.1) TAUZT=0.0
TAUTOT=DSQRT((TAUXL+TAUXT)**2+(TAUZL+TAUZT)**2)
IF(J.EQ.1) TAUW=TAUTOT
USTAR=DSQRT(TAUW*32.176/DEN)
YPLUS=Y(IX,J)*8/DSQRT(REYB)*USTAR/VISK
UPLUS=U(IX,J,K)*8/USTAR
YP=Y(IX,J)*8*12./REYB**0.5
WRITE(6,608) YP,TAUXL,TAUXT,TAUZL,TAUZT,TAUTOT,YPLUS,UPLUS,J
608 FORMAT(8D15.6,16)
9 CONTINUE
WRITE(6,609)
609 FORMAT(IX,'VALUES OF SHEAR ARE GIVEN IN LBF/FT**2')
IF(K.GT.1) GO TO 10
WRITE(6,610) (RZ(IX,J,K),J=1,NX)

```

```
610 FORMAT(6D20.6)
10 CONTINUE
11 RETURN
END
```

```

SUBROUTINE POT(IX)
  IMPLICIT REAL*8(A-R,U-Z)
  COMMON U(2,100,10),V(2,100,10),W(2,100,10),WZ(2,100,2),EM(2,100,10
1),Y(2,100),X(2),Z(10),REYX(2),VALU= (100),Q0,C,B,VISK,VISD,DEN,XX,R
2EY0,DX1,STSEL
  COMMON N(2),KK,LL,MM,NN,KKK,MMX,LLX,NUMBER
C THIS SUBROUTINE CALCULATES THE POTENTIAL FLOW OVER A CYLINDER
  NX=N(IX)+1
  C=48.0/12.0/B+XX
  DO 1 K=1,KKK
    U(IX,NX,K)=1.-((C-X(IX))**2-Z(K)**2)/((C-X(IX))**2+Z(K)**2)**2
1  W(IX,NX,K)=2.0*(C-X(IX))*Z(K)/((C-X(IX))**2+Z(K)**2)**2
    WZ(IX,NX,1)=2.0/(C-X(IX))**3
  RETURN
END

```

VIII. VITA

William Frederick Klinksiek was born in New York City, New York, on August 18, 1945. He graduated from Wakefield High School in Arlington, Virginia in June 1963 and was married that summer to the former Sharon Ruth O'Brien.

In September 1963 he entered Virginia Polytechnic Institute and received his Bachelor of Science in Mechanical Engineering with Honors in August 1966. During his undergraduate training he was an active member of Tau Beta Pi, Phi Kappa Phi, Student Section of the American Society of Mechanical Engineers and was a member of the Board of Directors of the Association of Married Students.

In September 1966, he entered the graduate school of Virginia Polytechnic Institute as a research assistant where he received his Master of Science in Mechanical Engineering in September 1967.

Since September 1967, he has been employed as an Instructor in the Department of Mechanical Engineering at Virginia Polytechnic Institute and State University while advancing his graduate training.

William Frederick Klinksiek

AN IMPLICIT NUMERICAL SOLUTION OF THE TURBULENT
THREE-DIMENSIONAL INCOMPRESSIBLE BOUNDARY-LAYER EQUATIONS

by

William Frederick Klinksiek

ABSTRACT

A method of solving the three-dimensional, incompressible turbulent boundary-layer equations was developed using a Crank-Nicholson implicit finite-difference technique, with the turbulent stress terms modeled with an eddy-viscosity model obtained from mixing length theory. The method was applied to two three-dimensional flow geometries for which experimental data exists and a comparison with this data showed excellent agreement.

The complete computer program was sufficiently generalized for application to two-dimensional laminar and turbulent flows with arbitrary pressure gradients. The method was applied to several such test cases and the solutions agreed well with both theory and experiment.

An analysis was presented to determine the conditions for which the finite difference equations were stable and convergent. The results of this analysis demonstrated that the equations are generally stable and convergent. However, care must be exercised when writing the finite difference approximation to the continuity equation, because certain finite difference formulations of the continuity equation can lead to an instability when the initial values for the distribution of the velocity normal to the bounding surface cannot be accurately specified.